Universidade de Brasília

Instituto de Geociências - IGD

Programa de Pós-graduação em Geologia

# GENESIS OF THE MAFIC GRANOPHYRE AT VREDEFORT, SOUTH AFRICA: FIELD, PETROGRAPHIC, AND GEOCHEMICAL STUDIES OF THE IMPACT MELT ROCK DIKE ON FARM RENSBURGDRIF.

ANA RITA PEREIRA MACIEL

**Dissertação de Mestrado nº 482**

BRASÍLIA – DF

OUTUBRO DE 2021

# GENESIS OF THE MAFIC GRANOPHYRE AT VREDEFORT, SOUTH AFRICA: FIELD, PETROGRAPHIC, AND GEOCHEMICAL STUDIES OF THE IMPACT MELT ROCK DIKE ON FARM RENSBURGDRIF.

GÊNESE DO GRANÓFIRO MAFICO DE VREDEFORT, ÁFRICA DO SUL: ESTUDOS DE CAMPO, PETROGRAFIA, E GEOQUÍMICA PARA O DIQUE DE ROCHA FUNDIDA DE IMPACTO NA FAZENDA RENSBURGDRIF.

ANA RITA PEREIRA MACIEL

**Dissertação de Mestrado nº 482**

Dissertação de Mestrado apresentada ao Programa de Pós-Graduação em Geologia do Instituto de Geociências da Universidade de Brasília, como requisito parcial para obtenção do grau Mestre em Geologia, na área de concentração Geologia Regional.

Orientador: Prof. Dr. Wolf Uwe Reimold

Co-orientadora: Profª. Drª. Natalia Hauser

BRASÍLIA – DF

2021

ANA RITA PEREIRA MACIEL

**GENESIS OF THE MAFIC GRANOPHYRE AT VREDEFORT, SOUTH AFRICA: FIELD, PETROGRAPHIC, AND GEOCHEMICAL STUDIES OF THE IMPACT MELT ROCK DIKE ON FARM RENSBURGDRIF.**

Dissertação de Mestrado apresentada ao Programa de Pós-Graduação em Geologia do Instituto de Geociências da Universidade de Brasília, como requisito parcial para a obtenção do grau de Mestre em Geologia, na área de concentração Geologia Regional.

29 de outubro de 2021

_____

Prof. Dr. Wolf Uwe Reimold (Presidente – UnB)

_____

Prof. Dr. Tiago Luis Reis Jalowitzki (UnB)

_____

Prof. Dr. Cristiano de Carvalho Lana (UFOP)

Ficha catalográfica elaborada automaticamente,
com os dados fornecidos pelo(a) autor(a)

Pereira Maciel, Ana Rita
Pg GENESIS OF THE MAFIC GRANOPHYRE AT VREDEFORT, SOUTH AFRICA: FIELD STUDY, PETROGRAPHY, AND GEOCHEMISTRY FOR THE IMPACT MELT ROCK DIKE ON FARM RENSBURGDRIF. / Ana Rita Pereira Maciel; orientador Wolf Uwe Reimold; co-orientador Natalia Hauser. -- Brasília, 2021.
115 p.

Dissertação (Mestrado - Mestrado em Geologia) -- Universidade de Brasília, 2021.

1. Vredefort Dome, . 2. Impact Melt Rock. 3. Mafic Granophyre. I. Reimold, Wolf Uwe, orient. II. Hauser, Natalia, co-orient. III. Título.

***“It always seems impossible until it’s done.”***

**Nelson Mandela**

# AGRADECIMENTOS

Agradeço primeiramente a minha mãe e ao meu companheiro Gabriel pela paciência, compreensão e suporte emocional. Agradeço aos meus orientadores Uwe Reimold e Natália Hauser pelo apoio, disposição e orientação.

Agradeço também aos amigos do programa de pós-graduação pela convivência e constante aprendizado e aos amigos da vida pelo incentivo e companheirismo durante toda essa jornada.

Muito obrigada aos funcionários do Instituto de Geociências, principalmente aos técnicos dos laboratórios de Laminação, Microscopia e Geocronologia, pelos favores e serviços prestados.

O presente trabalho foi realizado com o apoio da Coordenação de Aperfeiçoamento de Pessoal do Nível Superior – Brasil (CAPES) – Código de Financiamento 001 e apoio da Sociedade de Geologia da Afica do sul por meio do *REI Fund*.

**Por fim, obrigada a todos que acreditaram em mim durante todo esse longo e difícil período.**

# ABSTRACT

The Vredefort impact structure in South Africa is currently the largest impact structure known on Earth, with an original diameter estimated 250-300 km. Vredefort is also one of the oldest impact structures known on Earth (~2 Ga). The Vredefort Dome represents the deeply eroded central uplift of this large, complex impact structure. The formation of the impact melt rock of this structure – the Vredefort Granophyre – has been the subject of debate for more than 50 years. This impact melt rock was long considered a regionally remarkably uniform lithology in terms of chemical composition and along clast populations - essentially independent of the compositions of local wall rocks. Mafic inclusions were observed only locally where a dike cuts across an occurrence of metamorphosed dioritic – so-called epidiorite – or basaltic – Dominion Group Metalava - country rock. The genesis of this “normal” Felsic Granophyre has been traditionally explained by wholesale melting of target rocks, at various proportions of mainly granite plus quartzite and shale, or with an additional Ventersdorp Supergroup volcanic component. In 2011, the presence of a Mafic Granophyre phase was reported, allegedly along the margins of a dike of felsic Granophyre on the Kopjeskraal property, in the NW of the Vredefort Dome. It was proposed that two successive intrusions of melt from a differentiating impact melt sheet initially present in the Vredefort crater structure had generated this composite dike. Subsequently, it was recognized that the dike was indeed of composite nature but that the mafic phase occurred in the central part along the extension of the dike. It was hypothesized that mixing Felsic Granophyre with a local occurrence of likely epidiorite could explain the formation of the mafic phase. The second possible mafic component, Dominion Group Lava (DGL), was also considered. The current project was aimed at clarifying the formation of the Vredefort Granophyre by multidisciplinary analysis of the extension of this same dike on Farm Rendsburgdrif. Samples collected along the dike and along a profile perpendicular across the dike were analysed. The analyses indicated the presence of two distinct phases, whereby the mafic (clast-poor) phase was observed in the central part of the dike and the (felsic) clast-rich phase at the margins. Geochemical data indicate that the Mafic Granophyre composition is a mixture between the felsic phase and mafic host rock. The isotope data for Dominion Group metabasalt fall far off the Granophyre and epidiorite data array, which supports that DGL may not have been a precursor for the Mafic Granophyre phase and, apparently, did not play a significant role in the formation of Vredefort Granophyre. In this way, our results strongly mitigate against the hypothesis that Mafic Granophyre represents a differentiation from the original impact melt body and favor the epidiorite assimilation/admixture hypothesis for the formation of Mafic Granophyre.



**Keywords: VREDEFORT DOME, IMPACT MELT ROCK, MAFIC GRANOPHYRE, EPIDIORITE, DOMINION GROUP METALAVA, ISOTOPE GEOCHEMISTRY.**

# RESUMO

A estrutura de impacto Vredefort na, África do Sul, é a maior estrutura de impacto conhecida na Terra, com um diâmetro original de 250-300 km. Vredefort é também uma das mais antigas estruturas de impacto conhecidas na Terra (~2 Ga). O Domo de Vredefort representa a elevação central desta grande e complexa estrutura, que se encontra bastante erodida. A formação da rocha fundida de impacto desta estrutura – Vredefort Granophyre – vem sendo debatida por muitos anos. Esta rocha por muito tempo foi considerada como uma litologia regionalmente uniforme. Foram observadas inclusões maficas apenas localmente, na região onde um dique atravessa uma ocorrência de epidiorito. A gênese do Granófiro "normal", félsico, tem sido tradicionalmente atribuída à fusão de rochas alvo, em várias proporções tanto de granito, quartzito e xisto, quanto com um componente adicional de basalto proveniente do Supergrupo de Ventersdorp. Em 2011, foi relatada a presença de uma fase máfica ao longo das margens de um dique de granófiro na propriedade de Kopjeskraal, no NW do domo de Vredefort. Para explicar a sua formação, propuseram que o melt máfico teria sido alojado primeiro nos diques, seguido por um segundo pulso a partir da camada sobreposta de melt de impacto. Posteriormente, foi reconhecido que a fase máfica ocorria na porção central do dique. Desta forma, uma hipótese para explicar a formação dessa fase máfica, a partir de uma mistura do Granófiro Félsico com uma ocorrência local de epidiorito, foi proposta. As rochas máficas do Dominion Group lava (DGL) também foram consideradas como um possível componente máfico. O projeto atual tem como objetivo esclarecer a formação do Granófiro de Vredefort por meio da análise multidisciplinar da extensão deste mesmo dique sobre a Farm Rendsburgdrif. As amostras coletadas ao longo do dique e por meio de um perfil perpendicular à ele foram analisadas petrograficamente, geoquimicamente (elementos traços e maiores) e isotópicamente (Sr-Nd). As análises indicaram a presença de duas fases distintas, onde a fase mafica (pobre em clastos) foi observada na parte central do dique, enquanto a fase felsica (rica em clastos) nas margens. Os trends dos dados geoquímicos indicaram que a composição da Granófiro Mafico seria uma mistura entre a fase félsica e a rocha encaixante máfica. Os dados isotópicos do metabasalto do Grupo Dominion (DGL) caíram muito longe do campo de dados dos Granófiros e do epidiorito, confirmando que o DGL não pode ter sido um precursor da fase máfica e, que aparentemente, não desempenhou um papel significativo na formação do Granófiro máfico. Desta forma, nossos resultados mitigam fortemente a hipótese de que a a fase máfica representa uma diferenciação do corpo fundido do impacto original e favorece a hipótese de assimilação do epidiorito para a formação do mesmo.



**Keywords: DOMO DE VREDEFORT, ROCHA FUNDIDA DE IMPACTO, GRANÓFIRO MÁFICO, EPIDIORITO E GEOQUÍMICA ISOTÓPICA.**

# FIGURE CAPTIONS

# FIGURE CAPTIONS (CHAPTER 4)

# TABLE HEADINGS

# TABLE OF CONTENTS

# 1. CHAPTER: INTRODUCTION

The deeply eroded Vredefort impact structure (VIS), in north-central South Africa, is centered roughly 130 km southwest of Johannesburg, in Archean and Paleoproterozoic rocks of the central Kaapvaal craton (e.g., Gibson and Reimold, 2008; Gibson, 2019). The impact structure covers the entire region of the economically important Witwatersrand Basin (ibid). The VIS is the largest known impact structure on Earth with an estimated original diameter of 250-300 km (e.g., Henkel and Reimold, 1999; Gibson and Reimold, 2008; Gibson, 2019). It has been variably discussed whether this large structure represents a complex impact structure with central peak or with peak ring, or perhaps represents a multi-ring impact basin (Grieve et al., 2008).

The Vredefort Dome in the centre of the structure represents the deeply eroded central uplift (or peak ring) of this large, complex impact structure. Detailed multidisciplinary geoscientific analysis of the Dome has made this structure one of the best-studied impact structures in the world and has significantly contributed much to the general understanding of large impact cratering processes (e.g., Gibson and Reimold, 2008; Reimold and Koeberl, 2014; Gibson 2019 and references therein; Gottwald et al., 2020).

Importance of the impact process.

Largely as a direct result of Space exploration, impact cratering has become widely accepted over the past decades as one of the most important processes in the Solar System (e.g., Taylor, 2001; Rothery et al., 2018; Gottwald et al., 2020). The surfaces of all solid bodies in our planetary system are densely covered with impact structures of a vast range of sizes and different morphologies (e.g., Melosh, 2011; Osinski and Pierazzo, 2013). In contrast to the extensive records of impact bombardment of other planetary surfaces in the Solar System, only just about 208 impact structures have so far been identified on Earth (Gottwald et al., 2020; Kenkmann, 2021). The endogenous processes on our highly dynamic planet, i.e., weathering, erosion, sedimentation, burial, plate tectonics, etc., have effectively deleted the major part of Earth’s impact record. In addition, two thirds of the Earth´s crust are covered with oceans above relatively young oceanic crust.

According to Reimold and Koeberl (2014), the main purposes of searching for and studying impact structures include:

(1) identification and then confirmation of an impact structure;

(2) improving the terrestrial impact cratering record to evaluate how cratering intensity may have changed over geological time; this includes the dating of impact structures (actually of impact-generated lithologies or -modified minerals, and thereby, of the impact events);

(3) investigations related to the understanding of the physical and chemical processes inherent to impact cratering, projectile-target rock interaction, and impact breccia formation;

(4) the dependence of the final character of an impact structure on the individual conditions related to the nature (geological composition, stratigraphy, tectonic arrangements such as effects of structural defects or non-horizontal stratigraphy) of the target rock(s);

(5) improving the impact-related scaling relationships such as the function of energy released in relation to crater size or melt rock volume, or the variance of stratigraphic uplift with crater diameter, for different target rock types and configurations;

(6) correlation of impact magnitude and post-impact environmental effects, and

(7) basic investigations related to impact-characteristic shock metamorphism.

Impact structures on Earth are the only hands-on laboratories for impact cratering studies in the Solar System (with exception of the relatively limited supply of shocked and impact-generated meteorites, also from Mars and Moon, and some rock samples from the Moon).

### 1.1. Impact-generated melt rocks

Terrestrial impact structures, especially those formed in crystalline targets, have significant occurrences of one or more types of impact-generated melt rock (e.g., Reimold, 1998; reviews by Dressler and Reimold, 2001, 2004; French and Koeberl, 2010; Osinski and Pierazzo, 2013). Basically, this involves (1) impact melt rock (Stöffler and Grieve; 2007, for impactite nomenclature), and (2) the so-called pseudotachylitic breccias (in the following abbreviated PTB, in accordance with Reimold, 1995, 1998, and Gibson and Reimold, 2008). PTB was in earlier Vredefort literature referred to as pseudotachylyte or pseudotachylite. However, in the present structural geological

literature, the terms pseudotachylyte or pseudotachylite are considered synonymous with friction melt.

Impact melt rock is formed early in the evolution of an impact structure in a regime relatively close to the point of impact where target rock is essentially bulk melted due to very high shock pressures and associated post-shock temperatures. This melt is then mixed to various degrees with target rock clasts of different degrees of shock metamorphism. Impact melt can be variably formed in crystalline basement or in supracrustal target rocks, but melt volume seems to be strongly enhanced in cases of impact into crystalline targets.

Pseudotachylitic breccia is mostly rare in impact structures but at Sudbury (Canada) and Vredefort, the two largest impact structures known on Earth, voluminous, clast-bearing melt rock with a generally glassy or microcrystalline matrix, occurring in veins or irregular geometries, and containing angular to rounded clasts of wall rock lithologies (e.g., Stöffler and Grieve, 1994; Reimold et al., 2006) are abundant. The genesis of such material is still debated; some recent discussions were presented by Reimold et al. (2017) and Spray and Biren (2021). The main processes that have been implicated in the formation of such melt breccias are that pseudotachylitic breccias are shock-generated, that pre-impact fracture-fault systems, and that voluminous breccias of this type are formed during the decompression phase of impact when melting temperatures of rocks are suddenly exceeded during the ultradynamic uplift of initially shock compressed target rock in the region of the central uplift structure. This type of melt phase was termed by Reimold (1998) “pseudotachylitic breccia, PTB” to distinguish this impact-generated phase from tectonic or impact-related friction melt (pseudotachylite).

Melt rocks in impact structures are very important for the confirmation of an impact origin of a structure. The possible presence of a meteoritic component mixed into impact melt could be detected (e.g., Koeberl, 2014), or the presence of shock metamorphosed clasts (e.g., Reimold et al., 2017). Impact melt rocks may contain clast populations that comprise material derived from all parts of the transient crater cavity (Melosh, 1989), thus characteristically including clasts with diagnostic shock metamorphic effects. Dating of impact structures, i.e., of the associated impact events, has relied heavily on chronological analysis of impact melt rock, or of melt clasts in impact breccia known as suevite (e.g., Jourdan and Reimold, 2012).

Besides these melt rocks generated by the impact process, other impact-generated rocks may occur in impact structures: monomict breccias are shattered target rocks, petrographically equivalent to tectonically produced cataclasite, but they may carry some shocked mineral or lithic clasts. Lithic breccias are composed of clastic components only (no melt component). Suevite is a distinct rock type comprising mineral and lithic clasts of varied shock metamorphic degree, but invariably including a fragmental melt component (Stoffler and Grieve, 2007; and references there in).

## 1.2. The Vredefort Dome and its impact melt rocks

Boon and Albritton (1936) were the first to suggest that the ~90 km wide and roughly circular Vredefort Dome (at the time known as the Vredefort Ring) might be of impact origin, also based on the recognition by Shand (1916), Hall and Molengraaff (1925), and Nel (1927) of extensive volumes of melt rock – the so-called ‘‘pseudotachylyte’’ (Shand, 1916) – and the general observation of intense rock deformation.

The idea of meteorite impact was later debated by Daly (1947), who concluded that it was a more likely explanation for the origin of the Vredefort Dome than any other then-available endogenic hypothesis. Dietz (1947, 1959) promoted shatter cones as a recognition criterion for impact structures, and his prediction that the Vredefort Ring would contain this deformation feature (Dietz, 1960, 1961) was soon-after confirmed by Hargraves (1961).

Besides that, microdeformation features in quartz from Vredefort rocks (Carter, 1965, 1968) and of clasts in the so-called pseudotachylyte (Wilshire, 1971; Schwarzman et al., 1983) were considered as shock deformation, and Martini’s (1978) identification of coesite and stishovite in then renamed pseudotachylite did suggest an impact origin for the structure. However, a major sector of the geo-community, in particular in South Africa, continued to adhere to cryptoexplosive or cryptovolcanic ideas for the origin of the Vredefort Dome right into the 1990s (e.g., Nicolaysen and Ferguson, 1990).

Then, near-general acceptance of the impact origin for the Vredefort Structure came through the confirmation by Leroux et al. (1994) that the basal planar microdeformation features in quartz from the Vredefort Dome are a bona fide shock deformation effect (annealed Planar Deformation Features, PDFs). Kamo et al. (1996)

identifed shocked zircon in Vredefort melt rock, and Koeberl et al. (1996) determined a meteoritic component in Vredefort impact melt rock. Kamo et al. (1996) also dated the impact by U–Pb dating of single zircons from both impact melt rock and pseudotachylitic breccia to 2023 ± 4 Ma, within error limits of the results by Gibson et al. (1997), Moser (1997), and Spray et al. (1995).

The diameter of the Vredefort structure has been variably estimated in the literature. Simpson (1978) estimated a diameter of 100 to 130 km, based on a core radius of ~18 km. In the original paper citing evidence for an impact origin, Dietz (1961) estimated the structure's diameter at 120 km, based on a width of ~60 km for a "great ring syncline" surrounding the core. Martini (1991) estimated 150 km, based on a "circular fault scarp", whereas Bisschoff (1962) proposed a diameter of 160 km, based on the outer diameter of the surrounding "dolomite" (Transvaal Supergroup) basin. The largest diameter estimate of 300-400 km was tentatively suggested by Reimold and Wallmach (1991). A ca. 300 km crater diameter was estimated by the scaling of the distribution of shatter cones, pseudotachylitic breccia and shock deformation features in quartz (Therriault et al., 1997), which was then further supported by the geophysical modeling of the Vredefort-Witwatersrand system by Henkel and Reimold (1998) that also indicated an about 100 km wide central uplift based on the interpretation of reflection seismic data.

This latter size placed Vredefort into the elite triad of very large terrestrial impact structures, together with the Sudbury (~250 km, 1850 Ma) and Chicxulub (180–200 km, 66 Ma) structures (e.g., Grieve, 2001). Grieve and Therriault (2000) and Grieve et al. (2008) compared these three structures and concluded that they might well represent the only multi-ring impact basins (Spudis,1993) presently known on Earth.

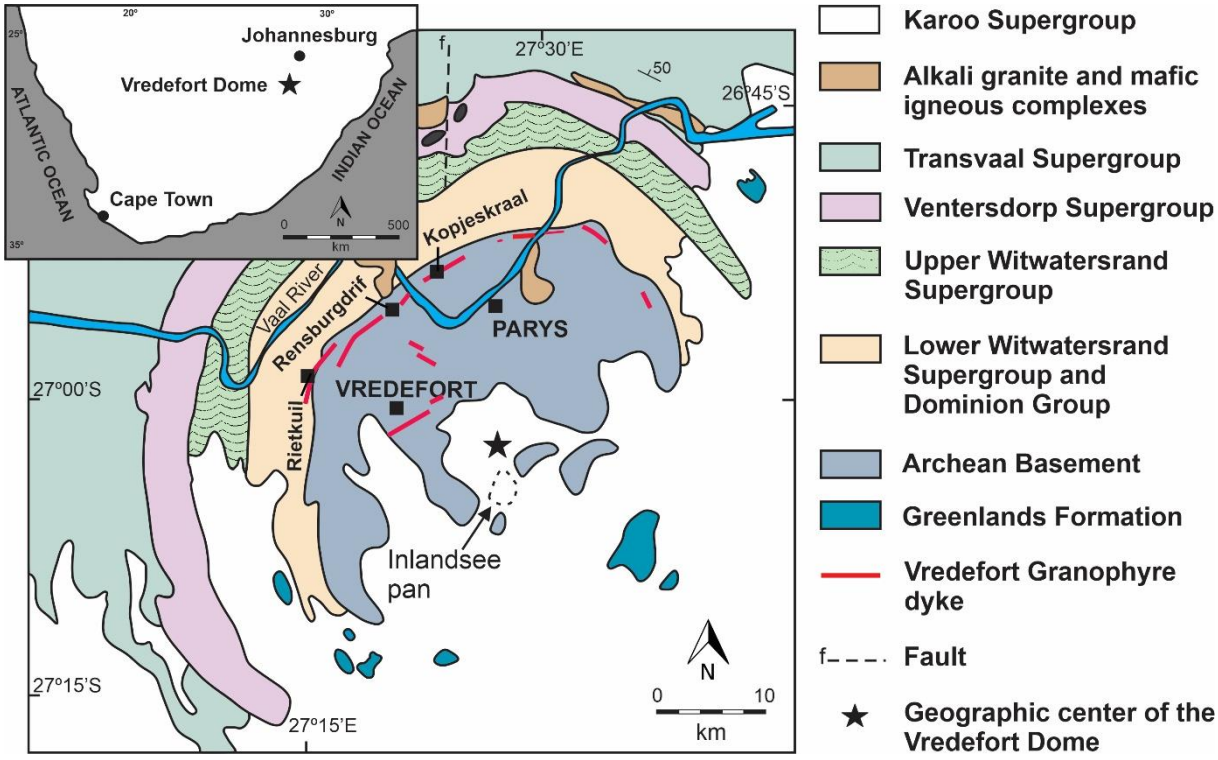


Figure 1 - Schematic geology of the Vredefort Dome (inset shows the location of the Vredefort impact structure within the southern African subcontinent). The sampling sites for this study - Rensburgdrif Farm, Kopjeskraal Farm, and Rietkuil Farm - are also referred. Modified after Reimold *et* al. (2017).

The Vredefort Dome is a prominent, ~90 km wide structural and topographic feature that presents excellent exposures for the investigation of deep levels of such a large central uplift feature (e.g., Gibson and Reimold, 2008; Gibson, 2019). Notably, the rocks of the actual central part of the dome structure have been exhumed to the current erosion level by up to 20-25 km from originally mid-crustal level.

The Vredefort impact structure involves the Vredefort Dome (central uplift, Fig. 1) and the surrounding Witwatersrand basin (ring basin). The core region of the dome is largely composed of an Archean Gneiss Complex subdivided into an inner zone of granulite-facies, historically known as Inlandsee Leucogranofels (ILG), and an outer, amphibolite-facies annulus of the so-called Outer Granite Gneiss (OGG). The collar around the core comprises up- and overturned supracrustal strata composed of a succession of locally occurring Dominion Group metalava, followed by the sequences of the Witwatersrand (metapelites and arenites), Ventersdorp (meta-lava) and Transvaal (carbonate plus arenite) supergroups. The collar strata were intruded by numerous sills of dioritic composition, known as epidiorite due to their metamorphic overprint (e.g., Reimold and Koeberl, 2014).

The impact melt rock of the VIS is known as the Vredefort Granophyre. The formation and emplacement of this lithology has been debated for nearly 100 years of research. Vredefort Granophyre (inter alia, Gibson and Reimold, 2008; Reimold et al., 1990, 2006; Therriault et al., 1996, 1997; Lieger, 2011; Wannek, 2015; Reimold et al., 2017 and references therein; Huber et al., 2020) occurs in a suite of 9 dikes of kilometer length and up to > 50 m width (compare Fig. 1). The melt rock has a granophyric (micropegmatitic) groundmass texture, from which the name derives. It contains clasts that in their majority are derived from granitoid of the Archean gneiss complex, with lesser contributions of quartzite and metapelite derived from Witwatersrand strata (see section on Regional Geology, below). In the past, mafic inclusions were observed only where a Granophyre dike cuts across an occurrence of epidiorite (metamorphosed diorite) within or near the inner collar of the dome (e.g., Therriault et al., 1996, 1997). Geochemically, the Granophyre was long considered to be of regionally homogeneous, chemically unique, felsic composition (e.g., Reimold and Gibson, 2006). Several past analyses of a mafic character were explained for a long time by local assimilation of mafic country rock (e.g., Reimold and Gibson, 2006; Gibson and Reimold, 2008 and references therein; Reimold et al., 2016, 2017, 2021).

### 1.3. The current Granophyre controversy

Granophyre dikes were emplaced after the crater modification stage (Gibson and Reimold, 2008). Structural similarity of granophyre dikes, notably their radial and concentric geometry with respect to the crater centre, with Offset Dikes at Sudbury suggested to some that they were emplaced by the same mechanism (Huber 2020; Huber et al., 2022). Correlation of melt temperature estimates of Offset Dikes with modelled cooling rates of the impact melt sheet at Sudbury suggests that Offset Dikes were emplaced up to ten thousand years after impact (Hecht et al., 2008). An impact melt origin of the Granophyre dikes is supported by the presence of shock metamorphosed clasts (Buchanan and Reimold, 2002), and by a Re–Os isotope study that indicated that Granophyre dikes have considerably higher Os contents than the country rocks considered likely impact target components, and significantly different Re–Os isotopic compositions than the essential target rocks (Koeberl et al., 1996). They observed a significant though small, up to only 0.2 %, chondritic component. Proposed mechanisms of dike formation discussed in the past are the injection of mafic

magma (Bisschoff, 1972; Nicolaysen, 1987) or gravity-controlled seepage of impact melt from the crater “cavity” into fractures through the crater floor (e.g., Dietz, 1961; French et al., 1989; French and Nielsen, 1990; Reimold et al., 1990; Therriault et al., 1996; Gibson and Reimold, 2008).

Almost all hypotheses about the emplacement of Granophyre dikes are based on geochemical and petrographic analysis of the matrix and country rock fragments in the dikes. In particular, the impact melt hypothesis for the origin of the dikes was tested through analyses of possible mixtures of various target rock types (French and Nielsen, 1990; Reimold et al., 1990; Therriault et al., 1997). The results suggested that the melt dikes formed from either impact melting and mixing of a suite of Vredefort target rocks or by assimilation mechanisms (total assimilation of wall rock by a parent magma). Emplacement was achieved in the course of an extensional regime during build-up and collapse of the central uplift structure, by gravitational settling of impact melt into fractures close to the center of the central uplift. (Reimold et al., 1990; Gibson and Reimold, 2008).

There has been uncertainty whether, and to what extent, a mafic melt component, derived in particular from the Ventersdorp metavolcanics that contribute to a voluminous package of the target sequence, contribute to the composition of the Granophyre melt (French and Nielsen, 1990; Reimold et al., 1990, 2017). Components from the Ventersdorp Lava have not been taken into account in some modelling efforts, as Granophyre dikes seemed to be generally devoid of fragments from this lithology (Reimold et al., 1990). Modelling of the Granophyre chemistry suggested that the impact melt rock could have been derived largely from melting of the lower supracrustal succession and upper-crustal granitic basement, as exposed in the dome (Reimold et al., 1990b; Therriault et al., 1997b), rather than from a mantle source or mantle-derived materials, as proposed by earlier workers (diorite or lamprophyre - Bisschoff,1969,1972).

A new stage of Granophyre studies was initiated when Lieger (2011; also, Lieger and Riller, 2012) identified a so-called mafic Granophyre phase on Farm Kopjeskraal, in the NW of the Dome. This phase apparently occurred along the margins of a dike of “normal” felsic Granophyre. They proposed that two successive intrusions of melt from a differentiating impact melt sheet above the Vredefort crater floor had generated a composite Granophyre dike. The idea was taken from the Sudbury Offset

dikes, for which others had proposed a model of multiple intrusions of impact melt phases (e.g., Hecht et al., 2008; see also Huber, 2020 and Huber et al., 2022).

Wannek (2015) recognized that the dike on this property was indeed of composite nature but that the mafic phase along the extension of the dike occurred in fact in the central part of the dike, in contrast to Lieger's (2011) finding. Her detailed mapping along the dike, furthermore, showed that geochemistry allows to generate the mafic melt rock by mixing normal felsic Granophyre with epidiorite that on this farm occurs prominently and extensively in relatively close vicinity to Granophyre (Wannek, 2015; see also Reimold et al., 2021). Thus, a new hypothesis of hybridization of normal felsic Granophyre by partial assimilation of a slab of epidiorite was developed (Wannek, 2015). Further support for this has since come from Rb-Sr, Sm-Nd, Pb-Pb, Re-Os and Se isotope data by Reimold et al. (2017, 2021).

### 1.4. Objectives for the present project.

This project is aimed at continuing the mapping, petrographic and geochemical studies of Wannek (2015) on Farm Kopjeskraal, in the NW sector of the Dome. The same Granophyre dike continues from Farm Kopjeskraal, north of the Vaal River, across Farm Rensburgdrif, south of the river (Fig. 1), all along relatively close to exposed epidiorite and, locally, Dominion Group metalava. Preliminary observations by W.U. Reimold and N. Hauser on Rensburgdrif in 2018 showed that large (up to meter sized) schlieren of medium-grained mafic material occur in the dike in this section. Therefore, it was proposed to produce a map at the scale of 1:10,000 of this study area and conduct detailed petrographic and geochemical, including isotope geochemical, investigations.

This project is aimed at further clarification of the formation of Vredefort Granophyre, by precisely defining the hosting geology and adding to the existing chemical and isotopic database on Felsic and Mafic Granophyre, as well as the Dominion Group metalava and epidiorite mafic country rock varieties.

The main objectives for this work, thus, are:

- Prepare a detailed map of the study area at the 1:10,000 scale.
- Conduct petrography and geochemistry to distinguish texturally and compositionally the phases of the Granophyre and the country rocks.

- Strontium and Sm-Nd isotope analyses will be used to determine possible mixtures between the Granophyre and the mafic country rocks (epidiorite and granite).

All these results, in comparison with the equivalent results by Wannek (2015) for the northeastern part of the dike, will contribute to a better understanding of Vredefort Granophyre genesis.

# 2. CHAPTER: GEOLOGICAL BACKGROUND

## 2.1. Kaapvaal Craton – Archean Basement Complex

The Kaapvaal craton of Southern Africa (Fig. 2) comprises a series of granite-greenstone fragments of 3.6–2.7 Ga (e.g., Schmitz et al., 2004; Anhaeusser, 2014; Gibson, 2019). Tectono-magmatic analysis has led to the recognition of a shield that formed through amalgamation of individual micro-continental blocks between 3.6 and 3.1 Ga, with a culmination in widespread granitoid magmatism at ca. 3.1 Ga (e.g., De Wit et al., 1992; Poujol et al., 2003; Schmitz et al., 2004; Lana et al., 2004; see also Gibson, 2019). The central Kaapvaal craton experienced a major volcanic and intrusive magmatic event at 2.05–2.06 Ga (Bushveld Event, e.g., Buchanan et al., 2004).

The Archean Basement Complex in the core of the Vredefort Dome comprises two terranes that are transitional to each other (Lana et al., 2004). The bulk of the core comprises polydeformed, polymetamorphic, predominantly trondhjemitic, granodioritic and granitic gneisses that contain increasing proportions of meter-to-kilometer-scale mafic, ultramafic, pelitic-greywacke and banded ironstone (BIF) gneiss fragments in the more deeply exhumed central parts (Gibson, 2019).

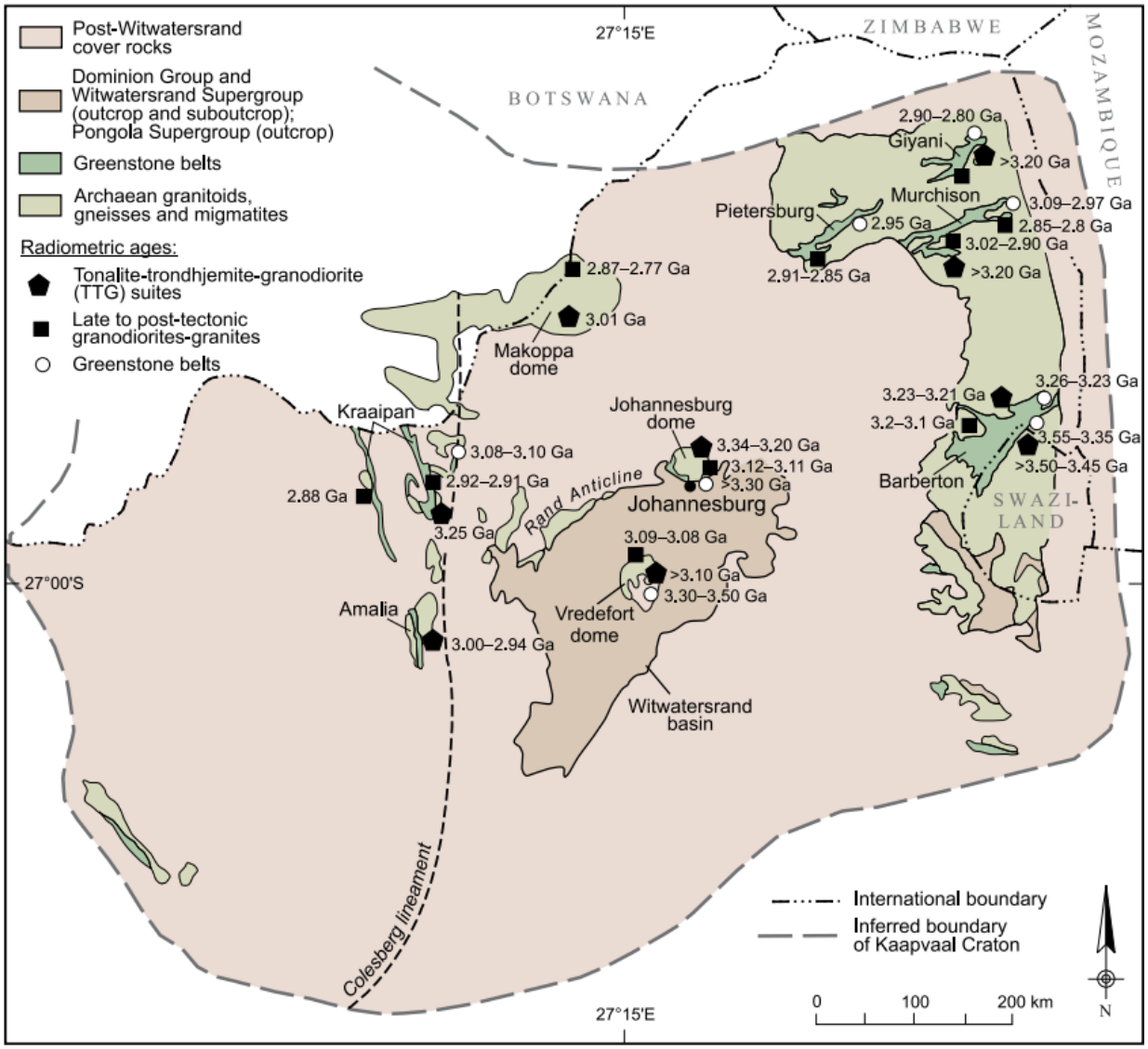


Figure 2 - The Kaapvaal craton with the Vredefort Dome in the geographically central part of the Witwatersrand Basin, as well as the various greenstone belts, e.g., the Barberton Greenstone Belt, recognized on the craton. A summary of radiometric age data was also provided (adapted from Eglington and Armstrong, 2004).

## 2.2. Geology of the Vredefort Dome

The ca. 90 km wide Vredefort Dome represents the deeply eroded central uplift of the Vredefort impact structure (e.g., Gibson and Reimold, 2008). It is located roughly in the center of the erosional remnant of the Witwatersrand basin (Fig. 2). The dome is well exposed in its northern and western sectors (e.g., Lana *et al*., 2003) but covered by Phanerozoic strata of the Karoo Supergroup in the eastern and southern parts. The Vredefort Dome comprises an approximately 40-km-wide core that exposes crystalline rocks of the Archean Basement Complex, and a 20–25 km-wide collar of younger (ca. 3.07 to 2.10 Ga) metamorphosed sedimentary and volcanic rocks of the

Dominion Group and the Witwatersrand, Ventersdorp and Transvaal supergroups. Both the core and collar rocks contain mafic intrusions that have been attributed to the 2.71 Ga Ventersdorp, 2.06 Ga Bushveld, and 1.1 Ga Kibaran-Umkondo events, repectively (Pybus, 1995; Reimold et al., 2000). Additionally, several small ultramafic to peralkaline granite intrusions occur in the collar (Fig. 1) that have also been correlated with the Bushveld event (Gibson, 2019, and references therein).

The presence of impact-diagnostic features, such as shatter cones, high-pressure quartz polymorphs, and decorated planar deformation features in quartz (Dietz, 1964; Hargraves, 1961; Carter, 1968, French, 1972), and planar fractures, twinning, and occurrence of reidite in zircon (Kamo et al., 1996; Kovaleva et al., 2018), in rocks of the dome leaves no doubt that the dome is the eroded remnant of a giant impact structure (see reviews by Grieve and Therriault 2000; Gibson and Reimold 2008). Shatter cones occur up to 60 km from the center of the Dome (Wieland et al., 2006), and the central part of the northern Witwatersrand Basin also contains extensive occurrences of pseudotachylitic breccias that have been attributed to the Vredefort impact event as well (e.g., Fletcher and Reimold, 1989; Killick and Reimold, 1990; Reimold et al., 2016). Widespread hydrothermal activity has affected the gold-bearing strata of the Witwatersrand Basin. This activity has also been linked with the impact event (e.g., Reimold et al., 2005; Hayworth et al., 2005).

### 2.2.1. The Archean basement core

The Archean Basement of the Vredefort Dome is dominated by predominantly trondhjemitic and granitic/granodioritic gneisses, granodiorites, and granites; tonalitic gneisses are relatively rare and appear to be confined to the innermost granulite zone (Fig. 3), with subsidiary mafic, ultramafic, meta-pelitic, and meta-ironstone xenoliths, possibly as old as 3.4–3.5 Ga (Hart et al., 1981; Lana et al., 2004; Armstrong et al., 2006; Gibson and Reimold, 2008; Gibson, 2019).

This gneiss terrane was originally divided into an inner zone, known traditionally as the Inlandsee Leucogranofels (ILG) terrane, of granulite metamorphic grade and an outer annulus known as the Outer Granite Gneiss (OGC) in amphibolite grade (e.g., Stepto, 1990; Bisschoff, 1999). However, subsequent mapping (Fig. 3; Lana, 2004; Lana *et al*., 2003b, c; see also Gibson, 2019 for a review) showed that a similar, diverse sequence of trondhjemitic-tonalitic-granodioritic lithologies with rather homogeneous

structural styles occurs throughout the entire core, although metamorphic grade varies with radial distance from the center of the structure.

The central and southeastern portions of the dome are covered by a thin veneer of Phanerozoic Karoo Supergroup shales and dolerite sills, with only a small, poorly exposed inlier of basement in the southeats, formed by the Archean Greenlands Formation (Minnitt et al., 1994), Gibson, 2019) that has been tentatively assigned an age of 3.4 Ga or possibly older (Gibson and Reimold, 2008). In contrast, the wider basement is well exposed in the northeastern to southwestern sectors of the core.

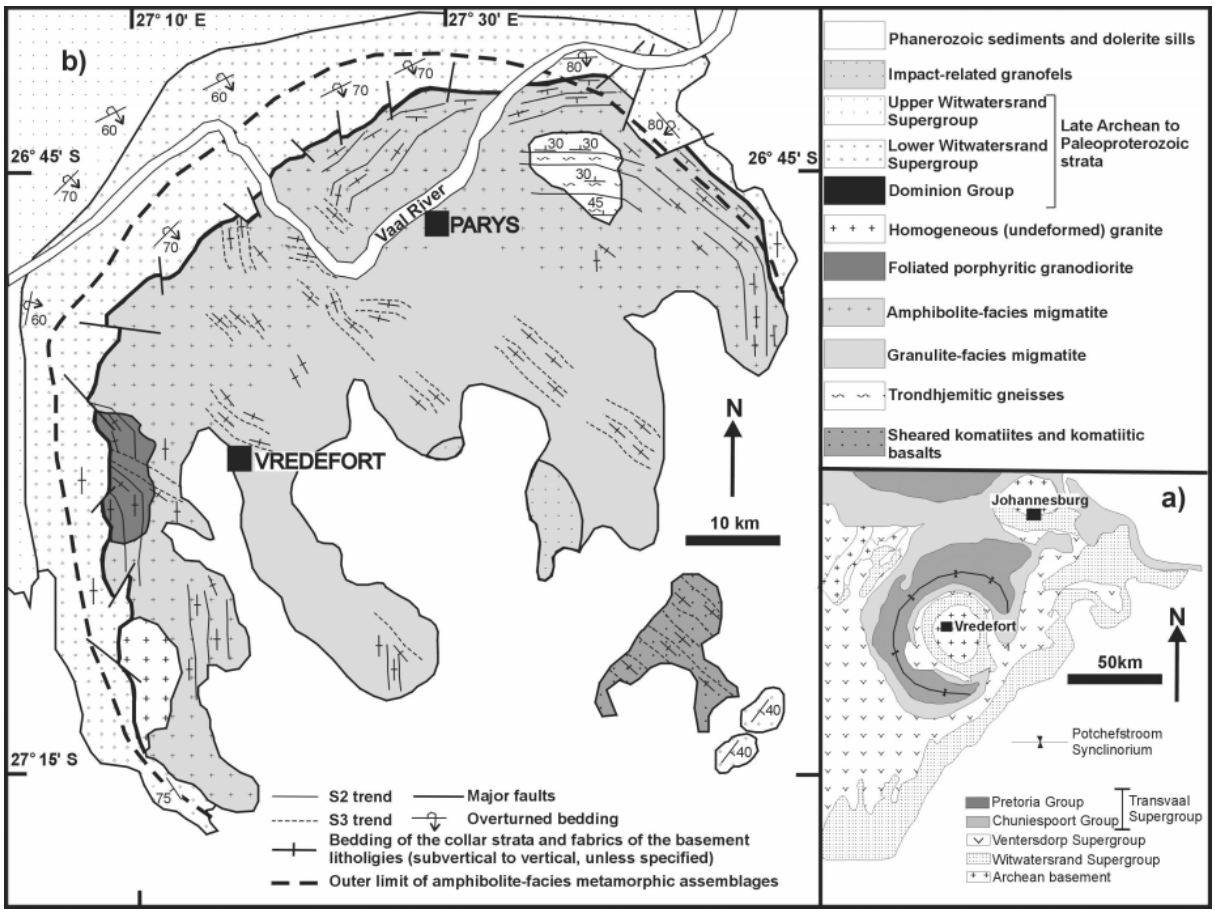


Figure 3 - a) Simplified geological map showing the distribution of Archean and Paleoproterozoic rocks in the Witwatersrand basin and the axis of the collar of the Vredefort Dome. b) Simplified geological map of the Vredefort dome showing the main lithologies and structures in the collar and core of the dome, and the eccentric distribution of the pre-impact amphibolite facies metamorphic isograd (after Lana *et al.,* 2003). Note that prominent structural trends are continuous across the entire crystalline core of the dome.

### 2.2.2. Collar lithologies

The collar rocks along a traverse outward from the contact with the Archean Basement comprise metalava of the Dominion Group, which was sequentially covered by quartzite, conglomerate, siltstone, shale and ironstone of the Witwatersrand Supergroup, bimodal lavas of the Ventersdorp Supergroup, and carbonate plus arenite of the Transvaal Supergroup (e.g., Gibson and Reimold, 2008; compare stratigraphic profile, Fig. 4). The collar strata were intruded by numerous sills of dioritic composition, known as epidiorite due to their metamorphic overprint (e.g., Pybus, 1995). They are interpreted as hypabyssal parts of feeder dikes for the 2.71 Ga Ventersdorp volcanism (ibid).

The collar rocks were also intruded by several alkali granitic and basic igneous bodies (the Schurwedraai, Baviaanskrans, Roodekraal, Rietfontein, and Lindequesdrift bodies). These complexes show Vredefort impact-related shatter coning and pseudotachylitic breccia development and, thus, must predate the impact event. Various ages between 2.2 and 2.05 Ga have been obtained for these rocks, with most works suggesting a syn-Bushveld age (e.g., Walraven and Elsenbroek, 1991; Gibson, 2019). The mafic intrusive Losberg Complex occurs in the collar and is geochronologically and geochemically linked to the Bushveld event (Coetzee and Kruger, 1994). The general stratigraphy for the Witwatersrand Basin region is illustrated in Figure 4.

## 2.3. Dominion Group

The Dominion Group is a volcano-sedimentary sequence of 3.07 Ga age, which is stratigraphically positioned directly above the Archean Basement and below the Witwatersrand Supergroup (Gibson, 2019). The Dominion Group is reasonably well exposed in the collar of the Vredefort Dome (Jackson, 1992, 1994). According to Nel (1927), the maximum thickness of the Dominion Group in the area is about 250 m. The pile of supracrustal sedimentary and volcanic strata was deposited associated with a series of rifting and basin-forming events. The Dominion Group was formed during a rifting stage that generated a bimodal sequence of felsic and basaltic andesite lavas with subsidiary rift-related clastic sediments (e.g., Jackson, 1994), now metamorphosed to mid-amphibolite grade (Gibson and Wallmach, 1995; Gibson, 2019).

## 2.4. Witwatersrand Supergroup

Between ca. 2.97 and 2.71 Ga (Robb and Robb,1998), up to 7 km of clastic sediments, with minor banded ironstones, were deposited and formed the Witwatersrand Supergroup. According to, for example, Gibson and Reimold (2008), the basal West Rand Group comprises predominantly shallow-marine to subtidal argillaceous-arenaceous sediments, whereas the overlying Central Rand Group is dominated by relatively coarser-grained fluviatile to subtidal arenaceous-rudaceous sediments (see also McCarthy et al., 2006). The Witwatersrand Supergroup hosts the world´s largest gold and uranium deposits and about 50 % of all gold ever mined on this planet has been produced from these deposits (Tucker et al., 2016). Gold mineralization occurs mostly in the conglomerates of the Central Rand Group (e.g., McCarthy et al., 2006). Significant debate has been carried out over the past decades regarding the origin of the gold and uranium mineralization – essentially between two opposing schools favoring either a purely hydrothermal process to have introduced gold-bearing solutions into the basin after deposition of the clastic sediment (Phillips and Powell, 2011), or the formation of detrital placer deposits that were later overprinted by epi- to hydrothermal solutions (Hayward et al., 2005; Reimold et al., 2005). These authors made a strong case that this authigenic gold mineralization originated from local solutions liberated throughout the basin as a direct consequence of the Vredefort impact (see also Gibson and Reimold, 2008).

## 2.5. Ventersdorp Supergroup

The Ventersdorp Supergroup represents a late Archean volcano-sedimentary supracrustal record on the Kaapvaal Craton. The Ventersdorp Supergroup is subdivided into the lower Klipriviersberg Group, the middle Platberg Group, and the upper Pniel Sequence, as indicated schematically in Figure 5 (Van der Westhuizen et al., 2006 and references therein).

Witwatersrand sedimentation was terminated by the extrusion of up to 3 km of tholeiitic flood basalts of the Klipriviersberg Group, followed by deposition of up to 2 km of localized rift sediments and felsic volcanics (Platberg Group) dated to 2.71 Ga (Armstrong et al., 1991).

## 2.6. Transvaal Supergroup

The Transvaal Supergroup is subdivided into the chemical sedimentary lithologies of the Chuniespoort Group in the lower and the predominantly clastic Pretoria Group in the upper part of the succession. The lowermost Pretoria Group is represented by the Duitschland/Rooihoogte and Timeball Hill formations, which are developed on the Chuniespoort Group carbonates and banded iron formation with a marked unconformity (Eriksson *et al*., 2006; Schröder *et al*., 2016). The Kaapvaal craton experienced widespread intrusion of ultramafic and mafic magmas at 2.06 Ga to produce the Bushveld Complex in the upper Transvaal Supergroup (Cawthorn *et al*., 2006).

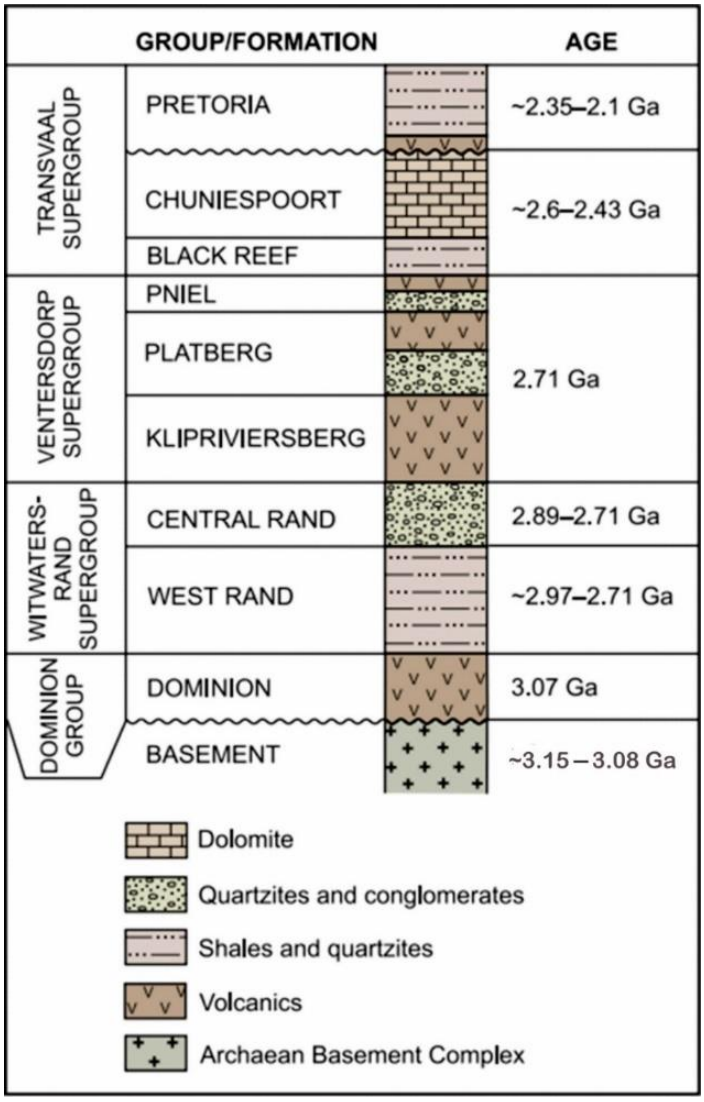


Figure 4 – Schematic stratigraphic column for the region of the Witwatersrand Basin after Gibson and Reimold (2008). Ages have been updated according to Gibson (2019).

## 2.7. Metamorphism in the Vredefort Dome

The Vredefort Dome exposes rocks that range in metamorphic grade from greenschist to granulite facies (ig. 5; see also e.g., Bisschoff, 1982; Gibson and Stevens, 1998; Gibson and Reimold, 2005; Gibson, 2019). The rocks in the dome are also variably affected by impact (shock) metamorphism. The impact induced thermal metamorphic overprint increases in grade radially inward from ~300 °C in the collar rocks to >1000 °C in the center of the dome (Gibson et al., 1998; Gibson, 2002; Gibson and Reimold, 2005; Ogilvie, 2010; Gibson, 2019).

The sedimentary strata of the Witwatersrand Supergroup and the Ventersdorp-age sills (epidiorite) were metamorphosed before the impact event (Bisschoff, 1982; Gibson and Wallmach, 1995), with the maximum grade of metamorphism increasing with stratigraphic depth from lower greenschist facies (~350 °C) in the Central Rand Group to mid-amphibolite facies (~600 °C) in the lower West Rand Group (Fig. 5; Gibson and Wallmach, 1995). Pressure-temperature constraints and geochronological data suggest that this metamorphism accompanied the 2.06 Ga Bushveld magmatism that also appears to be linked to the formation of the alkali granitic and mafic-ultramafic complexes of the dome (Gibson and Wallmach, 1995; Moser and Hart, 1996; Gibson et al., 2000).

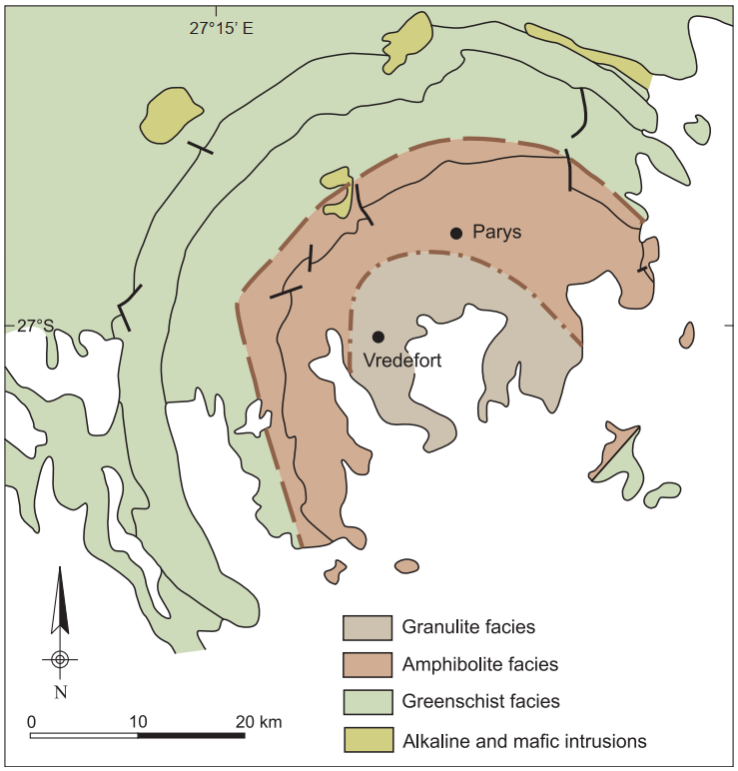


Figure 5 - Distribution of pre-impact metamorphic grades in the Vredefort Dome (from Gibson and Reimold, 2008). For stratigraphy, compare with Fig. 4.

# 3. CHAPTER: METHODOLOGY

## 3.1. Bibliographical research

This stage was characterized by a careful, strict, and extensive review of the literature related to impact cratering, the Vredefort Impact Structure, and the Granophyre, including the controversy about its origin. Scientific papers, maps, M.Sc./Ph.D. theses, and conference abstracts that address the study area and the research theme were selected.

## 3.2. Field work

Field work in the study area of the Vredefort Dome (Fig. 1) was realized during two weeks in July 2019, when detailed observations at 120 outcrop points, on the farms Rensburgdrif and Rietkuil (Fig. 1) were made. The Granophyre and country rocks on Farm Kopjeskraal were also inspected. Twenty-six samples were collected, of which 14 are from a profile across the Granophyre dike. The sampling locations are indicated in Fig. 8 (Chapter 4). The field work was aided by previous geological maps, as well as satellite imagery (Landsat 8, GoogleEarth). A geological map of the study area at the scale of 1:10,000 resulted from this work.

## 3.3. Petrography

Samples of the Granophyre (mafic and felsic) and country rocks (epidiorite and Dominion Group metalava) were selected for micropetrographic analysis. Twenty-six polished thin sections were made at the Lamination Laboratory of the Institute of Geosciences of the University of Brasília. The thin sections were studied with an Olympus polarizing microscope to investigate Granophyre matrix, country rock mineralogy and textures, and to study lithic clasts in Granophyre samples for provenance and shock deformation. The petrographic descriptions assisted in the further selection of samples for geochemical and isotopic analysis.

## 3.4. Electron probe microanalysis (EPMA)

Three samples (one each of Mafic Granophyre, Felsic Granophyre, and epidiorite) were selected for electron probe microanalysis of the main constituent minerals - plagioclase, pyroxene, and amphibole. These analyses were performed at the Naturhistorisches Museum Wien using a field-emission electron microprobe

analyzer (FE-EMPA) JEOL JXA 8530-F, equipped with five wavelength-dispersive spectrometers (WDS) and two energy-dispersive spectrometers (EDS). Operative conditions were 15 kV acceleration voltage, 20 nA beam current, and a fully focused beam. For quantification, a ZAF correction was applied. Natural and synthetic (non-commercial) reference minerals were used for calibration. Detection limits for major elements are: 136 ppm for Na, 115 ppm for Mg, 124 ppm for Al, 151 ppm for Si, 83 ppm for K, 169 ppm for Ca, 261 ppm for Mn, 297ppm for Ti, and 294 ppm for Fe.

### 3.5. Major and trace element geochemistry

Quantitative data for both major and trace element concentrations were acquired from sample powders at the Laboratoire G-Time of the Université Libre de Bruxelles (ULB), using inductively coupled plasma optical emission spectrometry (ICP-OES) and mass spectrometry (ICP-MS).

A total of 26 samples were crushed and pulverized using tungsten ware at the Geochronology Laboratory of the Institute of Geosciences, University of Brasília. Around 50 mg of powdered samples were accurately weighed ($\pm$ 0.1 mg) and mixed with ~1 g of a 4:1 ultrapure lithium metaborate ($Li_2O$) -tetraborate ($Li_2B_4O_7$) mixture by hand shaking. The mixtures were fused in graphite crucibles in a muffle furnace at 1000 °C for 10 minutes. After cooling down, the resulting beads were dissolved in 50 ml of 2N $HNO_3$ using stirring magnets for 5 hours. Twenty-four of these samples were analyzed in Brussels.

Following aliquoting, appropriate dilution, and addition of Y as internal standard, all major element concentrations were determined by quantification versus external calibration curves constructed using multi-element standard solutions of Si, Mg, Fe, Al, Ca, Na, Ti, K, P, Mn, and Cr on the Thermo Scientific iCAP 7000 Series ICP-OES at the ULB. Trace element concentrations were determined in a similar way on the same sample solutions using an Agilent Technologies 7700 Series ICP-MS at the ULB, after aliquoting, adequate dilution, and addition of Indium as internal standard. Oxide production was evaluated and corrected using standard element solutions of Pr and Nd, as well as Ba and Ce. Besides samples and replicates, international reference basalt BHVO-2 and andesite AGV-2 of the U.S. Geological Survey with certified chemical compositions were used to evaluate the accuracy and precision of the applied procedures. Based on the measurement of BHVO-2 replicates, the external

reproducibility expressed as relative standard deviation (RSD) is better than 5 % for most major and trace elements, except for K, Rb and Lu, for which they are better than 10 %, 7 %, and 10 %, respectively. Loss on ignition (LOI) was determined by weighing 0.5 g (± 0.1 mg) of sample into a ceramic crucible that was heated to 1000 °C in a muffle furnace for 1 hour. After cooling down to room temperature, the samples were weighed again to determine the weight percent (wt%) of lost volatiles. Major element and trace element compositions are presented in Table 1 (chapter 4).

Several additional samples (such as the NWU samples) were analyzed commercially by ICP-MS at SGS Geosol, Vespasiano, MG, Brazil (www.sgsgeosol.com.br), using their method ICP95A. Based on the information received from them, it is estimated that the accuracies for all major elements (concentration range as applicable to our samples) are of the order of 10 %. For trace element analysis, especially the Rare Earth Elements, the certified reference materials GRE-03 and GRE-05 were used, and accuracy at 95 % confidence level is quoted at the following levels (in % of the analytical value): Ce ± 2, Dy ± 4, Eu ± 2, Ga ± 4, Gd ± 3.6, Ho ± 0.3, La ± 36, Lu ± 0.1, Nb ± 44, Nd ± 33, Pr ± 9, Sm ± 5, Ta ± 9, Hf ± 7, Tb ± 0.5, Tm ± 0.1, Y ± 6, Yb ± 0.25, Zr ± 47, Sc ± 0.5, Ti ± 0.1 , Th ± 2.4, U ± 1, W ± 0.5. Three samples from the SGS Geosol sample batch were analyzed in duplicate, with generally excellent precision (values for major elements in wt%, trace elements in ppm, maximum deviations reported): $SiO_2$ 0.2, $TiO_2$ 0.3, $Al_2O_3$ 0.6, $Fe_2O_3$ 0.2, MnO 0.05, MgO 0.04, CaO 0.02, $K_2O$ 0.08, $Na_2O$ 0.01, $P_2O_5$ 0, LOI 0.04; V 12, Co 3, Ni 9, Cu 9, Zn 11, Ga 1.3, Rb 2.8, Sr 2, Y 1, Zr 19, Nb 1.3, Sn 0.2, Cs 0.23, Ba 67 (note, the other two values are 2 and 4, respectively), La 1.5, Ce 4.7, Pr 0.23, Nd 1.2, Sm 0.3, Eu 0.2, Gd 0.47, Tb 0.05, Dy 0.19, Ho 0.45, Er 0.06, Tm 0.01, Yb 0.1, Lu 0.02, Hf 0.61, Ta 0.11, W 1.3, 0.3, U 0.18. Considering that nugget effects may well have played a role with respect to several elements such as Zr, these precision data appear fully acceptable.

Regarding the major element abundances in duplicate analyses, reasonable coincidence was found within the 10 % limits advised by SGS – in fact, in many instances, the differences were much lower. For trace elements, numerous cases of exact coincidence of values were found, with considerable deviations noted primarily for Sr, Zr, and Ba, where especially elevated values may be affected by deviations of up to 5 %. In conclusion, our confidence in the commercially obtained

data is high. Where caution is advised for samples when major element totals do not add up to approximately 100 wt%.

### 3.6. Sr and Sm - Nd Isotopes

**Sm-Nd isotope analyses**

*Analyses at the Laboratory of Geochronology at UnB*

The Sm-Nd isotope analysis in the Laboratory of Geochronology of the University of Brasilia followed the method described by Gioia and Pimentel (2000). The rocks were pulverized, aliquots mixed with a mixed tracer solution (spike) enriched in $^{149}Sm$-$^{150}Nd$, prior to dissolution in Savillex capsules. The Sm and Nd fractions were loaded onto double evaporation filaments after Teflon powder and were extracted on Teflon columns containing LN-Spec resin (liquid resin HDEHP - di-Ethylhexyl phosphoric acid impregnated with Teflon powder).

The isotopic measurements of 14 samples were performed on a Thermo Scientific TRITON™ Plus Thermal Ionization Mass Spectrometry (TIMS) in static mode. Mass fractionation was corrected by normalizing the $^{143}Nd/^{144}Nd$ ratio to $^{146}Nd/^{144}Nd$=0.7219 and the $^{87}Sr/^{86}Sr$ ratio to 8.3752. The radioactive decay constant used for Sm-Nd was 6.54x10-12 a-1 (Lugmair and Marti, 1978). Samples AR-53 and AR-54 could not be analysed completely for technical reasons.

Four other samples (Arp38A, Arp 38G, Arp 38I, and Arp 38L) that could not be analyzed on TIMS were analyzed in solution in a Thermo-Fisher Neptune HR-MC-ICP-MS instrument at the same laboratory. The samples were introduced in the spectrometer using a nebulizer with a flux of 100uL/min. For Sm the tuned masses were $^{146}Nd$, $^{147}Sm$, $^{148}Sm$, $^{149}Sm$, $^{150}Sm$, $^{152}Sm$ and $^{154}Sm$. Five blocks of 10 cycles each with an integration time of 4.194 second was considered for each analysis. Normalization of the $^{147}Sm/^{152}Sm$ ratio was done after the laboratory factor 0.556083. For Nd the tuned masses were $^{142}Nd$, $^{143}Nd$, $^{144}Nd$, $^{145}Nd$, $^{146}Nd$, $^{147}Sm$, $^{148}Nd$ and $^{150}Nd$. Seven blocks of 10 cycles each with an integration time of 4.194 second was considered for each analysis. The $^{143}Nd/^{144}Nd$ proportions were normalized to $^{146}Nd/^{144}Nd$ = 0.7219; the decomposition constant was 6.54 × 10-12. The average $^{143}Nd/^{144}Nd$ obtained for the USGS BHVO-2 standard was 0.512970± 0.000002 (2SD) during the course of this study, which is consistent with the most recently published

values (e.g., 0.512986 ± 0.000009, Weis et al., 2005). Laboratory blanks were ~0.25 ng for Nd and ~0.04 ng for Sm. The uncertainties in Sm/Nd and $^{143}Nd/^{144}Nd$ ratios were better than ±0.5% (2 σ) and ±0.005% (2 σ), respectively, based on repeated analysis of the international BHVO-2 and BCR-1 rock standards. The measured $^{143}Nd/^{144}Nd$ sample ratios are expressed in Epsilon Neodymium notation ($\varepsilon_{Nd}$) as the fractional deviation in part per $10^4$ (units) from $^{143}Nd/^{144}Nd$ value of the Chondritic Uniform Reservoir (CHUR). Neodynium blanks were < 100 pg. The results were processed using the ISOPLOT/EX 4.15 software (Ludwig, 2008), and the TDM values were calculated based on the model by DePaolo (1981).

*Analyses at the University of Cologne*

Five samples (AR-53 and AR-54, ARp 38G, ARp 38I and ARp 38L) were analysed on a Thermo Fischer Neptune© MC-ICP MS at the Institut für Geologie und Mineralogie at Universität zu Köln (Cologne). Prior to sample digestion $^{87}Rb$–$^{84}Sr$, $^{149}Sm$–$^{150}Nd$ mixed isotope tracers were added to measure isotope composition, and the element abundances on the same aliquot (see Weyer et al. 2002). Subsequently, the samples were digested using the high-pressure acid digestion procedure for felsic samples as described in Hoffmann et al. (2011). In a first step, the samples were digested in 6 ml 14 M HNO 3/24 M HF (1:1) for 24 h on a hotplate at 120 °C. Subsequently, the sample solutions were dried down and re-digested in a (1:1) 14 M HNO3/24 M HF mixture at 180 °C using Parr pressure vessels for 2–3 days. Following this, 1 ml of 65% perchloric acid was added and dried down. To remove all residual organic matter and stabilise HFSE, additional 2 ml of 14 M HNO 3/trace HF were added and evaporated afterwards. To achieve sample-tracer equilibrium, all samples were taken up in 6 ml of 6 M HCl/0.06 M HF and the clear solutions were dried down after 1 day. Using the exponential law, measured ratios of $^{87}Sr/^{86}Sr$ and $^{87}Rb/^{85}Rb$ were normalised to 86Sr/88Sr = 0.1194 (Nebel et al. 2005), respectively, and Sr isotope results are given relative to a $^{87}Sr/^{86}Sr$ of 0.710240 for NBS 987. Rubidium was measured relative to NBS 984 ($^{87}Rb/^{85}Rb$ = 0.38554). Measured Nd isotope ratios were normalised to $^{146}Nd/^{144}Nd$ = 0.7219 using the exponential law and results are given relative to a $^{143}Nd/^{144}Nd$ of La Jolla of 0.511859. Total procedural blanks were, <39 pg for Nd, and <19 pg for Sm.

### *Sr isotope Analyses*

*Analyses at the Laboratory of Geochronology at UnB*

After sample digestion, an aliquot of sample solution was directly loaded onto Teflon® columns containing approximately 83 mg of Eichrom® Sr-Spec resin (50-100 µm) to separate the Sr fraction from the matrix. Rubidium concentration was not determined during this work. Strontium isotopic composition of selected samples was determined using a Thermo Scientific TRITON™ Plus Thermal Ionization Mass Spectrometer (TIMS) operating in the multidynamic mode. The average $^{87}Sr/^{86}Sr$ obtained for the NBS-987 standard was 0.71029 ± 0.00001 and 0.71028 ± 0.00002 (2SD) during the course of this study. This value agrees well, within the analytical error, with the most typically recommended value of 0.71025 (Thirlwall, 1991; Faure, 2001; Machado, 2013).

**4. CHAPTER:** Article to be submitted to Meteoritics and Planetary Science or Geochimica et Cosmochimica Acta.

# GENESIS OF THE MAFIC GRANOPHYRE AT VREDEFORT, SOUTH AFRICA: FIELD STUDY, PETROGRAPHY, AND GEOCHEMISTRY FOR THE IMPACT MELT ROCK DIKE ON FARM RENSBURGDRIF.

A. R. MACIEL[1], W. U. REIMOLD[1*], N. HAUSER[1], S. GODERIS[2], L. PITTARELLO[3], W. WEGNER[3], and M. FISCHER-GOEDDE[4], C. KOEBERL[5], C. S. M. SOUZA[1]

[1]Universidade de Brasília, Instituto de Geociências, Campus Darcy Ribeiro, 70297-400, Brasília, Brasil
[2]Vrije Universiteit Brussel, Research Unit: Analytical, Environmental, and Geo-Chemistry (AMGC)
[3]Naturhistorisches Museum Wien, Burgring 7, 1010 Wien, Austria
[4]Institut für Geologie und Mineralogie, Universität zu Köln, Zülpicher Str. 49a, D-50674 Köln, Gebäude 310a, Germany
[5]Department of Lithospheric Research, Althanstraße 14 (UZA II), 1090 Wien, University of Vienna, Austria
*Corresponding author: wolf.uwer@gmail.com

## ABSTRACT

The formation of the impact melt rock, the so-called Vredefort Granophyre, in the Vredefort Dome, the central uplift of the Vredefort impact structure in South Africa, has been debated for decades. Renewed debate was caused by the discovery that besides the previously known felsic variety of >66 wt% $SiO_2$, a second, more mafic phase occurs within a dike on Farm Kopjeskraal in the northwest sector of the Vredefort Dome. This so-called Mafic Granophyre, previously only observed at this locality, has been variably considered a second-stage injection into felsic impact melt seapage, both varieties derived from the melt sheet of the crater interior, or the product of admixture of a mafic country rock, the so-called epidiorite presumably related to the 2.7 Ga Ventersdorp Supergroup rifting-related metavolcanics, or the Dominion Group metalava, to Felsic Granophyre. It was suggested, however, that Mafic Granophyre may also occur in the southernly extension of this dike on farm Rensburgdrif. Here, new major and trace element data, as well as Sr and Sm-Nd isotopic systematics are reported for samples of both the mafic and felsic melt rock varieties from the same Granophyre dike but from Farm Rensburgdrif. That this mafic phase only occurs in the NW dike of impact melt rock on the Vredefort Dome could be evidence for this assimilation having occurred only locally at the core/collar boundary within the central uplift, as a result of stoping in of Granophyre impact melt into extensional fractures during the collapse phase of the central uplift. The analyses indicated the presence of two distinct phases, whereby the mafic (clast-poor) phase was observed in the central part of the dike and the (felsic) clast-rich phase at the margins. Geochemical data indicate that the Mafic Granophyre composition is a mixture between the felsic phase and mafic host rock. The isotope data for Dominion Group metabasalt fall far off the Granophyre and epidiorite data array, which supports that DGL may not have been a precursor for the Mafic Granophyre phase and, apparently, did not play a significant role in the formation of Vredefort Granophyre. In this way, our results strongly mitigate against the hypothesis that Mafic Granophyre represents a differentiation from the original impact melt body and favor the epidiorite assimilation/admixture hypothesis for the formation of Mafic Granophyre.

**Keywords: VREDEFORT IMPACT STRUCTURE, IMPACT MELT ROCK, VREDEFORT GRANOPHYRE, MAFIC GRANOPHYRE, EPIDIORITE.**

## 1. INTRODUCTION

The Vredefort impact structure (VIS), in north-central South Africa, is centered roughly 130 km southwest of Johannesburg, within Archean and Paleoproterozoic rocks of the central Kaapvaal craton. The VIS is the largest known

impact structure on Earth with an estimated original size of 250-300 km (e.g., Henkel and Reimold 1999; Gibson and Reimold, 2008; Gibson, 2019). It is also one of the oldest impact structures known on Earth with an age of 2.023 ± 4 Ma (Kamo et al., 2016). The Vredefort impact structure involves the Vredefort Dome (Fig. 1) and the surrounding Witwatersrand basin that, respectively, represent the deeply eroded central uplift structure of this large, complex impact structure, and the ring basin around the central uplift (Gibson and Reimold, 2008).

Melt rocks in confirmed or possible impact structures are very important. The possible presence of a meteoritic component mixed into impact melt (e.g., Koeberl, 2014) or the presence of shock metamorphosed clasts (e.g., French and Koeberl, 2010) could be detected. Impact melt rocks may contain clast populations that comprise material derived from all parts of the transient crater cavity, and thus, characteristically include clasts with diagnostic shock metamorphic effects.

The Vredefort Dome contains two types of impact generated melt rocks. The dome is the type locality for *pseudotachylyte/pseudotachylitic breccia* (PTB; Shand, 1916; Reimold, 1998; Reimold et al., 2017). Recent chemical and isotopic work has made a strong case that the massive occurrences of PTB in the Vredefort and Sudbury structures could be the result of melting during rapid decompression of the compressed crust in the center of the impact stucture (e.g., Reimold et al., 2017, and references therein; see also contrasting view by Spray and Biren, 2021).

The second impact-generated melt rock occurring at Vredefort – in fact, the *impact melt rock* of the Vredefort impact structure – is the so-called Vredefort Granophyre. The formation and emplacement of this lithology has long been debated (e.g., Hall and Molengraff 1925; Bisschoff, 1988; Reimold et al. 1990; Therriault et al. 1996; 1997; Reimold et al. 2006; Gibson and Reimold, 2008; Lieger, 2011; Wannek, 2015; Reimold et al. 2017, 2021, and further references therein). The Vredefort Granophyre occurs as a suite of 9 dikes of kilometer length and up to > 50 m width, which occurs along the boundary between the basement core and the supracrustal rocks of the collar of the Vredefort Dome (see below: Geology of the Vredefort Dome). These dikes are the only remnants of impact melt rock at Vredefort, as the structure is deeply eroded by maybe as much as 10 km (Gibson and Reimold, 2008). The melt rock has a granophyric micropegmatitic groundmass texture, from which the name Vredefort Granophyre derives. The clast population is dominated by fragments from

granitoid of the Archean Basement Complex, with lesser contributions of quartzite and metapelite derived from supracrustal Witwatersrand strata (see next section). In the past, comparatively rare mafic inclusions were only observed where a dike cuts across an occurrence of the so-called epidiorite (i.e., metamorphosed diorite) (e.g., Therriault et al., 1996, 1997) related to the Ventersdorp Supergroup. Geochemically, the Granophyre was long considered to be regionally of a homogeneous, chemically unique, felsic composition (with > 66 wt% $SiO_2$, e.g., Reimold and Gibson, 2006). Several previous analyses of mafic character were explained by local assimilation of mafic country rock (e.g., Therriault et al, 1996, 1997; Reimold and Gibson, 2006) only at sites where a Granophyre dike cuts across or close to an epidiorite occurrence.

A new stage of Granophyre study was initiated when Lieger (2011) and Lieger and Riller (2012) discussed a comparatively more mafic Granophyre phase apparently occurring along the margins of a dike of “normal” felsic composition on Farm Kopjeskraal, in the northwestern sector of the Vredefort Dome (Fig. 1). These authors proposed that two successive intrusions of melt from a differentiating impact melt sheet above the Vredefort crater floor had generated a composite felsic/mafic Granophyre dike. The idea was taken from the Offset Dikes of the Sudbury impact structure, which are regarded as produced by multiple intrusions of impact melt (e.g., Hecht et al., 2008 and references therein); also Huber,2020 and Huber et al., 2022).

Wannek (2015) reinvestigated the Granophyre dike on Kopjeskraal and recognized that the mafic phase occurred in the central part of the dike, in direct contrast to Lieger’s (2011) report. Wannek´s work, and the geochemical studies of Reimold et al. (2016, 2017, 2021), provided support for the hypothesis that the mafic impact melt rock could have been generated by admixture/assimilation of an epidiorite component to Felsic Granophyre.

In the present work, we are investigating the extension of this same Granophyre dike onto farms Rensburgdrif and Rietkuil to the south of Kopjeskraal, on the southern side of the Vaal River (Fig. 1). Field analysis, and petrographic and geochemical investigations are showing that the mafic impact melt rock phase is also present in this section of the dike. It is further investigated by new major and trace element, and Sr and Sm-Nd isotopic studies wether the “hybridization” hypothesis (admixture/assimilation of epidiorite to/by Felsic Granophyre) does represent the most likely generation process for the Mafic Granophyre variety. We are applying the

nomenclature of Felsic Granophyre and Mafic Granophyre for impact melt rock samples of more than and less than 66 wt% $SiO_2$, respectively.

## 2. GEOLOGICAL SETTING

The ca. 90 km wide Vredefort Dome (Fig. 1) represents the deeply eroded central uplift of the Vredefort impact structure. It is roughly located in the center of the erosional remnant of the Witwatersrand basin. The 50 km wide Potchefstroom Synclinorium is located along the northern margin of the dome. The dome is well exposed in its northern and western sectors. It comprises a ca. 40-km-wide core that exposes crystalline rocks of the Archean Basement Complex, as well as a 20 – 25 km wide collar of younger (3.07 to ~2.10 Ga) metamorphosed sedimentary and volcanic rocks of the Dominion Group and from the Witwatersrand, Ventersdorp, and Transvaal supergroups. Both core and collar contain mafic intrusions that have been attributed to the 2.71 Ga Ventersdorp, 2.06 Ga Bushveld, and 1.1 Ga Kibaran-Umkondo events (Pybus 1995; Reimold et al. 2000). Additionally, several ultramafic to peralkaline granite intrusions occurring in the collar have been correlated with the Bushveld event (Fig. 1; Reimold and Koeberl 2014; Gibson 2019).

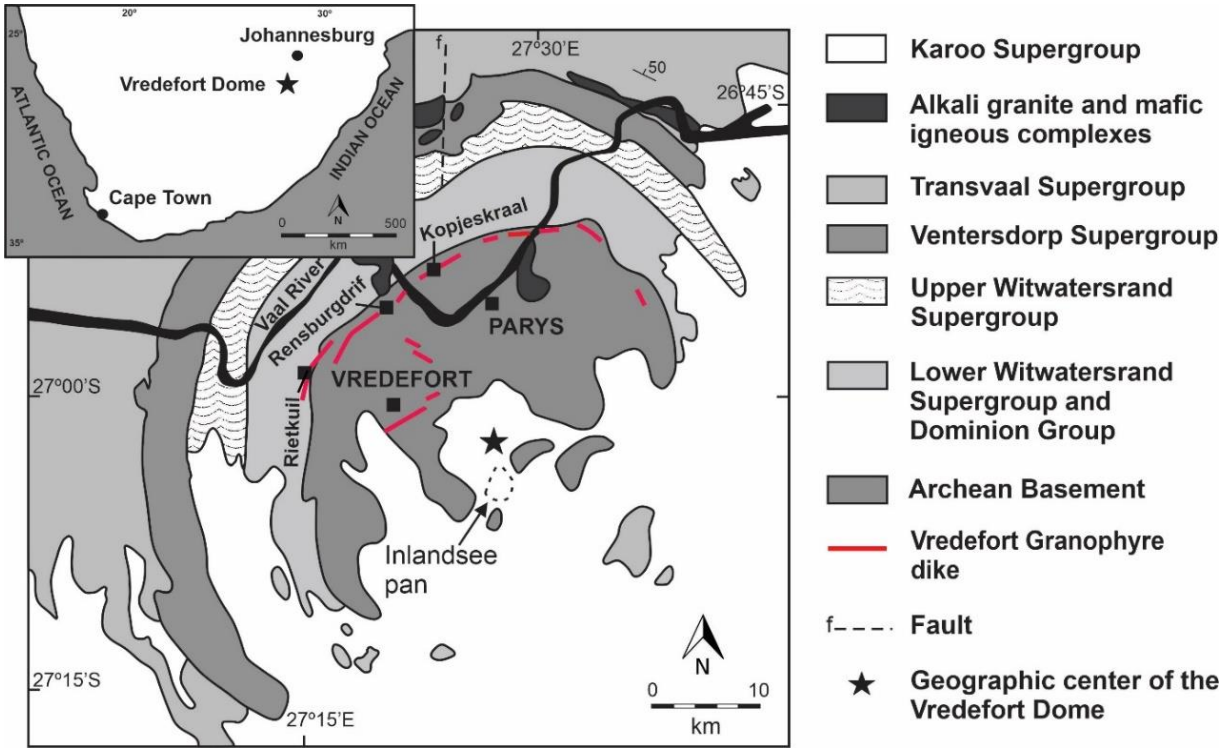


Figure 1 - Schematic geology of the Vredefort Dome (inset shows the location of the Vredefort impact structure within the Southern African subcontinent). The sampling areas for this study - Rensburgdrif, Kopjeskraal, and Rietkuil farms - are also referred. Modified after Reimold et al. (2017).

The presence of impact-diagnostic features, such as shatter cones, high-pressure quartz and zircon polymorphs, decorated planar deformation features in quartz, and unambiguous shock microdeformation in zircon in rocks of the dome leaves no doubt that the dome is the eroded remnant of an impact structure (Reimold and Koeberl 2014; Gibson and Reimold 2008; Kovaleva et al. 2018).

The Archean Basement Complex of the core of the dome is dominated by trondhjemitic and granodioritic to granitic gneisses, granodiorites, and granites. Tonalitic gneisses are relatively rare and appear to be confined to the innermost granulite zone (cf. below) were also subsidiary mafic, ultramafic, metapelitic, and meta-ironstone xenoliths, possibly as old as 3.5–3.4 Ga, occur (Hart et al., 1981; Armstrong et al., 2006; Gibson and Reimold, 2008; Lana et al. 2004; Gibson, 2019). The collar rocks include meta-lavas of the Dominion Group, quartzite, conglomerate, metapelites, and banded iron formation of the Witwatersrand Supergroup, hypabyssal volcanic of the Ventersdorp Supergroup, and carbonate and arenites of the Transvaal Supergroup (Gibson and Reimold 2008). The Dominion Group is a volcano-sedimentary sequence of 3.07 Ga age, which is stratigraphically positioned directly above the Archean Basement and below the Witwatersrand Supergroup (Gibson, 2019). The Dominion Group is reasonably well exposed in the collar of the Vredefort Dome (Jackson, 1992, 1994). The collar strata are intruded by sills of dioritic composition, referred as epidiorite due to their metamorphic overprint (e.g., Pybus 1995). They have been thought to be related to the 2.71 Ga Ventersdorp Supergroup (Pybus 1995; Reimold et al. 2000). There are several peralkaline and mafic intrusive complexes in the collar that have all been related to the Bushveld magmatic event at 2.06 Ga (Walraven 1990). All these strata and complexes predate the impact event and are affected by shock metamorphism and, in many cases, macro- to mesoscopic occurrences of impact-generated pseudotachylitic breccia or shatter cones.

The Vredefort Dome experienced post-impact temperatures that increase from the collar towards the center. They are interpreted to reflect a combination of centripetally increasing shock heating and uplift of progressively deeper crustal levels subsequent to the impact (Ivanov 2005; Gibson 2019). The Dome exposes rocks that range in metamorphic grade from greenschist to granulite facies (Gibson and Reimold 2005). Numerical modelling results (Ivanov 2005) showed that the rocks increase in post-shock temperature overprint radially inward from ~300 °C in the collar rocks to

>1000 °C in the center of the dome, which was shown to be consistent with the petrographic findings of Gibson and Reimold (2005).

# 3. METHODOLOGY

## 3.1 Field work and petrography

The field work was supported by previous geological maps (mainly Bisschoff, 1999) as well as satellite images (Landsat 8; GoogleEarth). A geological map of the study area was produced at the scale of 1:10,000. Samples of Granophyre and country rocks were collected throughout the study area. Twenty-six polished thin sections of the Granophyre varieties and host rocks (epidiorite and Dominion Group meta-lava - DGL) were investigated with an Olympus polarizing microscope. Three samples (one of Mafic Granophyre, Felsic Granophyre, and epidiorite each) were selected for electron probe microanalysis of the main minerals, i.e., plagioclase, pyroxene, and amphibole. These analyses were performed at the Naturhistorisches Museum Wien with a field-emission electron micro-analyzer of the type JEOL JXA 8530-F, equipped with five wavelength-dispersive spectrometers (WDS) and two energy-dispersive spectrometers (EDS). Operating conditions were 15 kV acceleration voltage, 20 nA beam current, and a fully focused electron beam. Detection limits for major elements are: 136 ppm for Na, 115 ppm for Mg, 124 ppm for Al, 151 ppm for Si, 83 ppm for K, 169 ppm for Ca, 261 ppm for Mn, 297ppm for Ti, and 294 ppm for Fe.

## 3.2 Sample processing and major and trace element geochemistry

Quantitative data for both major and trace element concentrations were acquired from sample powders at the Laboratoire G-Time of the Université Libre de Bruxelles (ULB), using inductively coupled plasma optical emission spectrometry (ICP-OES) and mass spectrometry (ICP-MS).

A total of 27 samples were crushed and pulverized using tungsten ware at the Geochronology Laboratory of the Institute of Geosciences of the University of Brasília (UnB). Around 50 mg of powdered samples were accurately weighed ($\pm$ 0.1 mg) and mixed with ~1 g of a 4:1 ultrapure lithium metaborate ($Li_2O$) -tetraborate ($Li_2B_4O_7$) mixture by hand shaking. The mixtures were fused in graphite crucibles in a muffle furnace at 1000 °C for 10 minutes. After cooling down, the resulting glass beads were dissolved in 50 ml of 2N $HNO_3$ using stirring magnets for 5 hours. Twenty-four of these

samples were analysed at Brussels, the remaining three NWU samples were analysed commercially at SGS GEOSOL.

Following aliquoting, appropriate dilution, and addition of Y as internal standard, all major element concentrations were determined by quantification versus external calibration curves constructed using multi-element standard solutions of Si, Mg, Fe, Al, Ca, Na, Ti, K, P, Mn, and Cr on the Thermo Scientific iCAP 7000 Series ICP-OES at the ULB. Trace element concentrations were determined in a similar way on the same digested sample solutions using an Agilent Technologies 7700 Series ICP-MS at the ULB, after aliquoting, adequate dilution, and addition of an In internal standard. Oxide production was evaluated and corrected using standard element solutions of Pr and Nd, as well as of Ba and Ce. Besides samples and replicates, international reference basalt BHVO-2 and andesite AGV-2 of the U.S. Geological Survey with certified chemical compositions were used to evaluate the accuracy and precision of the applied procedures. Based on the measurement of BHVO-2 replicates, the external reproducibility expressed as relative standard deviation (RSD) is better than 5 % for most major and trace elements, except for K, Rb and Lu, for which they are better than 10 %, 7 %, and 10 %, respectively. Loss on ignition (LOI) was determined by weighing 0.5 g (± 0.1 mg) of sample into a ceramic crucible that was heated to 1000 ˚C in a muffle furnace for 1 hour. After cooling down to room temperature, the samples were weighed again to determine the weight percent (wt%) of lost volatiles. Major element compositions are presented in Table 1 and trace element compositions are presented in Table 2.

Several samples were analyzed commercially by ICP-MS at SGS Geosol, Vespasiano, MG, Brazil (www.sgsgeosol.com.br), using their method ICP95A. Based on the information received from them, it is estimated that the accuracies for all major elements (concentration range as applicable to our samples) are of the order of 10 %. For trace element analysis, especially the Rare Earth Elements (REE), the certified reference materials GRE-03 and GRE-05 were used, and accuracy at 95 % confidence level is quoted at the following levels (in % of the analytical value): Ce ± 2, Dy ± 4, Eu ± 2, Ga ± 4, Gd ± 3.6, Ho ± 0.3, La ± 36, Lu ± 0.1, Nb ± 44, Nd ± 33, Pr ± 9, Sm ± 5, Ta ± 9, Hf ± 7, Tb ± 0.5, Tm ± 0.1, Y ± 6, Yb ± 0.25, Zr ± 47, Sc ± 0.5, Ti ± 0.1 , Th ± 2.4, U ± 1, W ± 0.5. Three samples from this SGS Geosol sample batch were analyzed in duplicate, with generally excellent precision (values for major elements in wt%, trace elements in ppm, maximum deviations reported): $SiO_2$ 0.2, $TiO_2$ 0.3, $Al_2O_3$ 0.6, $Fe_2O_3$

0.2, MnO 0.05, MgO 0.04, CaO 0.02, $K_2O$ 0.08, $Na_2O$ 0.01, $P_2O_5$ 0, LOI 0.04; V 12, Co 3, Ni 9, Cu 9, Zn 11, Ga 1.3, Rb 2.8, Sr 2, Y 1, Zr 19, Nb 1.3, Sn 0.2, Cs 0.23, Ba 67 (note, the other two values are 2 and 4, respectively), La 1.5, Ce 4.7, Pr 0.23, Nd 1.2, Sm 0.3, Eu 0.2, Gd 0.47, Tb 0.05, Dy 0.19, Ho 0.45, Er 0.06, Tm 0.01, Yb 0.1, Lu 0.02, Hf 0.61, Ta 0.11, W 1.3, 0.3, U 0.18. Considering that nugget effects may well have played a role with respect to several elements such as Zr, these data are fully acceptable.

Regarding the major elements, reasonable coincidence was found within the 10 % limits advised by SGS – in fact, in many instances, the differences were considerably lower. For trace elements, numerous cases of exact coincidence of values were found for duplicate analyses, with considerable deviations noted primarily for Sr, Zr, and Ba, where especially elevated values may be affected by deviations of up to 5 %. In conclusion, our confidence in the commercially obtained data is high. Where caution is advised is when major element totals do not reach approximately 100 wt%.

### 3.3 Isotope analysis

The isotope dilution, separation procedures and analytical method applied at UnB were reported by Gioia and Pimentel (2000). The samples were washed, and weathered parts were removed, then they were crushed, and pulverized to a very fine powder. Approximately 50 mg of rock powder were mixed with $^{149}Sm/^{150}Nd$ rapid solution and dissolved in Savillex capsules. All whole rock samples used for Sm-Nd extraction were subjected to conventional cation exchange techniques based on Teflon® columns containing LN-Spec resin (HDEHP - Di-(2-ethylhexyl) phosphoric acid supported by polytetrafluoroethylene powder).

#### *Isotope analyses by Thermo Scientific TRITON™ Plus Thermal Ionization Mass Spectrometer*

The Sm and Nd fractions of 13 samples were loaded onto double evaporation filaments and were extracted on Teflon columns containing LN-Spec resin (liquid resin HDEHP - di-Ethylhexyl phosphoric acid impregnated with Teflon powder).

The average $^{143}Nd/^{144}Nd$ obtained for the USGS BHVO-2 standard was 0.512970 ± 0.000002 (2SE) which is consistent with the most recently published values (e.g.,

0.512986 ± 0.000009, Weis et al., 2005, or 0.512950 ± 0.000005, Raczek et al., 2003). Laboratory blanks were ~0.25 ng for Nd and ~0.04 ng for Sm. The uncertainties in Sm/Nd and $^{143}Nd/^{144}Nd$ ratios were better than ±0.5% (2 σ) and ±0.005% (2 σ), respectively, based on repeated analysis of the international BHVO-2 and BCR-1 rock standards.

In addition, five samples (AR-53, and AR-54, ARp 38G, ARp 38I and ARp 38L) were also analysed on a Thermo Fischer Neptune© MC-ICP MS at the Institut für Geologie und Mineralogie, Universität zu Köln (Cologne). Prior to sample digestion 87Rb–84Sr, 149Sm–150Nd mixed isotope tracers were added to measure isotope composition, and the element abundances on the same aliquot (see Weyer et al. 2002). Subsequently, the samples were digested using the high-pressure acid digestion procedure for felsic samples as described in Hoffmann et al. (2011). In a first step, the samples were digested in 6 ml 14 M HNO 3/24 M HF (1:1) for 24 h on a hotplate at 120 °C. Subsequently, the sample solutions were dried down and re-digested in a (1:1) 14 M HNO3/24 M HF mixture at 180 °C using Parr pressure vessels for 2–3 days. Following this, 1 ml of 65% perchloric acid was added and dried down. To remove all residual organic matter and stabilise HFSE, additional 2 ml of 14 M HNO 3/trace HF were added and evaporated afterwards. To achieve sample-tracer equilibrium, all samples were taken up in 6 ml of 6 M HCl/0.06 M HF and the clear solutions were dried down after 1 day. Using the exponential law, measured ratios of 87Sr/86Sr and 87Rb/85Rb were normalised to 86Sr/88Sr = 0.1194 (Nebel et al. 2005), respectively, and Sr isotope results are given relative to a 87Sr/86Sr of 0.710240 for NBS 987. Rubidium was measured relative to NBS 984 (87Rb/85Rb = 0.38554). Measured Nd isotope ratios were normalised to 146Nd/144Nd = 0.7219 using the exponential law and results are given relative to a 143Nd/144Nd of La Jolla of 0.511859. Total procedural blanks were, <39 pg for Nd, and <19 pg for Sm.

After digestion, an aliquot of sample solution was directly loaded onto Teflon® columns containing approximately 83 mg of Eichrom® Sr-Spec resin (50-100 µm) to separate the Sr fraction from the matrix. Rubidium concentration was not determined during this work. Strontium isotopic composition of selected samples was determined using a Thermo Scientific TRITON™ Plus Thermal Ionization Mass Spectrometer (TIMS) operating in the multidynamic mode. The average 87Sr/86Sr obtained for the NBS-987 standard was 0.71029 ± 0.00001 and 0.71028 ± 0.00002

(2SD within run). This value agrees well, within the analytical error, with the most typically recommended value of 0.71034 ± 0.00026 of the National Institute of Standard and Technology. Mass fractionation was corrected by normalizing the 87Sr/86Sr ratio to 8.3752. Strontium and Sm-Nd isotopic ratios for all Felsic and Mafic Granophyre and potential precursor rocks (i.e., epidiorite, granite, and meta-basalt from the Dominion Group Lava) were recalculated to the age of the impact event at 2.02 Ga (Kamo et al., 1996).

***Isotope analyses by Thermo-Fisher Neptune MC-ICPMS***

Four other samples (ARp 38A, ARp 38G, ARp 38I and ARp 38L) were analyzed in solution in a Thermo-Fisher Neptune MC-ICPMS instrument at the University of Brasília laboratory. The samples were introduced in the spectrometer using a nebulizer with a flux of 100 uL/min. For Sm, the tuned masses were $^{146}$Nd, $^{147}$Sm, $^{148}$Sm, $^{149}$Sm, $^{150}$Sm, $^{152}$Sm and $^{154}$Sm. Five blocks of 10 cycles each with an integration time of 4.194 second was considered for each analysis. The normalization factor used was the $^{147}$Sm/$^{152}$Sm (true value of 0.556083). For Nd the tuned masses were $^{142}$Nd, $^{143}$Nd, $^{144}$nd, $^{145}$Nd, $^{146}$Nd, $^{147}$Sm, $^{148}$Nd and $^{150}$Nd. Seven blocks of 10 cycles each with an integration time of 4.194 second was considered for each analysis. After subtracting any (rare) $^{144}$Sm interference, $^{143}$Nd/$^{144}$Nd ratios were corrected for instrumental mass fractionation using the exponential fractionation law and assuming $^{146}$Nd/$^{144}$Nd = 0.7219.

The average $^{143}$Nd/$^{144}$Nd obtained for the USGS BHVO-2 standard was 0.512970 ± 0.00002 (2SE) which is consistent with the most recently published values (e.g., 0.512984 ± 0.000006, Yang et al., 2009 by MC-ICPMS or 0.512986 ± 0.000009, Weis et al., 2005 or 0.51295 ± 0.000005, Raczek et al., 2003 by ID-TIMS). TDM values were calculated based on the model by DePaolo (1981). The measured $^{143}$Nd/$^{144}$Nd sample ratios are expressed in Epsilon notation ($\varepsilon_{Nd}$) as the fractional deviation in part per $10^4$ (units) from $^{143}$Nd/$^{144}$Nd value of the Chondritic Uniform Reservoir (CHUR). Neodynium blanks were < 100 pg.

Those three samples (ARp 38G, ARp 38I and ARp 38L) were also analysed on a Thermo Fischer Neptune© MC-ICP MS at the Institut für Geologie und Mineralogie, Universität zu Köln (Cologne). Prior to sample digestion $^{87}$Rb–$^{84}$Sr, $^{149}$Sm–$^{150}$Nd mixed isotope tracers were added to measure isotope composition, and

the element abundances on the same aliquot (see Weyer et al. 2002). Subsequently, the samples were digested using the high-pressure acid digestion procedure for felsic samples as described in Hoffmann et al. (2011). In a first step, the samples were digested in 6 ml 14 M HNO 3/24 M HF (1:1) for 24 h on a hotplate at 120 °C. Subsequently, the sample solutions were dried down and re-digested in a (1:1) 14 M HNO3/24 M HF mixture at 180 °C using Parr pressure vessels for 2–3 days. Following this, 1 ml of 65% perchloric acid was added and dried down. To remove all residual organic matter and stabilise HFSE, additional 2 ml of 14 M HNO 3/trace HF were added and evaporated afterwards. To achieve sample-tracer equilibrium, all samples were taken up in 6 ml of 6 M HCl/0.06 M HF and the clear solutions were dried down after 1 day. Using the exponential law, measured ratios of 87Sr/86Sr and $^{87}Rb/^{85}Rb$ were normalised to 86Sr/88Sr = 0.1194 (Nebel et al. 2005), respectively, and Sr isotope results are given relative to a $^{87}Sr/^{86}Sr$ of 0.710240 for NBS 987. Rubidium was measured relative to NBS 984 ($^{87}Rb/^{85}Rb$ = 0.38554). Measured Nd isotope ratios were normalised to $^{146}Nd/^{144}Nd$ = 0.7219 using the exponential law and results are given relative to a $^{143}Nd/^{144}Nd$ of La Jolla of 0.511859. Total procedural blanks were, <39 pg for Nd, and <19 pg for Sm.

# 4. RESULTS

## 4.1. Field Observations

The roughly NE trending Granophyre dike on Rensburgdrif and neighboring farms straddles the boundary between the granitoid core (on the eastern side) and the metasedimentary collar of the Vredefort Dome (towards the northwest). The dike extends from Rensburgdrif towards the north-northeast across a portion of Farm Kommandonek and across the Vaal River onto the Eldorado and Kopjeskraal properties. To the south, it extends across Zuid Witbank to the Rietkuil property of Johannesburg Zoo. There was no indication for existence of mafic Granophyre or of mafic inclusions found at farm Rietkul. The dike was mapped over a length of 2.3 km on Farm Rensburgdrif from coordinates (UTM) 536304E / 7025546S to coordinates 535127E / 7023569S. In addition, a 500 m section further north on farm Kommandonek was visited, and some observations were made near the southwestern end of the dike on farm Rietkuil at 531646E / 7021491S (compare Figure 1). On Rensburgdrif, the dike trends in a slightly sinusoidal pattern in the general direction of ~N50E. Its width is

somewhat variable - over most of the mapped section, it is 20-30 m wide. The dike is exposed in the form of discontinuous, often curving segments formed on surface by agglomeration of submeter to meter sized boulders (Fig. 2a, b). Exposure occurs at different topographic levels, with an overall vertical gradient of 50 m.

The main country rocks in the study area are granite-gneiss, epidiorite, and metalava of the Dominion Group. Granite-gneiss is the most common host rock to Granophyre along the studied extent of the dike, with extensive outcrop. The granite-gneiss is medium- to coarse-grained and has a typical granitic composition of hypidiomorphic alkali-feldspar, plagioclase, quartz, and biotite. The rock presents a gneissic texture with leucosome-rich stromatic migmatite in places, containing granitic leucosomes and trondhjemitic melanosomes.

The Granophyre cuts epidiorite only close to the southern bank of the Vaal River (536213E / 7025581S) (Fig. 1). Here, outcrops of epidiorite are scarce and strongly weathered, and they are often located in dense bush with difficult access. Epidiorite has a medium-grained granoblastic texture of mainly amphibole and plagioclase and shows fractures perpendicular to regional strike in roughly NE-SW direction. DGL is not well exposed in the study area, with only a few outcrops south of a main fault (534995E / 7023458S) (compare map, Fig. 4). The crystalline, dense, dark-green rock is very fine-grained and consists of mafic minerals, quartz, and feldspar. In some cases, it is possible to notice a slight foliation. This lithology from the Vredefort Dome has been described in detail by Jackson (1992, 1994) and in regional occurrence by Marsh et al. (2006). Both granite-gneiss and epidiorite contain PTB veinlets up to 10 cm width, and network breccias of up to meter size, with well-rounded clasts of the mafic rock that are especially well exposed close to the homestead, on Farm Kopjeskraal.

The contact between the Granophyre dike and epidiorite on Farm Rensburgdrif is not exposed. The closest epidiorite occurrence is ca. 100 m from the dike at 536144E / 7025150S. Where the dike cuts granite-gneiss, the contact is frequently irregular (Fig. 2c, d). Fractures, joints, and color changes are observed in

the host rocks closest to the contact with the dike, which could indicate that the Granophyre intrusion affected the wall rocks mechanically and thermally.


Figure 2 - (a) Field photograph giving a general view of the granophyre dike outcrops on Farm Rensburgdrif, in the form of a chain of boulders with variable width of up ca. 30 m. Note some clasts visible on the weathered surfaces of the boulders. (b) A closer approximation of the outcrop showing sets of joints with vertical orientations and parallel to the strike of the dike. c) Panoramic view of the SW contact between Archean Granite (A) and Granophyre in the southern part of Farm Rensburgdrif. d) Outcrop of Granophyre at contact between Archean granite and Granophyre.

The Granophyre comprises two distinct textural phases. The first one is medium-grained (0.5 to 0.8 mm grain size) and hosts abundant clasts primarily derived from granite (85%), with minor contributions from quartzite and shale (together 10%), and epidiorite (< 5%). The second textural phase occurs in the central part of the dike and is finer-grained (< 0.5 mm) and slightly darker than the other phase. It has seemingly a dominance of smaller clasts compared to the first phase, which are also derived from these same country rock types at similar proportions of each type found in the felsic. The contact between these two Granophyre phases is gradational and runs parallel to the assumed contact between the dike and the host rock.

Over its entire extension, the dike is not homogeneous with respect to amount, average size, and geometry of clasts, as well as flow patterns that are indicated by the alignment of matrix minerals and small clasts of granite and quartzite. Dike margins are generally rich in visible clasts, which are elongated and angular, up to 15 cm in length, and commonly aligned parallel to the dike margin (Fig. 3a). Most elongate clasts are aligned parallel to the strike of the dike (Fig. 3b). In contrast, the central portions of the dike are apparently comparatively more clast-poor (clast-poor Granophyre, Fig. 3d). Here, fragments are more rounded and only up to 3 cm in size (Fig. 3e). Overall, in the dike, large clasts (10-30 cm in size) are considerably less abundant (< 5 %) than smaller clasts < 5 cm in size, which make up 10 to 20 vol.% estimated over the entire dike section mapped.

Several sets of joints were observed along the dike with different orientations: vertical and parallel to the strike of the dike, horizontal and perpendicular to the dike walls (Fig. 3g), and in two directions oblique to the walls of the dike dipping in the direction of its strike. A few joints show displacement of up to 10 cm; some are filled with quartz. Individual clasts within the dike are often substantially fractured (Fig. 3h). Shear zones are entirely absent. Different orientations had also been recorded on Rensburgdrif by Reimold et al. (1990). No PTB veinlets were observed along the Granophyre dike, in contrast to the single observation reported by Reimold et al. (1990). The map prepared for the study area is shown in Fig. 4. Note that the map has been superposed onto a section of the Geological Map of the Vredefort Dome (Bisschoff 1999). It is obvious that the present mapping does not match entirely with Bisschoff´s (1999) findings. This was first noted in the field. The main difference is seen in the southwestern sector, to the SW of a prominent NW-SE trending fault that does not displace the Granophyre dike but where several country rock types were recorded with discordance between the two mappings. The prominent fault is causing significant right-lateral offset of strata – and it appears possible that these discrepancies may be related –

at least in part - to this roughly radially (with respect to the center of the Vredefort Dome) trending structural feature.

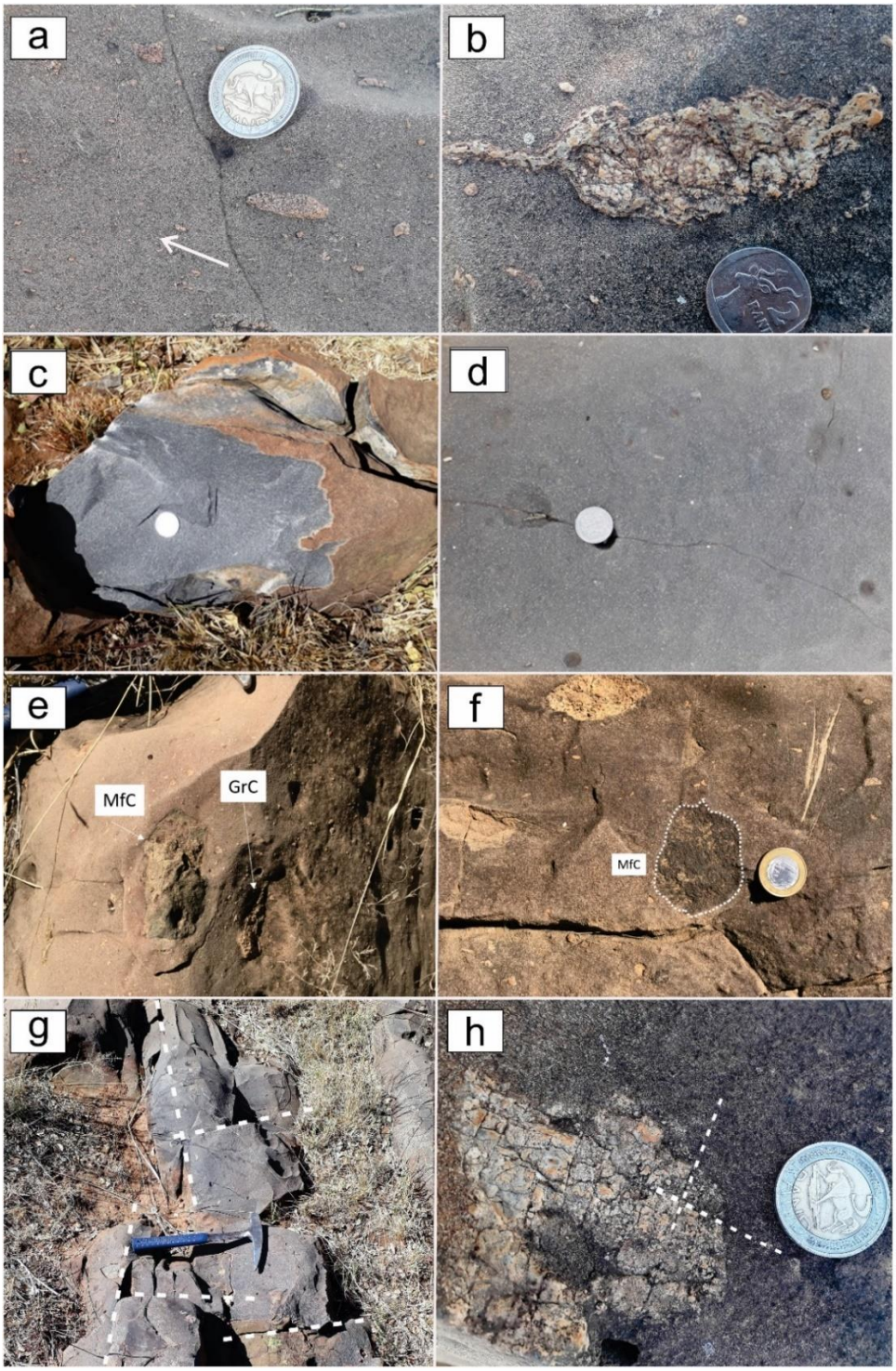


Figure 3 – (a, b) Clasts of different sizes and shapes from clast-rich Granophyre: (a) Alignment of granite clasts parallel to the strike of the dike, and (b) an elongated, apparently plasticized clast of quartzite. (c, d) Clast-poor Granophyre: in (d) holes in the dike are shown, probably due to weathering out of former clasts (e, f) Note mafic clasts in Granophyre on Rensburgdrif and Kopjeskraal farms, respectively. (g) Two sets of joints parallel and perpendicular to the strike of the dike represented by white dotted lines. Note the joint displacement of ~ 5 cm along the other joint. (h) Multiple fracture sets cutting through a quartzite clast (~5 cm wide) and extending into the surrounding Granophyre matrix. Scaling info: length of hammer 28 cm, diameters of 5 Rand (images a and h) and 2 Rand (images b, c and d) coins 26 and 22 mm, respectively. MfC: Mafic clast, and GrC: granite clast

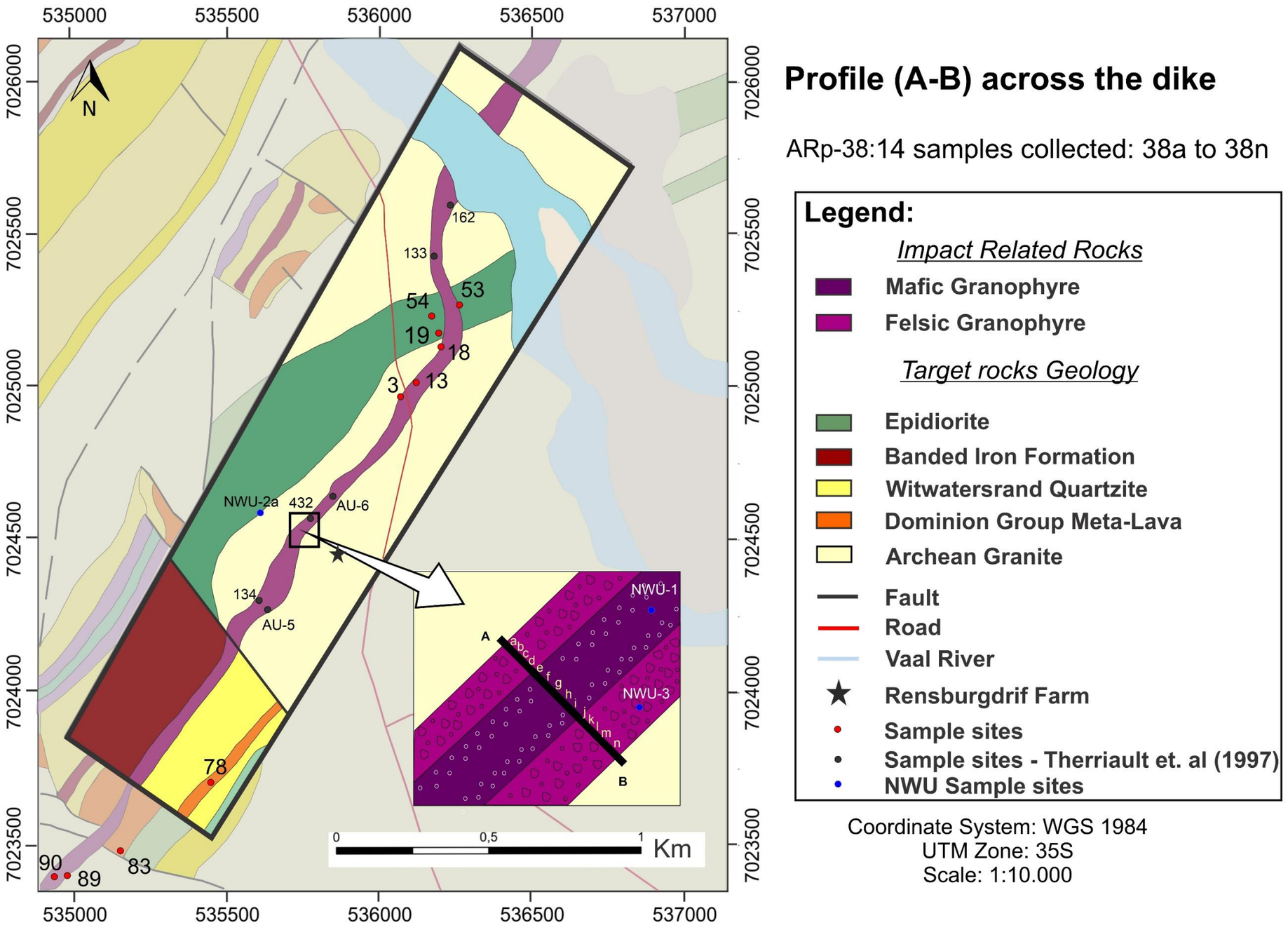


Figure 4 - Geological map (Scale 1:10.000) of the study area close to Rensburgdrif Farm. Granophyre dike at SW from the Vaal River. The background map is adapted from the geology of the Vredefort Dome map, Bischoff (1999) 1:50.000 scale, whereby equivalent lithologies are kept in the same though faded colors. Schematic map of the Granophyre dike on farm Rensburgdrif, indicating sampling sites of this investigation.

## 4.2. Petrography including mineral chemistry

Based on their chemical compositions, the samples of the clast-rich phase identified in the field are classified as Felsic Granophyre that is chemically defined as impact melt rock with "> 66 wt% $SiO_2$" (see section 4.3. Geochemistry), and samples of the clast-poor variety are classified as Mafic Granophyre with < 66 wt% $SiO_2$ (compare Wannek, 2015; Reimold et al., 2017). In the present section, optical and electron microscopic observations are discussed for these Granophyre types, as well as the mafic country rocks (epidiorite and DGL).

***Felsic Granophyre***

In thin section, the Felsic Granophyre on farm Rensburgdrif is characterized by a very fine-grained matrix of orthopyroxene, plagioclase, orthoclase, quartz, biotite, and opaque minerals (magnetite and ilmenite). Lithic clasts are mainly derived from granite, quartzite, minor shale, and – rarely – a medium-grained epidiorite. The proportion of groundmass in the Felsic Granophyre varies from 30 to 40 vol%. Some of the fine-grained minerals in the matrix may actually represent remnants of completely annealed microclasts.

The Felsic Granophyre displays a relatively uniform modal composition, but there are textural variations related to the abundances of the main modal components. Clast-rich samples (Felsic Granophyre) have fine-grained matrix with short prismatic (100-300 µm), zoned pyroxene crystals, and with plagioclase laths (800-1200 mm). Interstitial areas consist of granophyric intergrowth of quartz and alkali feldspar, which are mainly found interstitial to plagioclase blades (Fig. 5a). This kind of intergrowth often displays rosette and radial symplectite-like patterns (Fig. 5b). Apatite is an accessory mineral and occurs in the form of fine needles, and tiny, euhedral ilmenite crystals form another accessory mineral. Many pyroxene crystals are partially altered to amphibole and biotite. Some portions of the groundmass are rich in annealed quartz – likely remnants of part-melted granitic or quartzitic microclasts.

Most of the lithic clasts are extensively recrystallized to finest grained mosaics of felsic minerals. However, it is still often possible to determine the contact between clasts and matrix. Inclusions of metasedimentary rocks are fine- to medium-grained, angular, usually show a clastic texture, and are predominantly composed of quartz, with minor amounts of feldspar, and form subrounded inclusions in Granophyre groundmass. Granitoid clasts may still indicate igneous texture and are composed of

rounded relic quartz grains and feldspar (more alkali feldspar than plagioclase) that may display local melting at grain boundaries. Quartzite inclusions have experienced at least two episodes of recrystallization (see also Buchanan and Reimold, 2002). During the early episode of recrystallization, overgrowth rims developed on rounded quartz crystals. In remnant, not completely annealed quartz clasts, it is possible to notice evidence of deformation that may be ascribed to shock metamorphism, such as undulatory extinction and mosaicism. In the second episode of annealing, the original quartz grains were completely annealed to finest grained mosaics (Fig. 5c). Both vermicular texture indicative of incipient melting of quartz crystals (Buchanan and Reimold, 2002) and checkerboard texture developed in plagioclase of granitoid clasts illustrate partial melting (Fig. 5d).

Some pyroxene crystals are chemically zoned, as illustrated in the backscattered electron image of Figure 5e. A mosaic of fine-grained quartz crystals is also noted in the backscattered electron image of Figure 5f, which clearly represents a small, annealed clast.

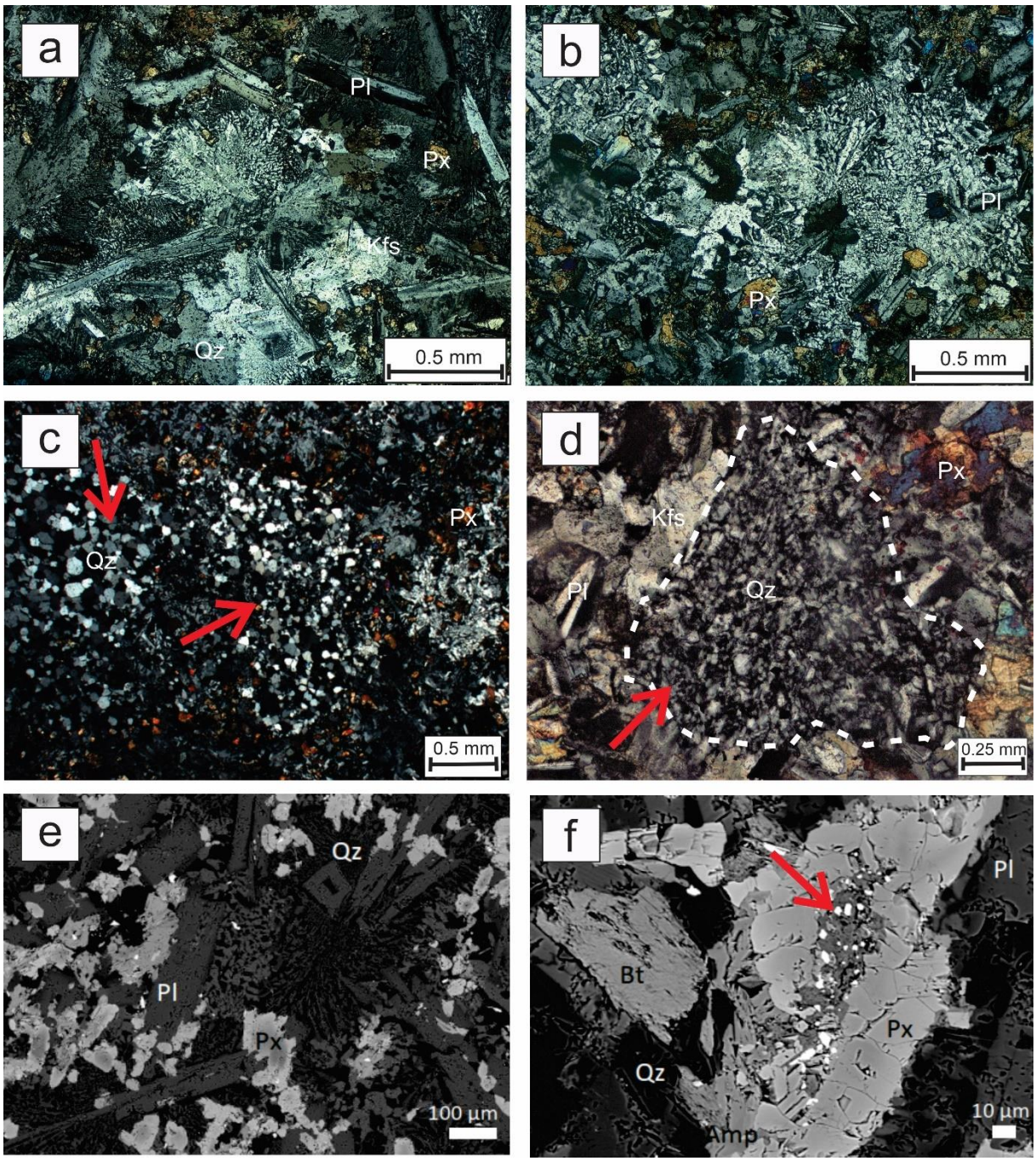


Figure 5 - Cross-polarized light photomicrographs of a Felsic Granophyre sample: (a) Felsic Granophyre matrix of large plagioclase laths and short prismatic hypersthene crystals. Interstitial areas are composed of microgranophyric intergrowths of quartz and feldspar (both plagioclase and K-feldspar). (b) Similar view – in this photomicrograph the intergrowth displays radial and rosette patterns of quartz and feldspar. (c) Rounded clasts composed of aggregates of equigranular quartz indicated by the red arrow). (d) Note incipient melting of a quartz crystal along crystallographic planes (vermicular quartz indicated by a red arrow). (e, f) Backscattered electron (BSE) images for selected matrix areas in Felsic Granophyre of sample AR-38M: (e) Micropegmatitic intergrowths of quartz and feldspar in interstices between dark grey plagioclase (Pl) laths and light grey, granular pyroxene crystals. Iron enrichment is indicated by the comparatively lighter rims on such crystals. (f) Pyroxene (Px), biotite (Bt), quartz (Qz), and amphibole (Amp) crystals in matrix of Felsic Granophyre.

### *Mafic Granophyre*

Mafic Granophyre (i.e., the clast-poor Granophyre variety) has more plagioclase and orthopyroxene than the felsic type. The matrix is comparatively slightly coarser-grained and has a granular texture, pyroxene crystals are zoned and somewhat larger (200-400 µm), and subhedral crystals of quartz and feldspar (400-800 µm) are prominent. The presence of ophitic intergrowth of prismatic pyroxene and plagioclase crystals and micropegmatitic quartz and K-feldspar pockets in groundmass defines a hypidiomorphic texture (Fig. 6a, b). The few biotite crystals present are subhedral to euhedral, and magnetite and ilmenite occur as anhedral to euhedral crystals that are commonly embedded in biotite. Pyroxene is to a minor extent replaced by biotite, amphibole, and chlorite.

Besides the same clast types being present as in the felsic phase, a number of lithic clasts composed of fine-grained aggregates of euhedral mafic crystals (Fig. 6c, d) were observed in this work for the first time. They were observed significantly more often in thin sections of Mafic Granophyre. These mafic clasts have sizes of up to 2 mm. The clasts are angular to rounded and have irregular margins, indicating that they were extensively corroded – presumably thermally.

Small amygdales, up to 5 mm in size, are also common in samples of both Granophyre varieties. The amygdales are commonly distorted by flow. They are partially to totally filled with mostly opaque phases, besides some phyllosilicate. Reaction aureoles with pyroxene of the matrix around the vesicles are often observed.

Backscattered electron images show that the amphibole is a secondary product of uralitization of pyroxene in Mafic Granophyre (Fig. 6e). The pyroxene in this phase is much more altered than in Felsic Granophyre samples (Figs. 6e and 6f). This observation was also reported by Wannek (2015) for the Mafic Granophyre from Farm Kopjeskraal.

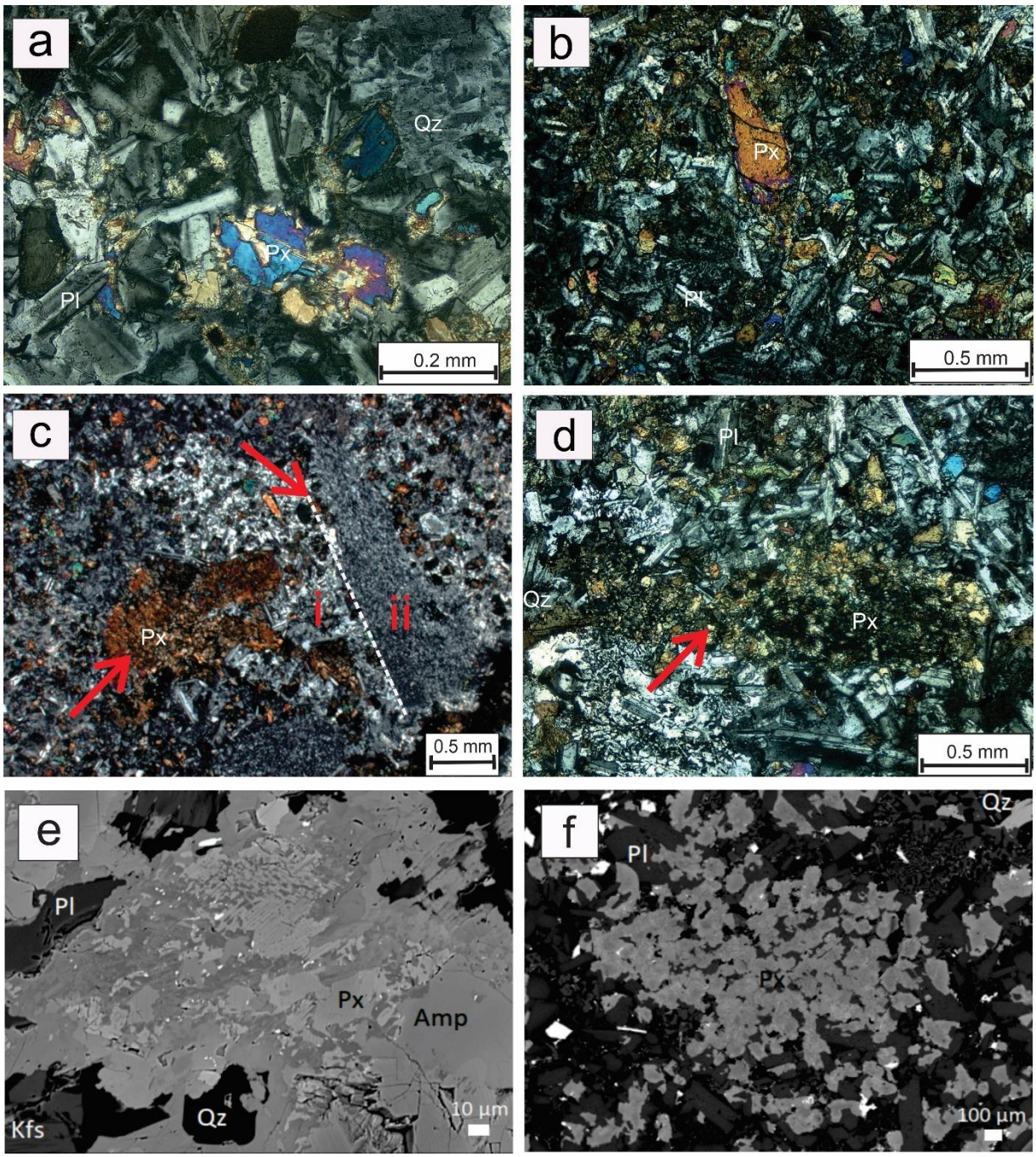


Figure 6 – (a-d) Cross polarized light photomicrographs of Mafic Granophyre samples from the ARp sample profile – see Fig. 8). (a) Typical granular texture of matrix with prismatic pyroxene crystals, subhedral crystals of quartz and alkali feldspar, and relatively smaller plagioclase laths. (b) Zoomed image of an augite crystal between plagioclase laths. (c, d) Small aggregates of prismatic pyroxene crystals. (c) Besides the mafic clast, note a lithic clast composed of two different granular products of annealing: (i) on the left, very small crystals of quartz, feldspar, and pyroxene, and on the right (ii) a partial melt of extremely fine-grained, felsic groundmass. (d) Granophyre matrix with a mafic clast that mostly consists of small crystals of pyroxene. (e, f) Backscattered electron images for selected matrix areas in Mafic Granophyre: (e) A typical pyroxene crystal of the matrix. Most of the image comprises uralitized clinopyroxene. (f) Altered pyroxene in the matrix. The small crystals have highly irregular shapes, which speaks for partial resorption of the pyroxene crystals.

***Epidiorite***

The epidiorite of the study area is affected by metamorphism, obliterating the original igneous texture of the protolith. The epidiorite is composed of amphibole (60%), plagioclase (30%), and biotite, quartz, and oxides (roughly at 10% each). Crystal size is medium- to coarse-grained, up to 3 mm. Most amphibole crystals are euhedral to subhedral, but most are deformed with jagged edges and show strong alteration (Fig. 7a, b). Amphibole is interpreted as a secondary product of uralitization of primary subhedral augite crystals (in accordance with Pybus, 1995 description of epidiorite). Plagioclase crystals are euhedral to subhedral, and also strongly altered (Fig. 7c, d). Chlorite and epidote are frequently observed as alteration products after amphibole. Apatite occurs as small, needle-shaped inclusions in plagioclase.

In backscattered electron (BSE) images, it is possible to notice the mosaic texture on the rims of some amphibole crystals (Fig. 7e), likely also a result of metamorphic overprint. Amphibole crystals have compact cores, whereas their outer zones appear porous (Fig. 7e) and apparently have experienced alteration. The assemblage of ilmenite, titanite, amphibole, and plagioclase crystals with irregular crystal margins represents the secondary products of alteration and/or metamorphic overprint (Fig. 7f).

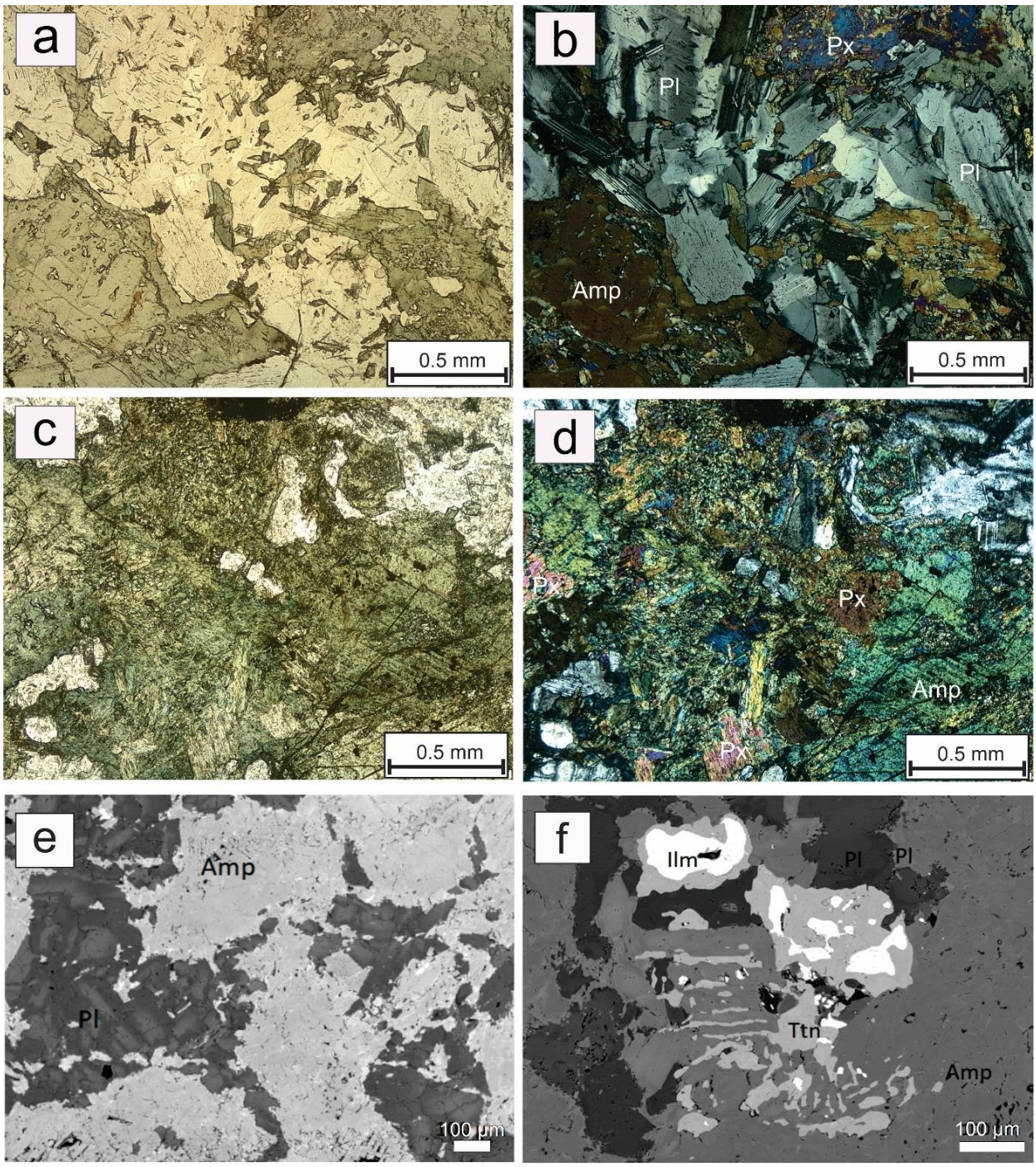


Figure 7 - Parallel (a, c) and cross polarized light (b, d) photomicrographs for an epidiorite sample (AR-54). (a, b) Subophitic equigranular texture of deformed amphibole crystals and subhedral plagioclase crystals. The pyroxene shows cleavage traces with approximately 90º angles between them and has small inclusions of quartz. Plagioclase crystals are zoned (c, d) Remnant pyroxene, totally altered to amphibole due to uralitization. The original igneous texture (subophitic) can still be recognised on the right. (e, f) Backscattered electron images of the same sample: (e) Medium-grey amphibole crystals with comparatively compact cores, and outer zones that appear porous and seemingly have experienced alteration. (f) Ilmenite (Ilm), titanite (Ttn), amphibole (Amp), and plagioclase (dark grey) with irregular crystal shapes. This assemblage may represent secondary products after alteration/metamorphic overprint of primary amphibole. The relatively larger amphibole crystal on the right contains small inclusions of feldspar (dark gray) and quartz (black).

***Mineral chemistry***

Mineral chemical analyses by electron microprobe were obtained for a sample each of Felsic Granophyre (sample ARp-38M), Mafic Granophyre (ARp-38G), and epidiorite (AR-54). Specifically, compositions of pyroxene, feldspars, and amphibole were determined (Appendix 4-6 Supplementary Material) and are compared with analyses from Reimold et al. (1990), Therriault et al. (1996), and Wannek (2015) (Fig. 8a-c).

The orthopyroxene (Fig. 8a) in Felsic Granophyre is primarily hypersthene ($En_{46-73}Fs_{25-51}Wo_{2-4}$). There are also some occurrences of clinopyroxene along rims of orthopyroxene laths. Orthopyroxene is often partially replaced by green pleochroic amphibole (ferri-actinolite to hornblende in composition). In Mafic Granophyre, hypersthene ($En_{51-59}Fs_{37-46}Wo_4$) as well as pigeonite and augite compositions ($En_{31-39}Fs_{23-27}Wo_{35-42}$) were identified.

There is clear evidence of Fe enrichment in the rim areas of pyroxene crystals, an effect that was also described by Wannek (2015) for Felsic Granophyre from Farm Kopjeskraal.

Feldspar analyses are shown in Fig. 8c. Alkali feldspar in the groundmass of both Granophyre types is generally K-rich. In the Mafic Granophyre, the composition is $An_{0-3}Ab_{13-37}Or_{60-86}$, whereas in Felsic Granophyre even more K enriched compositions ($An_{0.3-0.8}Ab_{13-14}Or_{84-86}$) are observed. Plagioclase compositions in Felsic Granophyre are predominantly labradorite of $An_{25-59}Ab_{40-73}Or_{0.7-1.3}$, and oligoclase to labradorite of $An_{19-57}Ab_{46-80}Or_{0-2}$ in the Mafic Granophyre.

In the epidiorite sample, plagioclase compositions of $An_{36-82}Ab_{17-63}Or_{0.1-0.6}$ were determined, with some crystals being strongly zoned from cores of $An_{67.9-80.6}Ab_{19.2-31.5}Or_{0.1-0.6}$ to rims of $An_{55.4}Ab_{44.2}Or_{0.4}$ - showing dominantly bytownite and labradorite compositions. Most of the amphibole analyses in the epidiorite sample correspond to actinolitic hornblende compositions, with few occurrences of magnesium-hornblende and actinolite (Fig. 8b).

In general, the microprobe results are consistent with previously published data. Wannek (2015) reported comparatively wider compositional ranges for plagioclase ($An_{26-51}Ab_{48-72}Or_{1-2}$) and pyroxene ($En_{50-78}Fo_{20-47}Wo_{2-4}$) for Felsic Granophyre, and for plagioclase ($An_{16-61}Ab_{39-81}Or_{1-2}$) and pyroxene ($En_{36-60}Fo_{23-28}Wo_{9-36}$) in Mafic Granophyre than observed here. However, Wannek (2015) did not differentiate between core and rim analyses. For her epidiorite sample, she reported a

range of plagioclase compositions of $An_{40-76}Ab_{24-59}Or_{0-1}$, which is narrower than our data spread. For amphibole in epidiorite on Farm Kopjeskraal, she determined hornblende compositions (see Fig. 8b). Wannek (2015) also presented microprobe analyses for feldspar and amphibole from Dominion Group metalava on Farm Kopjeskraal. These data have been plotted into Figure 8, for comparison.

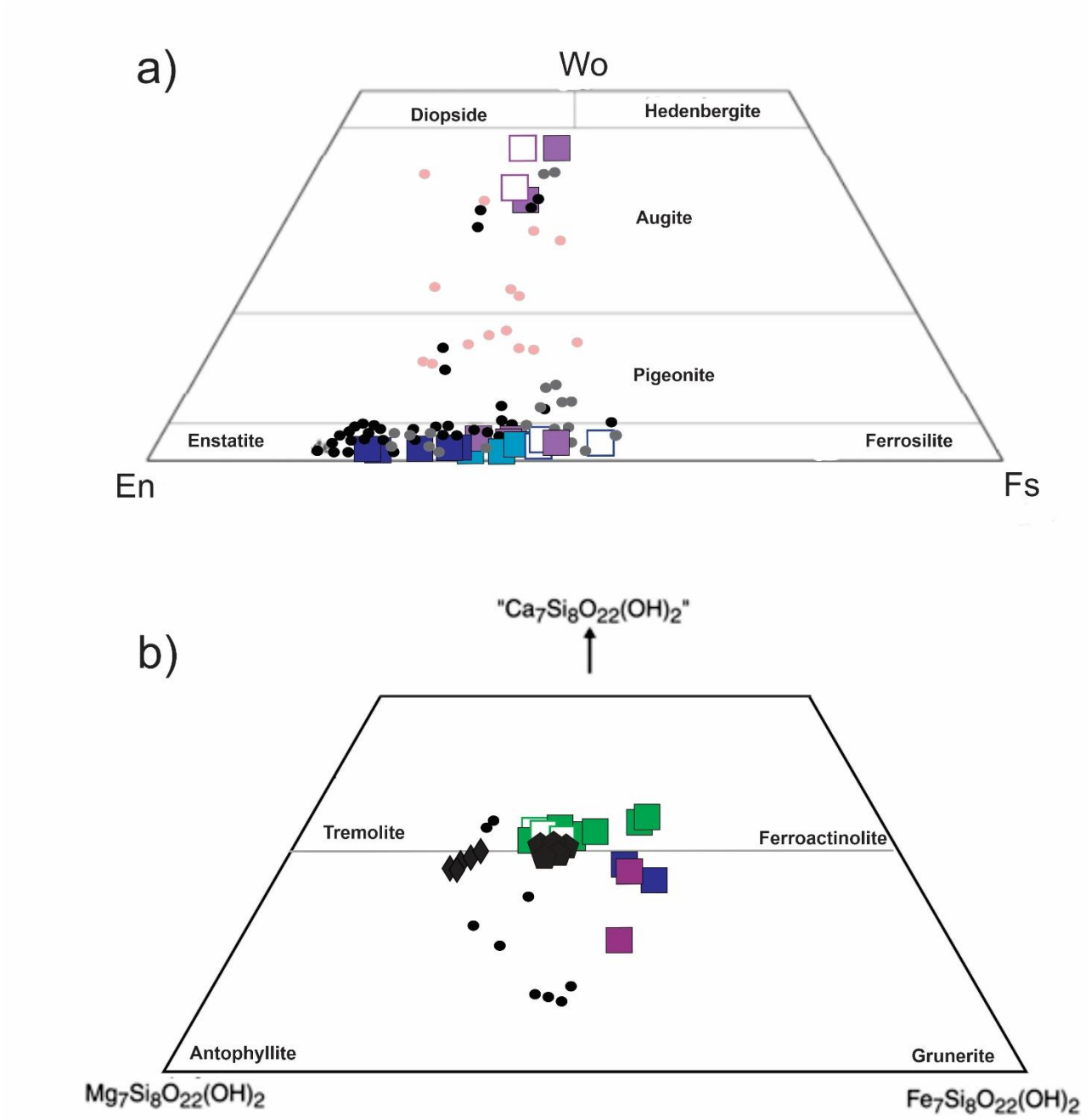

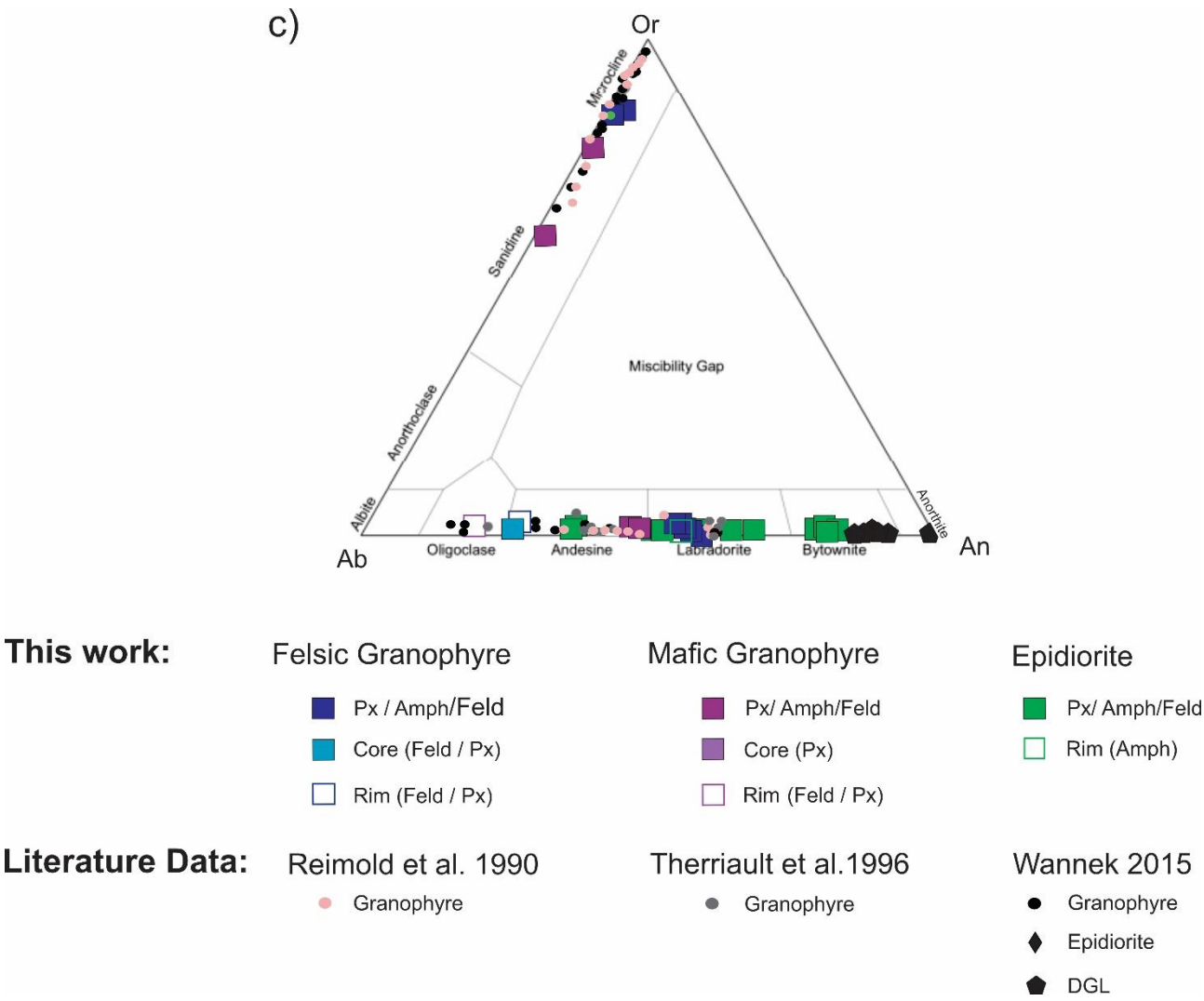


Figure 8 - Mineral compositions obtained by electron microprobe analysis for samples of Felsic and Mafic Granophyre, epidiorite, and Dominion Group meta-lava (DGL). For comparison, mineral compositions for Felsic Granophyre from Therriault et al. (1996), Reimold et al. (1990), and Wannek (2015), Mafic Granophyre from Wannek (2015), and for epidiorite and DGL from Wannek (2015) are plotted as well. (a) Pyroxene - px, (b) amphibole - amph, and (c) feldspar - feld.

### 4.3. Geochemistry

Twenty-six samples were collected from the Granophyre dike on Rensburgdrif and adjacent farms (Appendix 1). A comprehensive profile (samples ARp-38a-n, inset in Fig. 9) was sampled across the dike, with 14 samples spaced at 2 m each and covering an appropriate dike width of 30 m (Fig. 4). This profile includes samples of both Felsic and Mafic Granophyre. The other 13 samples were collected along the dike and comprise epidiorite (sample AR-54, NWU-2a), Felsic Granophyre (samples AR-3,13,18,19,53,78,83,90; NWU-1,3), and Mafic Granophyre (AR-89) as indicated in Fig. 9. Chemical compositions for these samples are listed in Table 1. Published major and trace element contents for Granophyre samples and main target rock types were compiled for comparison with our data from Hall and Molengraaff (1925); Willemse (1937); Reimold et al. (1990); Jackson (1994); Pybus (1995); Therriault et al. (1997); Lieger and Riller (2012), Wannek (2015), and Huber et al. (2020). These data are compiled in Appendix 2 in the Supplementary Material.

The new major and trace element data confirm the existence of Mafic Granophyre (<66 wt% $SiO_2$) also on Rensburgdrif Farm, which had been suggested by Lieger (2011) but not demonstrated with complete chemical analyses. It is demonstrated here that the mafic phase occurs indeed in the central portion of the dike, whereas the felsic (clast-rich) phase occurs along the dike margins, as shown clearly in the ARp profiles for major and trace elements in Figure 9. In addition, sample 38b from close to the western margin of the dike has more mafic character than the normal Felsic Granophyre. Note that the epidiorite and granite sample locations in these profiles are from the closest occurrences of these lithologies outside of the Granophyre dike, from the respective dike margins.

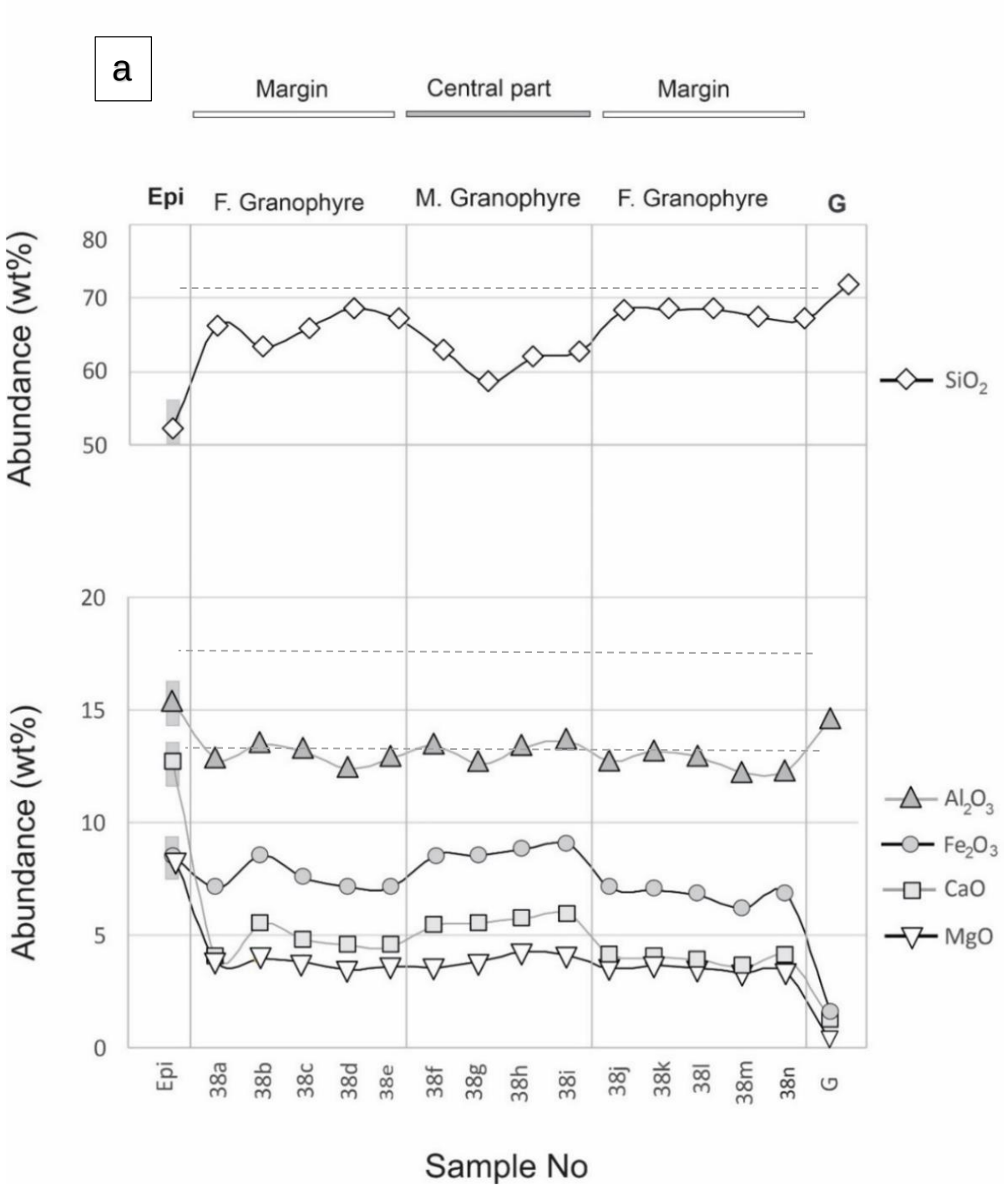
a
Margin
Central part
Margin
Epi
F. Granophyre
M. Granophyre
F. Granophyre
G
Abundance (wt%)
80
70
60
50
20
15
10
5
0
SiO2
Al2O3
Fe2O3
CaO
MgO
Epi
38a
38b
38c
38d
38e
38f
38g
38h
38i
38j
38k
38l
38m
38n
G
Sample No

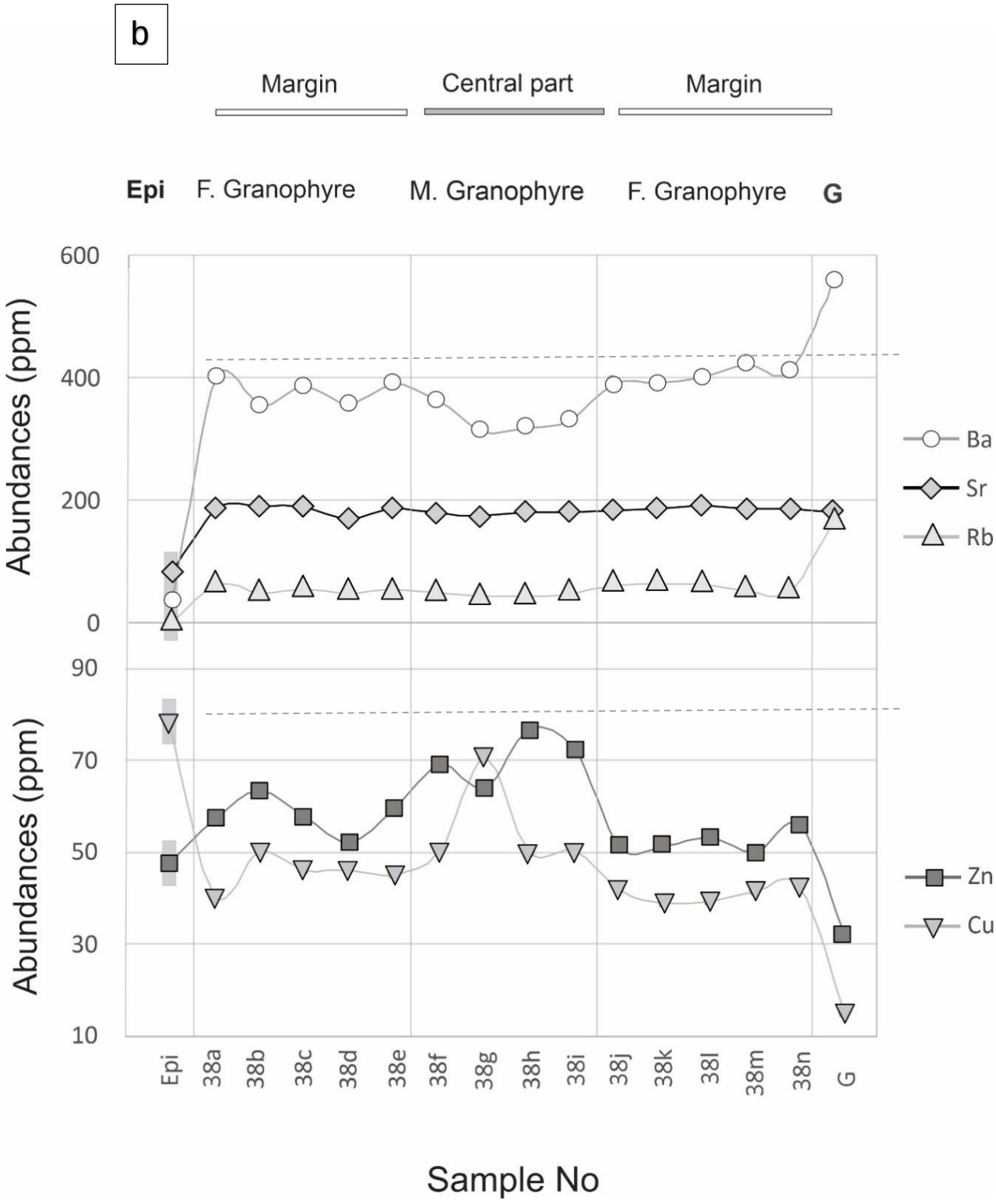


Figura 9 – Major (a) and trace (b) element data for the samples from the profile across the dike (ARp-38a-n). The mafic portion is in the central part of the dike. A possible mafic inclusion may also be present in the 38b sample from closer to the western edge of the dike. Note that the epidiorite and granite samples plotted are indeed from Rensburgdrif but do not originate from the immediate vicinity of the dike. These data are to give a general impression how these lithologies would plot in comparison to the Granophyre.

Our major and trace element analyses of Granophyre samples define two fields for the felsic and the mafic samples that agree with Wannek's (2015) distinction of Felsic and Mafic Granophyre compositions. The mafic Granophyre of this work is equivalent to the granular textured Granophyre reported by Therriault et al. (1997) on the core-collar boundaries dike.

Main oxides versus $SiO_2$ plots (Haker diagrams) are also used for comparing our data with those from literature (Fig. 10). The data define good negative correlations between CaO, MgO, $Fe_2O_3$ and $Al_2O_3$ (slightly scattered), with $SiO_2$. Conversely, $K_2O$ and $Na_2O$ define a positive correlation against $SiO_2$. The Granophyre data define two separate fields, which clearly correspond to the data for Felsic and Mafic Granophyre from the work of Wannek (2015) and one analysis from Huber et al. (2020). In general, mafic samples are characterized by similar to higher $Al_2O_3$ (a), $K_2O$ (b), $Fe_2O_3$ (d), and MgO (e) contents at a given SiO2 content (Fig. 10). Both Granophyre types contain indistinguishable $Na_2O$ (c) contents, while mafic samples have lower $K_2O$ (f) than felsic samples. Felsic Granophyre displays $SiO_2$ abundances between 66 (actually 65.89 – sample 38c has a composition that is right on the limit between Mafic and Felsic Granophyre compositions, but in terms of petrography is more akin to Felsic Granophyre) and 69.77 wt%, whereas Mafic Granophyre has $SiO_2$ abundances between 58.55 and 65.89 wt%. In Figure 10, epidiorite samples AR-54 and NWU-2 plots with data available from the literature (Pybus 1995; Wannek 2015). This lithology is characterized by higher CaO and MgO contents, similar to higher $Al_2O_3$ and $Fe_2O_3$ contents, and lower $SiO_2$, $K_2O$ and $Na_2O$ contents, compared to Mafic and Felsic Granophyre. On the other hand, the granite sample has opposite compositional character compared to epidiorite. Additionally, DGL samples (after Jackson 1994) plot into the compositional field defined by epidiorite. Significant gaps separate the fields of Mafic Granophyre and the two mafic endmembers, epidiorite and DGL.

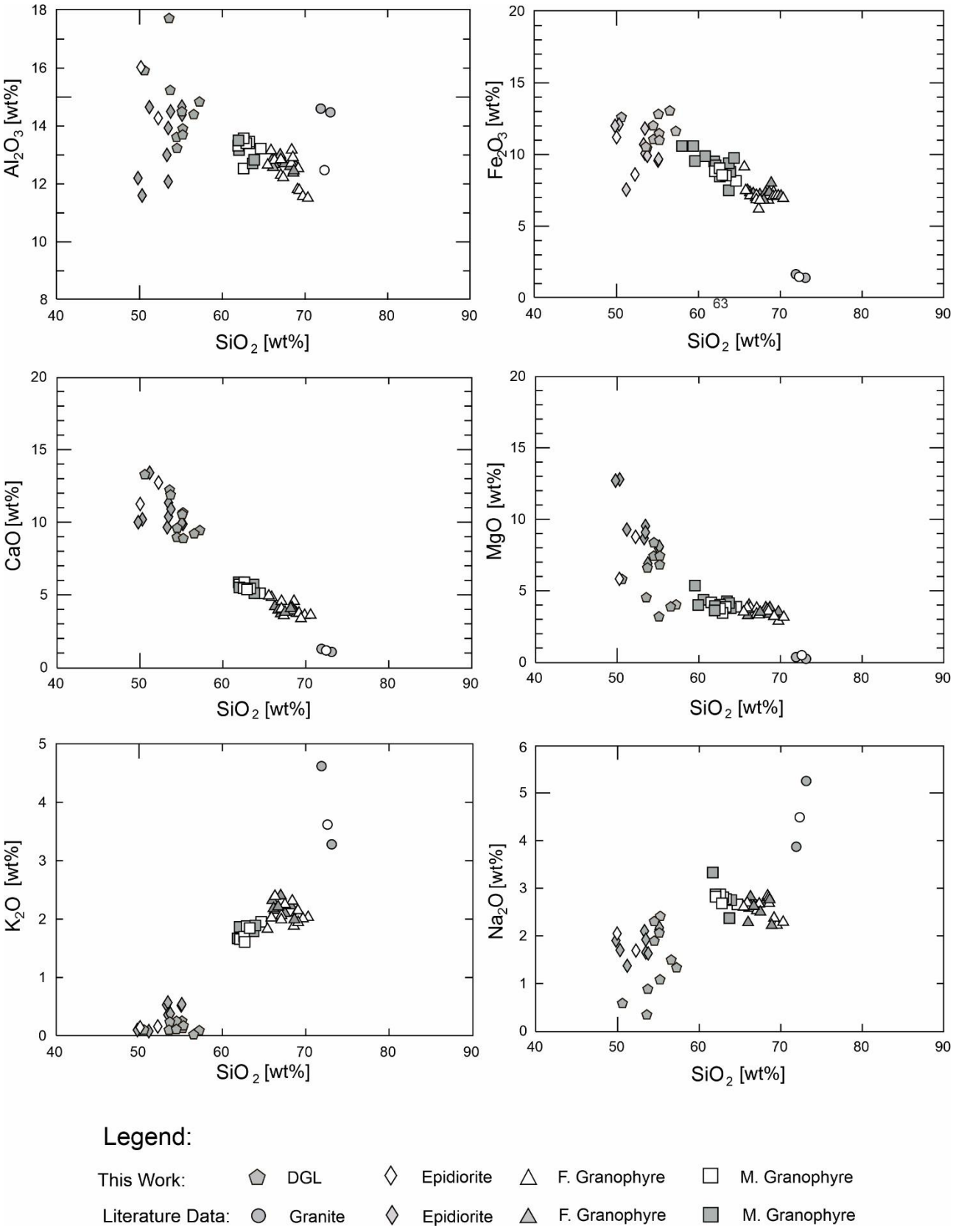


Figure 10 - Selected Harker type diagrams for Felsic and Mafic Granophyres, epidiorite, Dominion Group Lava (DGL), and granite. The Felsic Granophyre samples have essentially >66 wt% $SiO_2$. Literature data were taken from Hall and Molengraaff (1925), Willemse (1937), Reimold et al. (1990), Jackson (1994), Pybus (1995), Therriault et al. (1997), Lieger and Riller (2012), Wannek (2015), and Huber et al. (2020).

Trace element data are compiled in Appendix 8 (Supplementary Material). Twenty-four Granophyre samples and two samples of epidiorite were analyzed for their REE abundances. Chondrite-normalized (Sun and McDonough, 1989) REE patterns for these samples are compared with those from Reimold et al. (1990) and Wannek (2015) (Fig. 12). The REE patterns of Granophyre samples are similar, characterized by enrichment of light-REE (L-REE) over heavy-REE (H-REE), whereas epidiorite displays an almost flat pattern. The Granophyre patterns are somewhat similar to patterns for granitoids of the core of the Vredefort Dome, as, e.g., shown by Reimold et al. (1990). Dominion Group Lava REE abundance patterns are akin to the epidiorite patterns but characterized by significantly higher element abundances. Abundances for both Granophyre types are much alike and are very similar to the abundances determined by previously works (Reimold et al., 1990; Wannek, 2015). It is interesting to note that the Vredefort epidiorite REE patterns differ strongly from the field for Ventersdorp Supergroup samples after Gottwald et al. (2020).

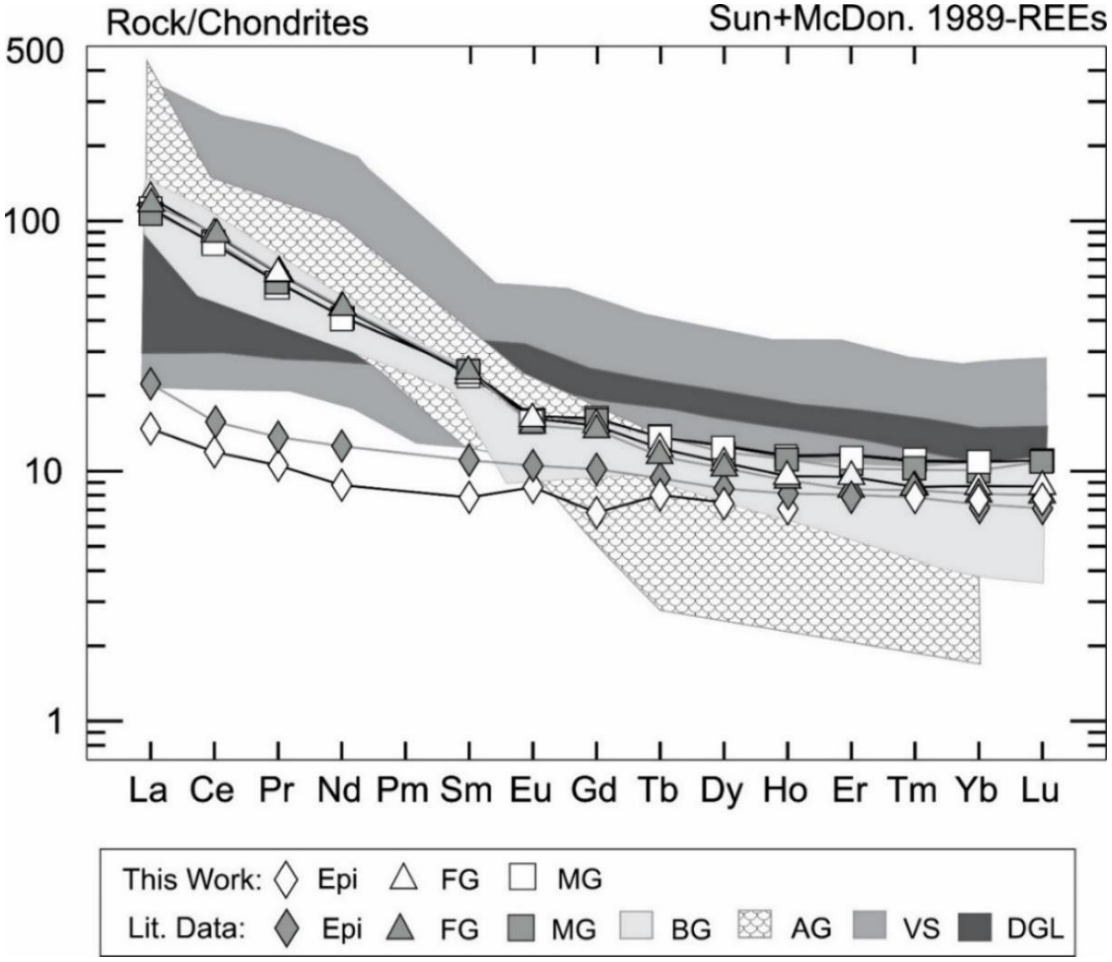


Figure 11 - Chondrite-normalized (Sun and McDonough 1989) rare-earth element patterns for averages of samples of Felsic and Mafic Granophyre and epidiorite. For comparison, literature data are plotted as follows - BG: Bronzite Granophyre after Reimold et al. (1990); AG: Archean Granite (Reimold et al. 1990); FG: Felsic Granophyre (Wannek 2015), MG: Mafic Granophyre (Wannek 2015), Epi: Epidiorite (Wannek 2015); DGL: Dominion Group Metalava (Jackson 1994); VS: Ventersdorp Supergroup (Gumsley et al. 2020).

Table 1 - Major and Trace element data for epidiorite, granite, and Felsic and Mafic Granophyre. Major element data are presented in wt%, and total Fe as $Fe_2O_3$. LOI – Loss on Ignition. Trace element data are presented in ppm.

a) Major element data

| Sample | AR-54 | ARp-38A | ARp-38B | ARp-38C | ARp-38D | ARp-38E | ARp-38F | ARp-38G | ARp-38H | ARp-38I |
|---|---|---|---|---|---|---|---|---|---|---|
| Lithology | Epidiorite | Felsic Granophyre | Mafic Granophyre | Felsic Granophyre | Felsic Granophyre | Felsic Granophyre | Mafic Granophyre | Mafic Granophyre | Mafic Granophyre | Mafic Granophyre |
| $SiO_2$ | 52.26 | 66.31 | 63.29 | 65.89 | 68.59 | 67.09 | 62.90 | 58.55 | 61.97 | 62.60 |
| $TiO_2$ | 0.39 | 0.47 | 0.57 | 0.53 | 0.50 | 0.49 | 0.65 | 0.55 | 0.59 | 0.60 |
| $Al_2O_3$ | 15.36 | 12.82 | 13.45 | 13.15 | 12.38 | 12.84 | 13.42 | 12.57 | 13.33 | 13.60 |
| $Fe_2O_3$ | 8.61 | 7.13 | 8.57 | 7.57 | 7.14 | 7.16 | 8.60 | 8.56 | 8.86 | 9.09 |
| MnO | 0.16 | 0.17 | 0.17 | 0.14 | 0.13 | 0.14 | 0.14 | 0.14 | 0.14 | 0.15 |
| MgO | 8.77 | 3.84 | 3.97 | 3.80 | 3.49 | 3.63 | 3.54 | 3.84 | 4.27 | 4.12 |
| CaO | 12.73 | 4.02 | 5.55 | 4.82 | 4.55 | 4.55 | 5.47 | 5.55 | 5.77 | 5.96 |
| $Na_2O$ | 1.69 | 2.63 | 2.80 | 2.69 | 2.68 | 2.53 | 2.83 | 2.71 | 2.86 | 2.87 |
| $K_2O$ | 0.16 | 2.39 | 1.85 | 2.02 | 1.88 | 2.06 | 1.89 | 1.63 | 1.68 | 1.72 |
| $P_2O_5$ | 0.03 | 0.07 | 0.09 | 0.08 | 0.07 | 0.08 | 0.09 | 0.08 | 0.09 | 0.09 |
| LOI | 0.75 | 0.15 | 0.18 | 0.12 | 0.18 | 0.25 | 0.29 | 0.21 | 0.27 | 0.17 |
| Sum | 101.01 | 100.05 | 100.50 | 100.85 | 101.62 | 100.85 | 99.84 | 94.40 | 99.87 | 100.99 |

| Sample | ARp-38J | ARp-38K | ARp-38L | ARp-38M | ARp-38N | AR-89 | AR-19 | AR-53 |
|---|---|---|---|---|---|---|---|---|
| Lithology | Felsic Granophyre | Felsic Granophyre | Felsic Granophyre | Felsic Granophyre | Felsic Granophyre | Mafic Granophyre | Felsic Granophyre | Felsic Granophyre |
| $SiO_2$ | 68.35 | 68.39 | 68.53 | 67.36 | 67.07 | 64.69 | 67.51 | 69.18 |
| $TiO_2$ | 0.46 | 0.47 | 0.46 | 0.47 | 0.49 | 0.55 | 0.45 | 0.49 |
| $Al_2O_3$ | 12.71 | 13.17 | 12.91 | 12.22 | 12.30 | 13.22 | 12.75 | 12.53 |
| $Fe_2O_3$ | 7.12 | 7.04 | 6.82 | 6.20 | 6.85 | 8.16 | 6.81 | 7.37 |
| MnO | 0.14 | 0.14 | 0.15 | 0.13 | 0.13 | 0.14 | 0.14 | 0.14 |
| MgO | 3.53 | 3.67 | 3.57 | 3.31 | 3.37 | 3.88 | 3.53 | 3.20 |
| CaO | 4.12 | 4.05 | 3.91 | 3.57 | 4.03 | 5.08 | 3.97 | 3.74 |
| $Na_2O$ | 2.66 | 2.84 | 2.80 | 2.67 | 2.62 | 2.66 | 2.53 | 2.37 |
| $K_2O$ | 2.22 | 2.31 | 2.28 | 2.00 | 1.99 | 1.95 | 2.25 | 2.06 |
| $P_2O_5$ | 0.08 | 0.07 | 0.07 | 0.07 | 0.08 | 0.08 | 0.07 | 0.08 |
| LOI | 0.15 | 0.23 | 0.13 | 0.40 | 0.18 | 0.38 | 0.21 | 0.07 |
| Sum | 101.56 | 102.42 | 101.67 | 98.44 | 99.13 | 100.82 | 100.24 | 101.36 |

| Sample | AR-13 | AR-83 | AR-88 | AR-92 | AR-93 | NWU-1 | NWU-2a | NWU-3 |
|---|---|---|---|---|---|---|---|---|
| Lithology | Felsic Granophyre | Felsic Granophyre | Felsic Granophyre | Felsic Granophyre | Mafic Granophyre | Felsic Granophyre | Epidiorite | Felsic Granophyre |
| $SiO_2$ | 69.34 | 69.15 | 69.77 | 70.38 | 65.48 | 63.14 | 50.6 | 66.7 |
| $TiO_2$ | 0.47 | 0.42 | 0.47 | 0.41 | 0.56 | 0.61 | 0.59 | 0.47 |
| $Al_2O_3$ | 11.76 | 11.8 | 11.55 | 11.49 | 12.64 | 13.32 | 16.2 | 12.7 |
| $Fe_2O_3$ | 7.19 | 7.1 | 7.13 | 6.94 | 9.15 | 10.1 | 11.3 | 7.3 |
| MnO | 0.14 | 0.15 | 0.14 | 0.15 | 0.15 | 0.17 | 0.17 | 0.15 |
| MgO | 3.15 | 3.4 | 3.11 | 3.34 | 3.7 | 4.22 | 5.58 | 3.48 |
| CaO | 3.45 | 3.7 | 3.58 | 3.58 | 4.96 | 5.9 | 11.2 | 3.96 |
| $Na_2O$ | 2.29 | 2.42 | 2.3 | 2.33 | 2.64 | 1.5 | 2.13 | 2.05 |
| $K_2O$ | 1.98 | 2.16 | 2.02 | 2.04 | 1.84 | 2.6 | 0.29 | 2.3 |
| $P_2O_5$ | 0.09 | 0.09 | 0.11 | 0.09 | 0.11 | 0.11 | 0.07 | 0.08 |
| LOI | -0.2 | 0.02 | 0.28 | 0.04 | -0.11 | -0.66 | 1.1 | 0.2 |
| Sum | 99.66 | 100.41 | 100.46 | 100.79 | 101.12 | 101.0 | 99.2 | 99.4 |

b) Trace element data

| Sample | AR-54 | ARp-38A | ARp-38B | ARp-38C | ARp-38D | ARp-38E | ARp-38F | ARp-38G | ARp-38H | ARp-38I |
|---|---|---|---|---|---|---|---|---|---|---|
| Lithology | Epidiorite | Felsic Granophyre | Mafic Granophyre | Felsic Granophyre | Felsic Granophyre | Felsic Granophyre | Mafic Granophyre | Mafic Granophyre | Mafic Granophyre | Mafic Granophyre |
| Sc | 36.30 | 14.40 | 20.18 | 17.94 | 17.45 | 17.12 | 21.39 | 22.21 | 20.41 | 23.21 |
| Cr | 742.3 | 330.1 | 221.8 | 216.7 | 192.2 | 216.8 | 157.4 | 175.7 | 200.4 | 185.1 |
| Co | 82.00 | 166.1 | 93.26 | 73.78 | 119.3 | 111.8 | 83.71 | 106.0 | 108.2 | 99.42 |
| Ni | 186.3 | 119.0 | 98.70 | 96.82 | 92.53 | 99.35 | 88.33 | 90.87 | 101.6 | 93.93 |
| Cu | 78.51 | 40.59 | 50.16 | 46.15 | 46.34 | 45.25 | 50.28 | 70.46 | 50.10 | 50.42 |
| Zn | 47.45 | 57.01 | 63.30 | 57.70 | 52.06 | 59.32 | 69.00 | 64.00 | 76.61 | 72.32 |
| Rb | 1.46 | 64.26 | 49.69 | 55.32 | 48.51 | 55.65 | 50.37 | 45.39 | 43.92 | 48.24 |
| Sr | 83.45 | 185.2 | 190.3 | 188.1 | 169.6 | 187.2 | 179.2 | 173.5 | 180.9 | 181.8 |
| Y | 11.02 | 13.69 | 16.46 | 14.64 | 14.32 | 14.38 | 17.48 | 16.50 | 16.83 | 16.95 |
| Zr | 29.99 | 133.2 | 126.2 | 126.4 | 120.3 | 124.1 | 128.4 | 115.2 | 116.0 | 119.6 |
| Nb | 1.17 | 6.67 | 6.44 | 6.11 | 5.68 | 6.02 | 6.39 | 5.49 | 5.64 | 5.73 |
| Ba | 38.57 | 405.1 | 355.3 | 386.8 | 358.0 | 391.2 | 364.8 | 314.5 | 319.6 | 331.0 |
| La | 3.51 | 29.70 | 28.00 | 28.65 | 26.86 | 29.24 | 29.04 | 25.51 | 26.06 | 26.13 |
| Ce | 7.34 | 55.11 | 51.86 | 53.87 | 49.50 | 52.78 | 53.49 | 47.15 | 47.86 | 48.73 |
| Pr | 0.97 | 5.95 | 5.57 | 5.77 | 5.41 | 5.84 | 5.74 | 5.19 | 5.12 | 5.45 |
| Nd | 4.13 | 20.50 | 21.13 | 20.22 | 19.52 | 20.79 | 20.48 | 18.76 | 19.05 | 19.38 |
| Sm | 1.21 | 3.55 | 3.85 | 3.69 | 3.45 | 3.78 | 4.12 | 3.76 | 3.61 | 3.88 |
| Eu | 0.48 | 0.91 | 0.99 | 0.96 | 0.86 | 0.98 | 1.00 | 0.99 | 0.92 | 0.95 |
| Gd | 1.42 | 2.90 | 3.29 | 3.29 | 3.15 | 3.20 | 3.62 | 3.27 | 3.31 | 3.15 |
| Tb | 0.28 | 0.45 | 0.50 | 0.45 | 0.46 | 0.45 | 0.53 | 0.48 | 0.51 | 0.51 |
| Dy | 1.87 | 2.51 | 3.00 | 2.87 | 2.73 | 2.76 | 3.40 | 3.13 | 3.09 | 3.19 |
| Ho | 0.43 | 0.50 | 0.62 | 0.55 | 0.54 | 0.54 | 0.66 | 0.65 | 0.65 | 0.65 |
| Er | 1.28 | 1.45 | 1.85 | 1.63 | 1.60 | 1.59 | 1.98 | 1.93 | 1.86 | 1.90 |
| Tm | 0.18 | 0.20 | 0.26 | 0.25 | 0.22 | 0.21 | 0.29 | 0.28 | 0.27 | 0.29 |
| Yb | 1.32 | 1.39 | 1.76 | 1.58 | 1.51 | 1.48 | 2.00 | 1.73 | 1.81 | 1.85 |
| Lu | 0.21 | 0.19 | 0.25 | 0.23 | 0.22 | 0.22 | 0.30 | 0.30 | 0.26 | 0.26 |
| Hf | 0.82 | 3.56 | 3.43 | 3.54 | 3.40 | 3.54 | 3.54 | 3.20 | 3.23 | 3.36 |
| Ta | 0.15 | 0.74 | 0.57 | 0.56 | 0.63 | 0.73 | 0.54 | 0.58 | 0.56 | 0.56 |
| Pb | 1.37 | 10.42 | 7.99 | 8.70 | 8.63 | 8.88 | 7.85 | 7.17 | 7.62 | 6.80 |
| Th | 0.49 | 6.56 | 5.21 | 5.79 | 5.27 | 5.89 | 5.47 | 4.76 | 4.83 | 4.93 |
| U | 0.10 | 1.61 | 1.10 | 1.15 | 1.18 | 1.25 | 1.06 | 0.92 | 1.02 | 0.99 |

| Sample | ARp-38J | ARp-38K | ARp-38L | ARp-38M | ARp-38N | AR-89 | AR-19 | AR-53 |
|---|---|---|---|---|---|---|---|---|
| Lithology | Felsic Granophyre | Felsic Granophyre | Felsic Granophyre | Felsic Granophyre | Felsic Granophyre | Mafic Granophyre | Felsic Granophyre | Felsic Granophyre |
| Sc | 15.46 | 15.56 | 14.44 | 13.35 | 14.81 | 19.43 | 16.33 | 14.20 |
| Cr | 277.4 | 271.6 | 273.9 | 282.8 | 225.3 | 206.3 | 277.6 | 970.1 |
| Co | 75.42 | 81.84 | 89.80 | 114.52 | 119.46 | 152.42 | 99.86 | 28.02 |
| Ni | 116.4 | 106.9 | 107.0 | 99.79 | 88.36 | 97.38 | 104.6 | 119.5 |
| Cu | 41.87 | 39.06 | 39.34 | 41.65 | 42.56 | 52.18 | 39.65 | 58.03 |
| Zn | 51.02 | 51.32 | 53.18 | 49.90 | 55.90 | 65.83 | 52.70 | 55.41 |
| Rb | 62.06 | 64.35 | 63.64 | 54.07 | 52.09 | 51.56 | 65.52 | 54.24 |
| Sr | 183.9 | 185.6 | 190.5 | 185.9 | 187.2 | 194.0 | 194.4 | 209.2 |
| Y | 13.30 | 13.58 | 13.22 | 13.67 | 14.45 | 16.27 | 14.13 | 13.52 |
| Zr | 128.8 | 130.8 | 131.8 | 126.9 | 127.5 | 135.4 | 135.1 | 131.8 |
| Nb | 6.48 | 6.61 | 6.58 | 5.82 | 5.87 | 6.31 | 7.01 | 5.78 |
| Ba | 391.8 | 393.4 | 401.2 | 423.4 | 411.5 | 370.7 | 409.0 | 452.2 |
| La | 29.58 | 31.00 | 30.50 | 31.13 | 28.49 | 29.48 | 30.95 | 31.15 |
| Ce | 54.20 | 56.36 | 55.68 | 57.81 | 53.71 | 54.58 | 56.98 | 57.60 |
| Pr | 5.88 | 5.99 | 6.00 | 6.33 | 5.72 | 5.64 | 6.05 | 6.18 |
| Nd | 20.34 | 21.55 | 21.38 | 22.70 | 21.20 | 20.88 | 20.70 | 22.10 |
| Sm | 3.72 | 3.55 | 3.50 | 3.96 | 3.99 | 3.82 | 3.81 | 3.89 |
| Eu | 0.97 | 0.92 | 0.91 | 0.91 | 0.94 | 1.03 | 0.93 | 0.97 |
| Gd | 2.92 | 3.18 | 2.98 | 3.17 | 3.16 | 3.42 | 2.94 | 3.12 |
| Tb | 0.43 | 0.47 | 0.45 | 0.47 | 0.42 | 0.49 | 0.43 | 0.47 |
| Dy | 2.59 | 2.73 | 2.61 | 2.74 | 2.84 | 2.87 | 2.60 | 2.66 |
| Ho | 0.52 | 0.53 | 0.54 | 0.52 | 0.54 | 0.63 | 0.51 | 0.54 |
| Er | 1.52 | 1.49 | 1.44 | 1.53 | 1.61 | 1.81 | 1.38 | 1.47 |
| Tm | 0.22 | 0.21 | 0.21 | 0.21 | 0.23 | 0.25 | 0.21 | 0.21 |
| Yb | 1.40 | 1.42 | 1.36 | 1.39 | 1.48 | 1.65 | 1.43 | 1.37 |
| Lu | 0.24 | 0.21 | 0.22 | 0.21 | 0.23 | 0.25 | 0.21 | 0.21 |
| Hf | 3.81 | 3.68 | 3.71 | 3.48 | 3.38 | 3.64 | 3.72 | 3.45 |
| Ta | 0.63 | 0.67 | 0.73 | 0.80 | 0.66 | 0.70 | 0.84 | 0.42 |
| Pb | 9.88 | 10.50 | 10.02 | 9.20 | 8.83 | 9.55 | 9.63 | 9.01 |
| Th | 6.54 | 6.84 | 6.71 | 5.89 | 5.77 | 5.74 | 6.86 | 5.46 |
| U | 1.51 | 1.62 | 1.48 | 1.43 | 1.24 | 1.09 | 1.60 | 1.22 |

| Sample | AR-13 | AR-83 | AR-88 | AR-92 | AR-93 | NWU-1 | NWU-2a | NWU-3 |
|---|---|---|---|---|---|---|---|---|
| Lithology | Felsic Granophyre | Felsic Granophyre | Felsic Granophyre | Felsic Granophyre | Mafic Granophyre | Felsic Granophyre | Epidiorite | Felsic Granophyre |
| Sc | | | | | | | 39.0 | 14.0 |
| Cr | | | | | | | 10 | 240 |
| Co | 25.7 | 24 | 24.7 | 24.1 | 33.2 | 41.5 | 44 | 20 |
| Ni | 107 | 103 | 101 | 104 | 102 | 113.0 | 72 | 89 |
| Cu | 48 | 39 | 45 | 41 | 50 | 64.0 | 111 | 55 |
| Zn | 72 | 60 | 54 | 43 | 73 | 82.0 | 74 | 49 |
| Rb | 70 | 75.6 | 67.4 | 73.3 | 59.1 | 55.5 | 6 | 72 |
| Sr | 225 | 213 | 228 | 205 | 229 | 217.0 | 122 | 204 |
| Y | 13.27 | 12.37 | 13.17 | 12.53 | 15.33 | 18.0 | 16 | 13 |
| Zr | 144 | 138 | 140 | 138 | 137 | 131.0 | 48 | 131 |
| Nb | 6.27 | 6.56 | 5.9 | 6.6 | 5.93 | 6.0 | 2 | 6 |
| Ba | 474 | 416 | 460 | 412 | 404 | 365.0 | 96 | 393 |
| La | 22.6 | 20.8 | 22.5 | 21.1 | 22.6 | 20.5 | 4.5 | 23 |
| Ce | 45.1 | 40.6 | 43.5 | 41.8 | 43.4 | 41.1 | 8.8 | 43.5 |
| Pr | 4.6 | 4.41 | 4.66 | 4.34 | 4.65 | 4.2 | 1.04 | 4.76 |
| Nd | 17.4 | 16 | 17.1 | 16.1 | 17.4 | 15.8 | 4.9 | 16.6 |
| Sm | 3.2 | 2.7 | 3.1 | 2.9 | 3.1 | 3.0 | 1.3 | 3.1 |
| Eu | 0.74 | 0.64 | 0.77 | 0.68 | 0.77 | 0.8 | 0.56 | 0.69 |
| Gd | 2.59 | 2.43 | 2.78 | 2.46 | 2.99 | 3.0 | 1.9 | 2.9 |
| Tb | 0.38 | 0.37 | 0.41 | 0.38 | 0.44 | 0.5 | 0.36 | 0.42 |
| Dy | 2.36 | 2.12 | 2.37 | 2.14 | 2.78 | 3.0 | 2.48 | 2.39 |
| Ho | 0.44 | 0.43 | 0.47 | 0.4 | 0.53 | 0.6 | 0.52 | 0.47 |
| Er | 1.3 | 1.27 | 1.34 | 1.34 | 1.6 | 1.8 | 1.57 | 1.36 |
| Tm | 0.19 | 0.17 | 0.2 | 0.17 | 0.25 | 0.2 | 0.23 | 0.18 |
| Yb | 1.2 | 1.3 | 1.3 | 1.1 | 1.5 | 1.7 | 1.5 | 1.2 |
| Lu | 0.17 | 0.17 | 0.19 | 0.17 | 0.24 | 0.3 | 0.27 | 0.2 |
| Hf | 3.52 | 3.46 | 3.45 | 3.25 | 3.28 | 3.3 | 1.2 | 3.4 |
| Ta | 0.69 | 0.68 | 0.56 | 0.68 | 0.54 | 0.5 | 0.2 | 0.5 |
| Pb | | | | | | | | |
| Th | 6.1 | 6.4 | 5.9 | 6.3 | 5.6 | 5.2 | 0.9 | 6.3 |
| U | 1.61 | 1.78 | 1.49 | 1.76 | 1.29 | 1.2 | 0.3 | 1.8 |

### 4.4. Sr and Nd isotope analysis

All isotope analytical data are compiled in Table 2, and the results are displayed in the diagrams of Figure 13. In the $^{87}Rb/^{86}Sr$ versus $^{87}Sr/^{86}Sr$ diagram (Fig. 12a), all data fall onto a reference line that reflects potential mixing between two endmembers, Archean granite from the Basement Complex, as exemplified here by a grey gneiss from the Rand Granite Quarry (Reimold et al., 2017) at the one extreme with the highest $^{87}Rb/^{86}Sr$ ratios and $^{87}Sr/^{86}Sr$ ratios and the metabasalt from the Dominion Group Lava at the other extreme, with the lowest $^{87}Rb/^{86}Sr$ and $^{87}Sr/^{86}Sr$ ratios. Such a mixing trend is also suggested by the $^{87}Sr/^{86}Sr$ versus Sr diagram mixing diagram of Figure 12b. However, the impact melt rock (Granophyre) data here plot together with the values for epidiorite samples – clearly off the mixing trend from data for granite and DGL. In fact, both Felsic and Mafic Granophyre display strong affinity in their isotopic character to epidiorite samples.

The εNd (t= 2020 Ga, the impact age) values for Felsic Granophyre samples are between −11.18 (AR 53) and −12.65 (Arp 38K), and between -11.45 (ARp-38F) and -12,61(ARp-38B) for Mafic Granophyre. The $T_{DM}$ model ages are between 3.07 and 3.18 Ga for Felsic and 3.14 and 3.22 Ga for Mafic Granophyre (Table 2b).

Note that two samples of Felsic Granophyre (ARp38C and Arp38N) are distinct from the other melt rock samples in the $^{147}Sm/^{144}Nd$ versus $^{143}Nd/^{144}Nd$ diagram (Fig. 12c). However, there is no petrographic or geochemical evidence/reason that could explain this finding.

The newly analyzed epidiorite samples, in the $^{143}Nd/^{144}Nd$ versus Nd systematics, seem to be slightly depleted in Nd in comparison with the samples analyzed by Reimold et al. (2017). Mafic Granophyre data plot closer to epidiorite than granite so that admixture of Granophyre-like impact melt to the granite appears unlikely. In Rb-Sr and Sm-Nd isotopic systematics (Fig. 12), Mafic and Felsic Granophyre have similar isotopic compositions. Moreover, Mafic Granophyre has more affinity to the epidiorite than Felsic Granophyre. In contrast, Dominion Group metalava does not seem to be related to Granophyre based on its isotopic composition (Fig. 12d).

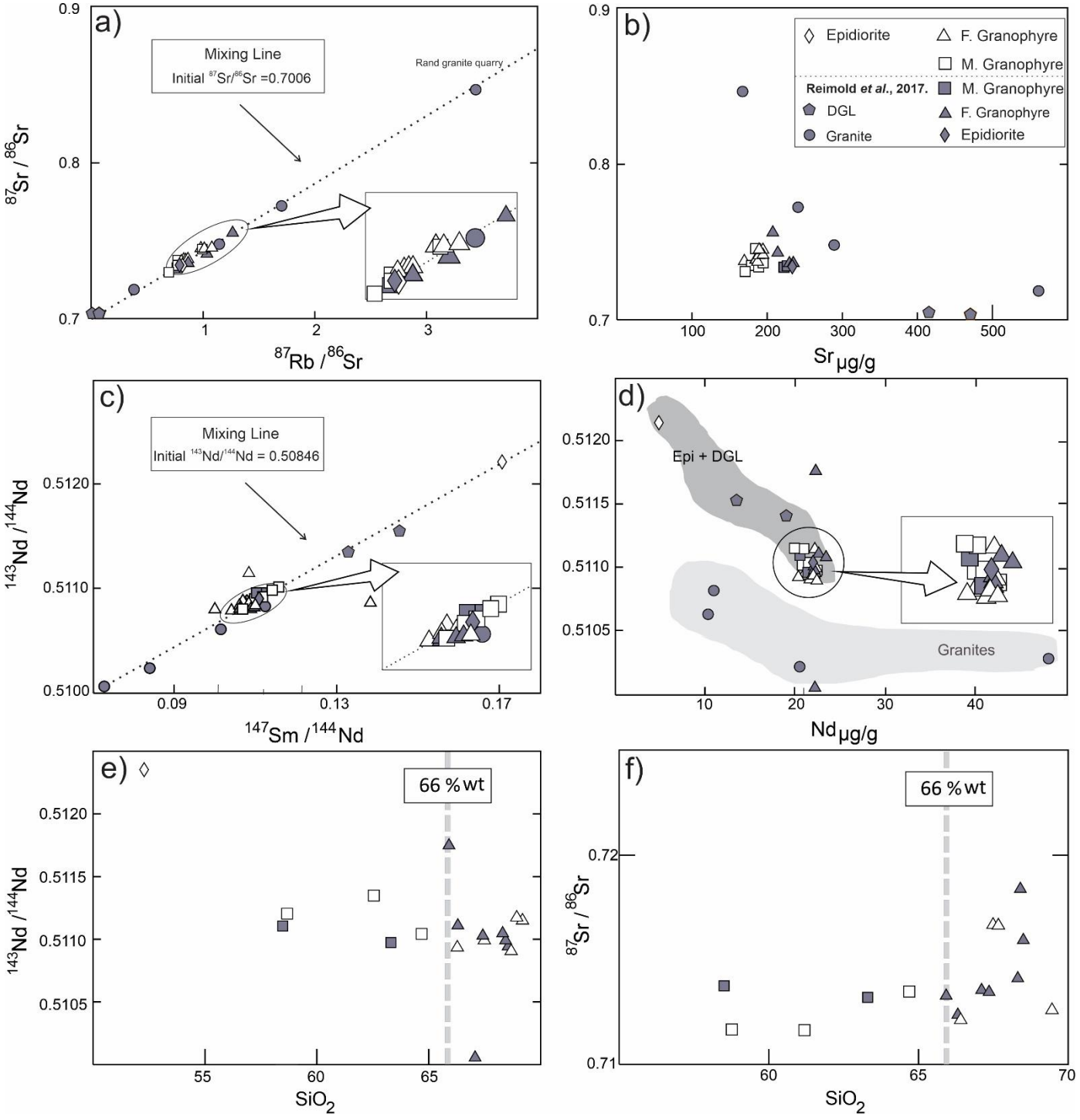


Figure 12 - Isotopic results for Mafic and Felsic Granophyre, and from the potential precursor rocks epidiorite, several granites, and Dominion Group metalava (data from Reimold et al. 2017). (a) $^{87}Rb$-$^{86}Sr$ versus $^{87}Sr$-$^{86}Sr$, and (b) Sr versus $^{87}Sr/^{86}Sr$. (c) $^{147}Sm/^{144}Nd$ versus $^{143}Nd/^{144}Nd$. (d) Nd versus$^{143}Nd/^{144}Nd$, showing a stronger data scatter for the precursor lithologies than in the other diagrams. The epidiorite values from this work are slightly depleted in Nd in comparison with the data from Reimold et al. (2017). Mafic and Felsic Granophyre data are similar, but the mafic samples plot closer to epidiorite than to any granite data. (e, f) $SiO_2$ versus$^{143}Nd/^{144}Nd$ and $^{87}Sr/^{86}Sr$ diagrams indicating the cutoff at 66 wt% $SiO_2$ between felsic and mafic samples.

Table 2 - Results of isotopic analysis of epidiorite and Granophyre from Farm Rensburgdrif. Samples analyzed at the University of Brasilia; fc = as measured and corrected for fractionation; $_{(T)}$ = measured values recalculated to impact time (2020 Ma). Uncertainties on isotope ratios are given as the least significant digits of the values as 2 sigma standard errors (2se). Samples ARp-38 (A, G, I, L) in light grey were analysed by ICP-MS at University of Brasília. Samples ARp-38 (G, I, L), AR-53, and AR-54 in dark grey were analysed at Institut für Geologie und Mineralogie at Universität zu Köln.

**a)**

| Sample | Lithology Type | Rb [µg/g] | Sr [µg/g] | $^{87}Rb/^{86}Sr$ | $^{87}Sr/^{86}Sr_{[fc]}$ | 2se | $^{87}Sr/^{86}Sr_{(T)}$ |
|---|---|---|---|---|---|---|---|
| AR-19 | F. Granophyre | 65.52 | 194.4 | 0.9753 | 0.74508 | 0.00001 | 0.71670 |
| AR-53 | F. Granophyre | 54.24 | 209.2 | | | | |
| AR-54 | Epidiorite | 1.46 | 83.4 | | | | |
| AR-53 | F. Granophyre | 60.35 | 218.1 | 0.8028 | 0.73460 | 0.00006 | 0.70367 |
| AR-54 | Epidiorite | 1.78 | 90.0 | 0.0572 | 0.70533 | 0.00008 | 0.71908 |
| AR-89 | M. Granophyre | 51.56 | 194.0 | 0.7683 | 0.73583 | 0.00002 | 0.71347 |
| ARp-38A | F. Granophyre | 64.30 | 185.2 | 1.0039 | 0.74548 | 0.00001 | 0.71627 |
| ARp-38B | M. Granophyre | 49.69 | 190.3 | 0.7548 | 0.73514 | 0.00003 | 0.71318 |
| ARp-38C | F. Granophyre | 55.32 | 188.1 | 0.8505 | 0.73812 | 0.00003 | 0.71337 |
| ARp-38D | F. Granophyre | 48.51 | 169.6 | 0.8271 | 0.73780 | 0.00001 | 0.71373 |
| ARp-38E | F. Granophyre | 55.65 | 187.2 | 0.8598 | 0.73847 | 0.00003 | 0.71345 |
| ARp-38F | M. Granophyre | 50.37 | 179.2 | 0.8127 | 0.73601 | 0.00001 | 0.71236 |
| ARp-38G | M. Granophyre | 45.39 | 173.5 | 0.7019 | | | |
| ARp-38I | M. Granophyre | 48.24 | 181.8 | 0.7669 | 0.73353 | 0.00002 | 0.71121 |
| ARp-38J | F. Granophyre | 62.06 | 183.9 | 0.9765 | 0.74685 | 0.00001 | 0.71844 |
| ARp-38K | F. Granophyre | 64.35 | 185.6 | 1.0031 | 0.74518 | 0.00002 | 0.71599 |
| ARp-38L | F. Granophyre | 63.64 | 190.5 | 0.9667 | 0.74503 | 0.00001 | 0.71690 |
| ARp-38M | F. Granophyre | 54.07 | 185.9 | 0.8410 | 0.73863 | 0.00002 | 0.71416 |
| ARp-38N | F. Granophyre | 52.09 | 187.2 | 0.8044 | 0.73691 | 0.00003 | 0.71350 |

**b)**

| Sample | Lithology Type | $SiO_2$ | Sm [µg/g] | Nd [µg/g] | $^{147}Sm/^{144}Nd$ | $^{143}Nd/^{144}Nd_{[fc]}$ | 2se | $\varepsilon Nd_{(0)}$ | $^{143}Nd/^{144}Nd_{(T)}$ | $\varepsilon Nd_{(T)}$ | TDM |
|---|---|---|---|---|---|---|---|---|---|---|---|
| AR-19 | F. Granophyre | 67.51 | 3.82 | 22.36 | 0.1041 | 0.510786 | 0.00001 | -36.30 | 0.509401 | -12.35 | 3.13 |
| AR-53 | F. Granophyre | 69.18 | 3.89 | 22.19 | 0.1069 | 0.510883 | 0.00002 | -34.41 | 0.509461 | -11.18 | 3.07 |
| AR-54 | Epidiorite | 52.26 | 1.21 | 4.31 | 0.1707 | 0.512211 | 0.00002 | -8.50 | 0.509941 | -1.76 | - |
| AR-89 | M. Granophyre | 64.69 | 3.87 | 21.45 | 0.1100 | 0.510879 | 0.00002 | -34.49 | 0.509416 | -12.07 | 3.17 |
| ARp-38A | F. Granophyre | 66.31 | 3.836 | 21.937 | 0.1065 | 0.510816 | 0.00002 | -35.72 | 0.509400 | -12.38 | 3.15 |
| ARp-38B | M. Granophyre | 63.29 | 3.91 | 21.46 | 0.1110 | 0.510864 | 0.00002 | -34.78 | 0.509388 | -12.61 | 3.22 |
| ARp-38C | F. Granophyre | 65.89 | 3.96 | 22.24 | 0.1084 | 0.511144 | 0.00001 | -29.32 | 0.509702 | -6.44 | 2.73 |
| ARp-38D | F. Granophyre | 68.59 | 3.69 | 20.52 | 0.1095 | 0.510896 | 0.00001 | -34.16 | 0.509440 | -11.59 | 3.13 |
| ARp-38E | F. Granophyre | 67.09 | 3.93 | 22.09 | 0.1083 | 0.510851 | 0.00001 | -35.03 | 0.509410 | -12.17 | 3.16 |
| ARp-38F | M. Granophyre | 62.90 | 4.17 | 22.73 | 0.1119 | 0.510935 | 0.00002 | -33.40 | 0.509447 | -11.45 | 3.14 |
| ARp - 38G | M. Granophyre | 58.55 | 3.85 | 20.79 | 0.1129 | 0.510949 | 0.00001 | -33.12 | 0.509448 | -11.44 | 3.15 |
| ARp - 38I | M. Granophyre | 62.60 | 3.76 | 20.26 | 0.1130 | 0.510951 | 0.00001 | -33.08 | 0.509448 | -11.43 | 3.15 |
| ARp -38G | M. Granophyre | 58.55 | 3.52 | 19.35 | 0.1101 | 0.510915 | 0.00008 | -33.61 | 0.509451 | -11.2 | 3.17 |
| ARp-38I | M. Granophyre | 62.60 | 3.34 | 17.85 | 0.1130 | 0.510904 | 0.00023 | -33.82 | 0.509402 | -12.2 | 3.29 |
| ARp-38J | F. Granophyre | 68.35 | 3.87 | 22.09 | 0.1068 | 0.510817 | 0.00001 | -35.70 | 0.509396 | -12.45 | 3.16 |
| ARp-38K | F. Granophyre | 68.39 | 3.87 | 22.11 | 0.1067 | 0.510805 | 0.00002 | -35.93 | 0.509386 | -12.65 | 3.18 |
| ARp-38L | F. Granophyre | 68.53 | 3.93 | 21.95 | 0.1089 | 0.510812 | 0.00001 | -35.79 | 0.509364 | -13.09 | 3.24 |
| ARp-38L | F. Granophyre | 68.53 | 3.41 | 19.42 | 0.1060 | 0.510838 | 0.00020 | -35.11 | 0.509428 | -11.6 | 3.16 |
| ARp-38M | F. Granophyre | 67.36 | 4.19 | 24.08 | 0.1061 | 0.510833 | 0.00001 | -35.38 | 0.509422 | -11.95 | 3.12 |
| ARp-38N | F. Granophyre | 65.89 | 5.01 | 22.07 | 0.1383 | 0.510859 | 0.00001 | -34.88 | 0.509020 | -19.83 | 4.51 |

# 5. DISCUSSION

The primary objective for this study was to investigate the extension of the Granophyre dike in the northwestern sector of the Vredefort Dome (Fig. 1), south of the Vaal River on and beyond Farm Rensburgdrif. The possibility that a mafic variety of Granophyre could occur in this section on Rensburgdrif, as suggested by Lieger (2011), was investigated. Field geological and petrographic characterization of the Granophyre was to be carried out, as well as new geochemical analyses, including Sr and Sm-Nd isotope analyses, to be obtained.

### *Field Observations*

The analysis of the profile across the dike (Fig.4) indicated in the field that the Granophyre appeared relatively uniform but still had some variables. There is a significant variation in the abundances of the main modal components. Two distinct phases were identified, whereby the clast-poor phase was observed in the central part of the dike, and the clast-rich phase at the margins. The contact between the Granophyre dike and epidiorite is not exposed on this property but generally within ca. 100 m from the western dike margin. Where the dike cuts granite, the contact is frequently distinct. In agreement with findings by Therriault et al. (1996), granite, quartzite, very little shale, and (locally) mafic clasts of contrasting sizes and mineral compositions occur. Several sets of joints along the dike with different orientations were observed, indicating that the dike solidified and thereafter was subject to brittle deformation, maybe during the phase of mechanical readjustment of the central uplift.

A geological map of the study area was produced at the 1:10,000 scale (Supplementary Material, Appendix 1). The background map to this figure was adapted from "The Geology of the Vredefort Dome" map (1:50.000 scale) by Bischoff (1999). Granophyre samples were collected along the dike in the margins and the central part. Target rocks (epidiorite and granite) were collected on outcrops located near the dike.

### *Petrography including mineral chemistry*

Clast-rich Granophyre samples (Felsic Granophyre) have fine-grained matrix with zoned pyroxene crystals and relatively large plagioclase laths. The clast-poor samples (Mafic Granophyre) have more pyroxene than the clast-rich phase (Felsic Granophyre). The matrix is slightly coarser-grained and has a granular texture,

plagioclase laths are smaller, pyroxene crystals are larger. In both granophyre types, amphibole is a secondary product of uralitization of subhedral pyroxene crystals. The round fragments of equigranular quartz aggregates found in the higher abundance in the clast-rich phase phase likely result from fine-grained recrystallization (annealing) of originally medium-grained quartz crystals of quartzitic or granitic lithic clasts.

The Mafic Granophyre, as observed on Farm Rensburgdrif, is equivalent to the rare “mafic" Granophyre samples already observed by earlier workers (Willemse, 1937 and Therriault et al., 1996), later by Lieger et al. (2011) and discussed by Lieger and Riller (2012), and most recently by Wannek (2015) and referred by Huber et al. (2020). Especially the work by Wannek (2015) provided observations on these two Granophyre types that allow us to state that these respective varieties on farms Kopjeskraal and Rensburgdrif are petrographically similar. This includes the similar proportion of groundmass, modal compositions, and hypidiomorphic texture types in the two different phases. Secondary biotite, chlorite, and amphibole in Granophyre were also noted by Therriault et al. (1996) and then related by Reimold and Gibson (2006) to the metamorphic grade in this limited to upper greenschist and lower amphibolite facies at the core-collar transition of the Vredefort Dome.

The medium- to coarse-grained granular pyroxenitic clasts found in Mafic Granophyre samples from Rensburgdrif must have been originally derived from mafic intrusive precursor lithologies. This pyroxene is also partially replaced by biotite, amphibole, and chlorite.

Mineral chemical results by Wannek (2015) show comparatively wider compositional ranges for plagioclase and pyroxene in both Felsic and Mafic Granophyre than have been observed here (Fig. 8). However, this author did not differentiate between analyses of cores and rims of such crystals. The pyroxene crystals observed in the Mafic Granophyre are larger and have a higher calcium content, explained by the presence of clinopyroxene (Fig. 7), indicating a more mafic composition. For the epidiorite sample of Wannek (2015), a range of plagioclase compositions narrower than our data was reported. However, in general, the two data sets are complementary.

### *Major and trace element geochemistry*

Our new major and trace element analyses of Granophyre samples define two fields for the felsic and the mafic samples that agree with Wannek's (2015)

distinction of Felsic and Mafic Granophyre compositions. The composition of Mafic Granophyre is characterized by less than 66 wt% $SiO_2$( range determined here for Rensburgdrif: 58.55 – 64.99 wt% $SiO_2$), whereas Felsic Granophyre has between 66 and 69.8 wt% $SiO_2$. Granite and epidiorite analyses bracket the Granophyre fields and could be considered endmembers of a mixing trend (Fig. 10). The meta-lava of the Dominion Group falls chemically between Mafic Granophyre and epidiorite. Major element abundances (especially $SiO_2$, $Al_2O_3$, MgO, and CaO) indicate that the Mafic Granophyre composition could, in principle, have formed by admixture of epidiorite or DGL to the Felsic Granophyre. This establishes a significant involvement of a mafic component in the formation of this Granophyre dike (Fig. 10) but does not allow to differentiate between the two optional mafic precursors.

As Mafic Granophyre has only been noted ever in this particular dike from the NW of the Vredefort Dome, its formation seems to be delimited to this locale. The trace element data in Table 2 (see also Fig. 9b) also allow us to distinguish between possible contributions to Felsic Granophyre from a mafic host rock. The HREE Mafic Granophyre pattern in Fig. 11 shows that epidiorite is more likely to represent the mafic component assimilated by Felsic Granophyre than DGL. If DGL had been admixed, the HREE abundance in Mafic Granophyre should have been strongly increased, which is not observed. This issue of DGL or epidiorite admixture is further pesued with assistance from isotopic evidence.

***Sr-Nd isotopes***

Rb-Sr and Sm-Nd isotopic ratios were determined for a series of samples of Granophyre and epidiorite to test the possibility that isotopic analysis could contribute to resolve the debate about the genesis of Mafic Granophyre from Vredefort, in comparison to the previous work of Reimold et al. (2017). It is remarkable that the formation of impact-generated melt rocks at 2.02 Ga apparently took place without essential isotopic fractionation. Another important observation is that the isotope data for Dominion Group meta-lava fall far off the Granophyre and epidiorite data array, which supports that DGL is an unlikely precursor for the Mafic Granophyre phase and, apparently, did not play a significant role in the formation of Vredefort Granophyre. This conclusion was previously reached by Reimold et al. (2017, 2021) based on their Rb-

Sr, Sm-Nd, Re-Os and Se isotopic data. In all four systems (Fig. 12), epidiorite is clearly favored as an endmember of mixing over DGL.

The εNd (t) values for Felsic Granophyre samples are between −11.18 (AR 53) and −12.65 (Arp 38K), and between -11.45 (ARp-38f) and -12,61(ARp-38B) for Mafic Granophyre. The $T_{DM}$ model ages are between 3.18 and 3.07 Ga for Felsic and 3.22 and 3.14 Ga for Mafic Granophyre (Table 2b). The basaltic-andesitic, ca. 2.7 Ga Ventersdorp Supergroup metavolcanics may have contributed to this mixture (see also Reimold et al. 2016, 2017). The presence of mafic clasts hosted by the Mafic Granophyre on Rensburgdrif and Kopjeskraal (this work; also, Wannek, 2015) provides strong support for this contribution. The $^{143}Nd/^{144}Nd$ versus Nd systematic shows that epidiorite has a strong contribution from the mafic component, the same was observed in the data reported by Reimold et al. (2017).

***Formation of the Mafic Granophyre***

Previous works (e.g., Therriault et al., 1997; Reimold and Gibson, 2006 and references therein) suggested that the genesis of Granophyre was explained by wholesale melting of several target rocks. The mafic character of selected Granophyre samples was explained for a long time by local assimilation of mafic country rock (possibly epidiorite that through time has been related to the Ventersdorp Supergroup). Lieger (2011) and Lieger et al. (2011) observed a Mafic Granophyre phase on Farm Kopjeskraal and suggested that a mafic phase could also occur on Rensburgdrif - but without providing proper geochemical evidence for this latter assertion. Lieger and Riller (2012) proposed that the chemical heterogeneity between fragment-rich and fragment-poor dike zones could be explained by variable assimilation of a mafic component. The mafic melt had been emplaced first in the dikes, and the more felsic and fragment-rich melts followed during a second emplacement pulse from the overlying impact melt sheet. Then, Wannek (2015) observed that the Mafic Granophyre actually occurs in the central part of the dike on Kopjeskraal, in contrast to Lieger (2011). Wannek (2015) and Reimold et al. (2017, 2021), based on extensive chemical and isotope geochemical evidence, proposed that the Mafic Granophyre on Kopjeskraal Farm was formed by local admixture (assimilation) of an epidiorite-type component during dike emplacement. The isotope data of Reimold et al. (2016, 2017) favored an epidiorite component instead of a DGL component.

According to, for example, Gibson and Reimold (2006), the distinctive clast population in the Vredefort impact melt rock, with strong metasedimentary and granitoid components, can only be explained by emplacement of the Granophyre from above, where the melt could assemble a clast population that involves all major supracrustal rock types (Transvaal Supergroup to Dominion Group), as well as Archean granitoid basement. Note again that the occurrence of Mafic Granophyre is not symptomatic for the 9 Granophyre dikes on the Vredefort Dome but that it is delimited to a single dike in the NW sector.

The compositional zoning in the dike could be explained by wall rock assimilation (e.g., Therriault *et al*., 1996, 1997), as the marginal zones of the dike are more enriched in wall rock material (granitoid) than the inner part of this dike. MgO and $SiO_2$ contents in fragment-poor Granophyre (3.9 wt% and 61.5 wt%, respectively) are intermediate between those of fragment-rich Granophyre (3.57 wt% MgO and 67 wt% $SiO_2$) and epidiorite country rock (8.8 wt% MgO and 52.3 wt% $SiO_2$). An additional sample of mafic composition was obtained in the eastern outer portion of the profile sampled across the dike (Fig. 4; Fig. 9).

The analyzed profile across the Rensburgdrif dike was sampled in an area where the immediate host rock is a granite gneiss on both sides of the Granophyre dike. The mafic phase is a zone that occurs in the interior of the dike, and the felsic phase is located along the margins.

The chemical and isotopic results for Granophyre, epidiorite and DGL samples show that the Mafic Granophyre is the result of assimilation of a mafic component, in all likelihood epidiorite (Reimold et al. 2017, 2021, and this work), by the Felsic Granophyre. Unfortunately, it was not possible to sample a profile across the dike exactly where it comes closest to the epidiorite in outcrop, due to the absence of sufficient outcrop at the northeastern end on Farm Rensburgdrif, as locally difficult access due to dense thornbrush vegetation hindered this. However, the two profile experiments done by Reimold et al. (2021) on Kopjeskraal and in the present study on Rensburgdrif, and the results of Wannek (2015) are consistent with respect to the occurrence of a Mafic Granophyre phase mainly in the central part of the dike. The few Granophyre samples collected in the relative vicinity of epidiorite on Rensburgdrif (e.g., AR-13 – 150 m from the nearest exposure of epidiorite; AR-53 – 100 m from epidiorite) have felsic composition. Only further work can provide clarity as to the more regional

distribution of, and the actual sizes of the likely raft-like occurrences of the mafic impact melt rock along this Granophyre dike at the NW core-collar boundary.

## 6. CONCLUSIONS

We have conducted a detailed multidisciplinary study of the Granophyre dike on Farm Rensburgdrif, south of the Vaal River, along the extension of the dike from farms Kopjeskraal and Eldorado, north of the Vaal River.

i. Analysis of the samples from a profile across the dike indicates that the Granophyre displays a relatively uniform mineral composition. Still, there is a significant variation in the abundance of the main modal components. Two distinct phases (felsic and mafic) of Granophyre were recognized, whereby the mafic phase (clast-poor) was observed in the inner part of the dike, as observed on Kopjeskraal to the north, and the felsic (clast-rich) type occurs closer to the dike margin.

ii. The Mafic Granophyre is equivalent to the rare “mafic" Granophyre samples already observed by previous workers (Willemse, 1937; Therriault et al., 1996), and then by Lieger et al. (2011), Lieger and Riller (2012), and Wannek (2015), in terms of matching petrographic and chemical characteristics.

iii. The relatively higher MgO and CaO contents in the Mafic Granophyre, compared to the Felsic Granophyre, favor a significant contribution from a mafic precursor to Felsic Granophyre towards the generation of Mafic Granophyre. Trace element data allow us to distinguish between possible contributions to Felsic Granophyre from a mafic host rock: based on evaluation of REE systematics, this mafic component is most likely derived from epidiorite.

iv. Other trace element data are less useful for the distinction of Mafic and Felsic Granophyre, except for Cu, Zn, Ba abundances that are comparatively higher in the Mafic Granophyre.

v. The Dominion Group meta-lava (DGL) isotope data plot far off the Granophyre and epidiorite data array in all Sr-Nd isotope diagrams (Fig. 12), which supports that this lithology is not a likely precursor for the Mafic Granophyre. The isotopic mixing trends strongly support formation of Mafic Granophyre as a mixture of Felsic Granophyre with epidiorite – as already supported by the Sr, Nd, Os, He isotope work of Reimold et al. (2017, 2021).

These results, in conjunction with the previous isotopic studies of Reimold et al. (2016, 2017; 2021), mitigate against the hypothesis that Mafic Granophyre represents a differentiate from the original impact melt body in the impact crater. They favor the epidiorite assimilation/admixture hypothesis for the formation of Mafic Granophyre. That phase seemingly only occurs in the NW dike of the Vredefort Dome is evidence for this assimilation to have occurred only locally at the core/collar boundary within the central uplift, as a result of stoping into mafic country rock by the Granophyre impact melt, during its descent along extensional fractures opened during the collapse phase of the central uplift. It is warranted to further pursue chemical/isotopic mapping to further delineate possible rafts of mafic contributor along the NW dike of Granophyre.

## 7. ACKNOWLEDGMENTS

The authors thank the Geological Society of South Africa for their REI Fund to support the field trip and Christo Meyer of Kopjeskraal Lodge for access and permission to collect samples on his property. We thank the Institute of Geosciences of the University of Brasilia for the use of laboratory infrastructure, including technicians. We are grateful to the technical staff of the geoscientific laboratories at the Vrije Universiteit Brussels, Research Unit: Analytical, Environmental, and Geo-Chemistry (AMGC), the Naturhistorisches Museum Wien, and the Department of Litosphere of Vienna University, and the Institut für Geologie und Mineralogie, Universität zu Köln for expert petrographic, chemical, and isotopic support. This is study was financed in part by the Coordenação de Aperfeiçoamento de Pessoal de Nível Superior - Brasil (CAPES) – Finance Code 001.

## 8. REFERENCES

Armstrong, R. A., Lana, C., Reimold, W. U., and Gibson, R. L. 2006. SHRIMP zircon age constraint on Mesoarchean crustal development in the Vredefort dome, central Kaapvaal craton, South Africa. In: Processes on the Early Earth., edited by Reimold, W.U., Gibson, R.L. Boulder, Colorado: Geological Society of America Special Papers. v. 405., pp. 233-253.

Bisschoff, A. A. 1982. Thermal metamorphism in the Vredefort Dome. Transactions of the Geological Society of South Africa 85:43-57.

Bisschoff, A. A. 1988. The history and origin of the Vredefort Dome. South African Journal of Science 84:413-417.

Bisschoff, A. A. 1999. The geology of the Vredefort Dome: explanation of geological sheets 2627CA, CB, CC, CD, DA, DC, and 2727AA, AB, BA, map 1:50,000 scale. Council for Geoscience, Geological Survey of South Africa, Petroria.

Gibson, R. L. 2002. Impact-induced melting of Archaean granulites in the Vredefort Dome, South Africa. I: Anatexis of metapelitic granulites. Journal of Metamorphic Geology 20:57-70.

Gibson, R. L. 2019. The Mesoarchaean Basement Complex of the Vredefort Dome, A Mid-Crustal Section Through the Central Kaapvaal Craton Exposed by Impact. In A. Kröner and A. Hofmann (eds.), The Archaean Geology of the Kaapvaal Craton, Southern Africa, Regional Geology Reviews., pp. 109-132.

Gibson, R. L., and Reimold, W. U. 2005. Shock pressure distribution in the Vredefort impact structure, South Africa. In: Large Meteorite Impacts and Planetary Evolution III v. 384., edited by Kenkmann, T., Hörz, F., and Deutsch, A. Geological Society of America Special Paper, pp. 329-349.

Gibson, R. L., and Reimold, W. U. 2008. Geology of the Vredefort Impact Structure: A Guide to Sites of Interest. Council for Geoscience, Pretoria, Memoir 97:181 pp.

Gibson, R. L., and Stevens, G. 1998. Regional metamorphism due to anorogenic intracratonic magmatism. Geological Society, London, Special Publications 138:121-135.

Gioia, S., and Pimentel, M. 2000. The Sm-Nd isotopic method in the Geochronology Laboratory of the University of Brasília. Anais da Academia Brasileira de Ciencias 72: 219-245.

Grieve, R., and Therriault, A. 2000. Vredefort, Sudbury, Chicxulub: Three of a Kind? Annual Review of Earth and Planetary Sciences 28: 305-338.

Gumsley, A., Stamsnijder, J., Larsson, E., Söderlund, U., Næraa, T., De Kock, M., Sałacińska, A., Gawęda, A., Humbert, F., and Ernst, R. 2020. Neoarchean large igneous provinces on the Kaapvaal Craton in southern Africa re-define the formation of the Ventersdorp Supergroup and its temporal equivalents. Geological Society of America Bulletin 132: 1829–1844

Hall, A. L., and Molengraaff, G. A. F. 1925. The Vredefort Mountain Land in the southern Transvaal and the northern Orange Free State. Verhandelingen, Koninklijke Akademie van Wetenschappen, Amsterdam 24:183 pp.

Hargraves, R. B. 1961. Shatter cones in the rocks of the Vredefort Ring. Trans. Geol. Soc. S. Afr. 64:147-154.

Hart, R. J., Nicolaysen, L. O., and Gale, N. H. 1981. Radioelement concentrations in the deep profile through Precambrian basement of the Vredefort structure. Journal of Geophysical Research: Solid Earth 86 (B11):10653-10661.

Henkel, H., and Reimold, W. U.1999. Magnetic Model of the Central Uplift of the Vredefort Impact Structure. LPSC XXX, Lunar and Planetary Institute, Houston, TX, Abstr. 1336.

Huber, M.S., Kovaleva, E. and Riller, U. 2020. Modeling the geochemical evolution of impact melts in terrestrial impact basins: Vredefort granophyre dikes and Sudbury offset dikes. Meteoritics. Planetary Science., 55: 2320-2337.

Ivanov, B. A. 2005. Numerical modeling of the largest terrestrial meteorite craters. Solar System Research 39:381-409.

Jackson, M. C. 1993. A review of the late Archean volcano-sedimentary Dominion Group and implications for the tectonic setting of the Witwatersrand Supergroup, South Africa. Journal of African Earth Sciences 15: 169-186.

Jackson, M. C. 1994. Geochemistry and metamorphic petrology of Dominion Group metavolcanics in the Vredefort area, South Africa. South African Journal of Geology 97 : 62-77.

Koeberl, C. 2014. The geochemistry and cosmochemistry of impacts. In: Treatise on Geochemistry, 2nd., edited by Holland, H.D. Amsterdam: Elsevier, pp.73-118.

Kovaleva, E., Huber, M.S., Roelofse, F., Tredoux, M., Praekelt, H. 2018. Pseudotachylite vein hosted by a clast in the Vredefort Granophyre: characterization, origin and relevance. South African Journal of Geology 121:51–68.

Lana, C., Gibson, R. L., Kisters, A. F. M., and Reimold, W. U. 2003. Archean crustal structure of the Kaapvaal craton, South Africa - evidence from the Vredefort dome. Earth and Planetary Science Letters 206:133-144.

Lana, C., Reimold, W. U., Gibson, R. L., Koeberl, C., and Siegesmund, S. 2004. Nature of the archean midcrust in the core of the Vredefort dome, Central Kaapvaal Craton, South Africa, Associate editor: B. R. Frost. Geochimica et Cosmochimica Acta 68:623–642.

Lieger, D. 2011. Structural and geochemical analyses of Fragment-rich pseudotachylite bodies and the Vredefort Granophyre of the Vredefort Impact Structure, South Africa. M.Sc. Thesis. Department of Earth Sciences, Freie Universität Berlin, Berlin, Germany, 212 pp.

Lieger, D., and Riller, U. 2012. Emplacement history of Granophyre dikes in the Vredefort Impact Structure, South Africa, inferred from geochemical evidence. Icarus 219., pp. 168-180.

Marsh, J. S. 2006. The Dominion Group - Chapter 6. In: The Geology of South Africa., edited by Johnson, M.R., Anhaeusser, C.R., and Thomas, R.J.: Geological Society of South Africa and Council for Geoscience, Pretoria., pp. 149-154

Pybus G.Q. 1995. Geological and mineralogical analysis of some mafic intrusives in The Vredefort Dome, Central Witwatersrand Basin. M.Sc. Thesis. University of the Witwatersrand, Johannesburg, South Africa. 376pp.

Raczek, I., Jochum, K. P., and Hofmann. A. W. 2003. Neodymium and strontium isotope data for USGS reference materials BCR-1, BCR-2, BHVO-1, BHVO-2, AGV-1, AGV-2, GSP-1, GSP-2 and eight MPI-DING reference glasses, Geostandard Newsletter, 27, 173 – 179.

Reimold, W. U. 1998. Exogenic and endogenic breccias: a discussion of major problematics. Earth Science Reviews 43:25-47.

Reimold, W. U., and Gibson, R. L. 2006. The melt rocks of the Vredefort impact structure - Vredefort Granophyre and pseudotachylitic breccias: Implications for impact cratering and the evolution of the Witwatersrand Basin. Chemie der Erde – Geochemistry 66:1-35.

Reimold, W.U., Horsch, H., and Durrheim, R. J. 1990. The “Bronzite” - granophyre from the

Vredefort structure - a detailed analytical study and reflections on the genesis of one of Vredefort's enigmas. Journal of Chemical Information and Modeling 53:1689-1699.

Reimold, W.U., Pybus, G.; Kruger, F., Layer, P., and Koeberl, C. 2000. The Anna's Rust Sheet and related gabbroic intrusions in the Vredefort Dome-Kibaran magmatic event on the Kaapvaal Craton and beyond?. Journal of African Earth Sciences 31. 499-521

Reimold, W.U., Cooper, G.R.J., Romano, R., Cowan, D.R., and Koeberl, C., 2006. Investigation of Shuttle Radar Topography Mission data of the possible impact structure at Serra da Cangalha, Brazil. Meteoritics and Planetary Science 41:237-246.

Reimold, W. U., Gentzmann, M., Hauser, N., Schmitt, R-T., Zaag, P., and Mohr-Westheide, T. 2016. A geochemical contribution to the discussion about the genesis of impact-related pseudotachylitic breccias: Studies of PTB in the Otavi and Kudu Quarries of the Vredefort Dome support the "In Situ Formation" hypothesis. South African Journal of Geology, 119:453-472.

Reimold, W. U., Hauser, N., Hansen, B. T., Thirlwall, M., and Hoffmann, M. 2017. The impact pseudotachylitic breccia controversy: Insights from first isotope analysis of Vredefort impact-generated melt rocks. Geochimica et Cosmochimica Acta 214:266-281.

Reimold, W. U., Schulz, T., König, S., Koeberl, C., Hauser, N., Wannek, D., Schimidt, R-T. 2021. Genesis of the mafic granophyre of the Vredefort Impact Structure (South Africa): Implications of new geochemical and Se and Re-Os isotope data. In Reimold, W. U., and Koeberl, C., eds., Large Meteorite Impacts and Planetary Evolution IV: Geological Society of America Special Paper 550: 235-254.

Spray, J., and Biren, M. 2021. Forthcoming. Distinguishing friction- from shock-generated melt products in hypervelocity impact structures. Large Meteorite Impacts and Planetary Evolution VI.

Sun, S.S. and McDonough, W.F. 1989. Chemical and isotopic systematics of oceanic basalts; implications for mantle composition and processes. In: Magmatism in the ocean basins. Saunders, A.D. and Norry, M.J. (Eds), Geological Society of London, London. 42: 313-345.

Therriault, A. M., Grieve, R. A. F., and Reimold, W. U. 1997. Original size of the Vredefort structure: Implications for the geological evolution of the Witwatersrand Basin. Meteoritics and Planetary Science 32, n. 1:71-77.

Therriault, A., Reimold, W.U., and Reid, A. M. 1996. Field relations and petrography of the Vredefort Granophyre. South African Journal of Geology 99:1-21.

Wannek D. S. 2015. Geologische Untersuchungen zur Genese des Vredefort Granophyrs im Nordwesten des Vredefort Doms. M.Sc. Thesis (unpubl.), Freie Universität Berlin, Berlin, Germany, 186pp.

Walraven F., Armstrong R. A., and Kruger F. J. 1990. A chronostratigraphic framework for the north-central Kaapvaal Craton, the Bushveld Complex and the Vredefort Structure. Tectonophysics 171:23–48

Weis, P., Beck, H.P., and Günther, D. 2005. Characterizing ablation and aerosol generation during elemental fractionation on absorption modified lithium tetraborate glasses using LA-ICP-MS. Analytical and Bioanalytical Chemistry 381, 212–224.

Willemse, J. 1937. On the old granite of the Vredefort region and some of its

associated rocks. Transactions of the Geological Society of South Africa 40:195–206.

Yang, L. 2009. Accurate and precise determination of isotopic ratios by MC-ICP-MS: A review. Mass Spectromy. Reviews, 28: 990-1011.

# 5. CHAPTER: DISCUSSION AND CONCLUSION

The primary purpose of this study was to investigate the extension of the Granophyre dike south of the Vaal River for the possible occurrence of two varieties of impact melt rock and their possible relationships to country rock. The formation of the impact melt rock dike related to the Vredefort impact structure can be understood by determining the geochemical and isotopic compositional, petrographic, and textural variability of Granophyre. Extensive petrographic and chemical investigations, including Sr and Sm-Nd isotope analysis of Granophyre and target rock samples, have been carried out for this work on the dike on farm Rensburgdrif.

## 5.1. Field Observations

The analysis of the profile across the dike (Fig.9) indicated in the field that the Granophyre had a relatively uniform appearance. Still, there is a significant variation in the abundances of the main modal components. Two distinct phases were identified, whereby the clast-poor phase was observed in the central part of the dike, and the clast-rich phase at the margins. The contact between the Granophyre dike and epidiorite is not exposed on this property but generally within ca. 100 m from the western dike margin. Where the dike cuts granite, the contact is frequently distinct. In agreement with findings by Therriault et al. (1996), granite, quartzite, very little shale, and (locally) mafic clasts of contrasting sizes and mineral compositions occur. Several sets of joints along the dike with different orientations were observed, indicating that the dike solidified and thereafter was subject to brittle deformation, maybe during the phase of mechanical readjustment of the central uplift in the consequence of the violent impact event.

A geological map of the study area was produced at the 1:10,000 scale (Supplementary Material, Appendix. 1). The background map to this figure was adapted from "The Geology of the Vredefort Dome" map (1:50.000 scale) by Bischoff (1999). The maps are very similar regarding the impact-melt rock occurrences and the dike position and orientation. The main difference between the maps is observed in the southwestern sector, to the SW of a prominent NW-SE trending fault that does not displace the Granophyre dike. In the southwestern section of the map, several host rocks were recorded with discordance between the two mappings. This may be related to the difference in scales and as the 1988 map was likely prepared to a large degree

based on stereoscopic interpretation of orthophotos.

### 5.2. Petrography including mineral chemistry

Clast-rich samples (Felsic Granophyre) have fine-grained matrix with short, zoned pyroxene crystals (10%), recrystallized, and relatively large plagioclase laths (30%), quartz (30%) and k-fledspar (25%) are subhedral. Mafic Granophyre (i.e., clast-poor zones) has more pyroxene (20%) than the first phase. The matrix is slightly coarser-grained and has a granular texture, plagioclase (25%) laths are smaller, pyroxene crystals are zoned and comparatively larger, and subhedral crystals of quartz (25%) and K-feldspar (15%) are easily recognized. In both phases, the amphibole is usually secondary product of uralitization of subhedral pyroxene crystals. The round fragments of equigranular quartz aggregates found in the Felsic phase, are likely resulted from fine-grained recrystallization (annealing) of originally medium-grained quartz crystals of a quartzitic or granitic clast.

The Mafic Granophyre, as observed on Farm Rensburgdrif, is equivalent to the rare “mafic" Granophyre samples already observed by earlier workers (Willemse, 1937 and Therriault et al., 1996), and then later by Lieger et al. (2011) and discussed by Lieger and Riller (2012), and most recently by Wannek (2015) and referred by Huber et al. (2022). Especially the work by Wannek (2015) provided observations on these two Granophyre types that allows us to state that these respective varieties on farms Kopjeskraal and Rensburgdrif are petrographically similar. This includes the similar proportion of groundmass, modal compositions, and hypidiomorphic texture types in the two different phases. The granular texture present in these Granophyre types was reported by Therriault et al. (1996) for the other core-collar dikes of the Dome as well. Secondary biotite, chlorite, and amphibole in Granophyre were also noted by Therriault et al. (1996) and then related by Reimold and Gibson (2006) to the metamorphic grade limited to upper greenschist and lower amphibolite facies at the core-collar transition of the Vredefort Dome.

The medium- to coarse-grained granular pyroxenitic clasts found in Mafic Granophyre samples from Rensburgdrif may have been originally derived from mafic intrusive precursor lithologies. This pyroxene is also partially replaced by biotite, amphibole, and chlorite.

Mineral chemical results by Wannek (2015) show comparatively wider compositional ranges for plagioclase and pyroxene in both Felsic and Mafic Granophyre than have been observed here (Fig. 8). However, this author did not differentiate between analyses of cores and rims of such crystals. The pyroxene crystals observed in the Mafic Granophyre are larger and have a higher calcium content, explained by the presence of clinopyroxene (Fig. 8), indicating a more mafic composition. For the epidiorite sample of Wannek (2015), a range of plagioclase compositions narrower than our data was reported.

### 5.3. Major and trace elements

Our new major and trace element analyses of Granophyre samples define two fields for the felsic and the mafic samples that agree with Wannek's (2015) distinction of Felsic and Mafic Granophyre compositions. The composition of Mafic Granophyre is characterized by less than 66 wt% $SiO_2$, whereas Felsic Granophyre has between 66 and 69.8 wt% $SiO_2$. Granite and epidiorite analyses bracket the Granophyre fields and could be considered endmembers of a mixing trend (Fig. 10). The meta-lava of the Dominion Group falls chemically between Mafic Granophyre and epidiorite. Harker diagrams show that Mafic Granophyre has a stronger affinity to epidiorite than to granite. Major element abundances (especially $SiO_2$, $Al_2O_3$, MgO, and CaO) indicate that the Mafic Granophyre composition could, in principle, have formed by admixture of epidiorite or DGL to the Felsic Granophyre. This establishes a significant involvement of a mafic component in the formation of this Granophyre dike (Fig. 10) but does not allow to differentiate between the two optional mafic endmembers.

The data define somewhat linear trends in the $Fe_2O_3$, MgO and CaO versus $SiO_2$ diagrams (Fig. 11). These trends show that the Mafic Granophyre composition is a mixture between the felsic phase and mafic host rock. Compared to the Felsic Granophyre, the mafic phase is significantly enriched in CaO, MgO, $Fe_2O_3$, Cu, and Zn. This could be due to the higher modal proportion of mafic and opaque minerals in the mafic endmembers. As Mafic Granophyre has only been noted ever in this particular dike from the NW of the Vredefort Dome, its formation seems to be delimited to this locale. Epidiorite generally has higher major element abundances than found in the Felsic Granophyre – in direct relation to the respective $SiO_2$ contents. The relatively

higher MgO and CaO contents favor that a significant contribution from epidiorite could have been incorporated into Felsic Granophyre towards the generation of Mafic Granophyre. The trace element data in Table 2 (see also Fig. 10b) also allow us to distinguish between possible contributions to Felsic Granophyre from a mafic host rock. The HREE Mafic Granophyre pattern in Fig. 12 shows that epidiorite is more likely to represent the mafic component assimilated by Felsic Granophyre than DGL. If DGL had been admixed, the HREE abundance in Mafic Granophyre should have been strongly increased, which is not observed.

However, the trace element Cr does not allow us to distinguish between possible contributions to felsic Granophyre from the host rock. Since, the Mafic Granophyre is depleted in Cr, for which, besides assimilation of an epidiorite component to Felsic Granophyre, must be considered a possible variability in the composition of the confirmed (Reimold et al., 1990) shale component. The West Rand shales of the Witwatersrand Supergroup, in part, are characterized by high Cr abundances (e.g., French et al., 1989). Discrepancies in Cr abundances are also noted between the data for Felsic Granophyre presented by Koeberl *et al*. (1996) and Reimold *et al*. (1990). And widely variable Cr abundances for mafic and Felsic Granophyre, were obtained by Wannek (2015).

### 5.4. Sr-Sm-Nd isotopes

Rb-Sr and Sm-Nd isotopic ratios were determined for a series of samples of Granophyre and epidiorite to test the possibility that isotopic analysis could contribute to resolve the debate about the genesis of Mafic Granophyre from Vredefort, in comparison to the previous work of Reimold et al. (2017, 2021). It is remarkable that the formation of impact-generated melt rocks at 2.02 Ga apparently took place without essential isotopic fractionation. Another important observation is that the isotope data for Dominion Group meta-lava fall far off the Granophyre and epidiorite isotope data array, which supports that DGL is an unlikely precursor for the Mafic Granophyre phase and, apparently, did not play a significant role in the formation of Vredefort Granophyre. This conclusion was previously reached by Reimold et al. (2017, 2021) based on their Sr, Sm-Nd, Re-Os and Se isotopic data. In all four systems (Fig. 12), epidiorite is clearly favored as an endmember of mixing over DGL.

The εNd (t) values for Felsic Granophyre samples are between −11.18 (AR 53) and −12.65 (Arp 38K), and between -11.45 (ARp-38f) and -12,61(ARp-38B) for Mafic Granophyre. The $T_{DM}$ model ages are between 3.18 and 3.07 Ga for Felsic and 3.22 and 3.14 Ga for Mafic Granophyre (Table 3b). These values are 1.10-1.18 units less negative than those for all other basement samples (~3.2 Ga), implying that the impact melt incorporates a component from a crust younger than the Archean granitoid precursor. The basaltic-andesitic, ca. 2.7 Ga Ventersdorp Supergroup metavolcanics may have contributed to this mixture (see also Reimold et al. 2016, 2017). The presence of mafic clasts hosted by the Mafic Granophyre on Rensburgdrif and Kopjeskraal (this work; also, Wannek, 2015) provides strong support for this contribution. The $^{143}Nd/^{144}Nd$ versus Nd systematic shows that epidiorite has a strong contribution from the mafic component, as observed in the data reported by Reimold et al. (2017).

### 5.5. Granophyre formation

Previously works (Therriault et al., 1997; Reimold and Gibson, 2006 and references therein) suggested that the genesis of Granophyre was explained by wholesale melting of target rocks. The mafic character of selected samples was explained for a long time by local assimilation of mafic country rock (possibly epidiorite that through time has been related to the Ventersdorp Supergroup). Lieger (2011) and Lieger et al. (2011) observed a Mafic Granophyre phase on Farm Kopjeskraal and suggested that a mafic phase could also occur on Rensburgdrif - but without providing proper geochemical evidence for this latter assertion. Lieger and Riller (2012) proposed that the chemical heterogeneity between fragment-rich and fragment-poor dike zones can be explained by variable assimilation of a mafic component. The mafic melt had been emplaced first in the dikes, and the more felsic and fragment-rich melts followed during a second emplacement pulse from the overlying impact melt sheet. Then, Wannek (2015) observed that the Mafic Granophyre actually occurs in the central part of the dike on Kopjeskraal, in contrast to Lieger (2011). Wannek (2015) and Reimold et al. (2017, 2021), based on extensive chemical and isotope geochemical evidence, proposed that the Mafic Granophyre on Kopjeskraal Farm was formed by local admixture (assimilation) of an epidiorite-type component during dike emplacement. The isotope data of Reimold et al. (2016, 2017) favored an epidiorite component instead a DGL component.

According to, for example, Gibson and Reimold (2006), the distinctive clast population in the Vredefort impact melt rock, with a strong metasedimentary and felsic igneous component, can only be explained by emplacement of the Granophyre from above, where the melt could assemble a clast population that involves all major supracrustal rock types (Transvaal Supergroup to Dominion Group), as well as Archean granitoid basement. Note again that the occurrence of Mafic Granophyre is not symptomatic for the 9 Granophyre dikes on the Vredefort Dome but that it is delimited to a single dike in the NW sector.

The compositional zoning in the dike can be explained by wall rock assimilation (e.g., Therriault *et al*., 1996, 1997), as the marginal zones of the dike are more enriched in wall rock material (granitoid) than the inner part of this dike. MgO and $SiO_2$ contents in fragment-poor zones (3.9 wt% and 61.5 wt%, respectively) are intermediate between those of fragment-rich zones (3.57 wt% MgO and 67 wt% $SiO_2$) and epidiorite country rock (8.8 wt% MgO and 52.3 wt% $SiO_2$). An additional sample of mafic composition was obtained in the eastern outer portion of the dike (Fig. 4).

The analyzed profile across the Rensburgdrif dike was sampled in an area where the immediate host rock is a granite gneiss on both sides of the Granophyre dike. The mafic phase occurs in the interior of the dike, and the felsic phase is located along the margins.

The chemical and isotopic results for Granophyre, epidiorite and DGL samples show that the Mafic Granophyre is the result of assimilation of a mafic component, in all likelihood epidiorite (Reimold et al. 2017, 2021, and this work), by the Felsic Granophyre. Unfortunately, it was not possible to sample a profile across the dike exactly where it comes close to the epidiorite in outcrop, due to the absence of sufficient outcrop at the northeastern end of Farm Rensburgdrif on the other side of the Vaal onto Farm Kommandonek (compare Fig. 1), as well as locally difficult access due to dense vegetation. However, the two profile experiments done by Reimold et al. (2021) on Kopjeskraal and in the present study on Rensburgdrif, and the results of Wannek (2015) are consistent with respect to the occurrence of a Mafic Granophyre occurring mainly in the central part of the dike. The few Granophyre samples collected in the relative vicinity of epidiorite on Rensburgdrif (e.g., AR-13 – 150 m from the nearest exposure of epidiorite; AR-53 – 100 m from epidiorite) have felsic composition. Only further work can provide clarity as to the more regional distribution of, and the

actual sizes of the likely raft-like occurrences of the mafic impact melt rock along this Granophyre dike at the NW core-collar boundary.

We have conducted a detailed multidisciplinary study of the Granophyre dike on Farm Rensburgdrif, south of the Vaal River, along the extension of the dike from farms Kopjeskraal and Eldorado, north of the Vaal River.

I. Analysis of the samples from a profile across the dike indicates that the Granophyre displays a relatively uniform mineral composition. Still, there is a significant variation in the abundance of the main modal components. Two distinct phases (felsic and mafic) of Granophyre were identified, whereby the mafic phase (clast-poor) was observed in the inner part of the dike, as observed on Kopjeskraal to the north, and the felsic (clast-rich) type occurs closer to the dike margin.

II. The Mafic Granophyre is equivalent to the rare “mafic" Granophyre samples already observed by previously workers (Willemse, 1937; Therriault et al., 1996), and then by Lieger et al. (2011), Lieger and Riller (2012), and Wannek (2015), in terms of matching petrographic and chemical characteristics.

III. The relatively higher MgO and CaO contents, and the isotopic results, in the Mafic Granophyre, compared to the Felsic Granophyre, favor a significant contribution from epidiorite to Felsic Granophyre towards the generation of Mafic Granophyre. Trace element data also allow us to distinguish between possible contributions to Felsic Granophyre from a mafic host rock – based on evaluation of REE systematics again most liely from epidiorite.

IV. Trace element data are less useful for the distinction of Mafic and Felsic Granophyre, except for Cu, Zn, Ba abundances that are higher in the Mafic Granophyre.

V. The Dominion Group metalava (DGL) isotope data plot far off the Granophyre and epidiorite data array in all Sr-Nd isotope diagrams (Fig. 12), which supports that this lithology is not a likely precursor for the Mafic Granophyre. The isotopic mixing trends strongly support formation of Mafic Granophyre as a mixture of Felsic Granophyre with epidiorite – as already supported by the isotope work of Reimold et al. (2017, 2021).

In conclusion, we can state that the results presented in this study, in conjunction with the earlier isotopic studies of Reimold et al. 2016, 2017, 2021),

mitigate against the hypothesis that Mafic Granophyre represents a differentiate from the original impact melt body. These results favor the epidiorite assimilation/admixture hypothesis for the formation of Mafic Granophyre. That this phase only occurs in the NW dike of impact melt rock on the Vredefort Dome is evidence for this assimilation having occurred only locally at the core/collar boundary within the central uplift.

## 6. REFERENCES


ANHAEUSSER, C. Archaean greenstone belts and associated granitic rocks - A review. **Journal of African Earth Sciences**, v. 100, p. 684-732, 2014.

ARMSTRONG, R. A., COMPSTON, W., RETIEF, E.A., WILLIAMS, I. S., WELKE, H.J. Zircon ion microprobe studies bearing on the age and evolution of the Witwatersrand triad. **Precambrian Research**, v. 53, n. 3–4, p. 243–266, 1991.

ARMSTRONG, R. A., LANA, C., REIMOLD, W. U., GIBSON, R. L. SHRIMP zircon age constraint on Mesoarchean crustal development in the Vredefort dome, central Kaapvaal craton, South Africa. In: Reimold, W.U., Gibson, R.L., (Eds.), Processes on the Early Earth, Geol. Soc. Amer., Boulder, Colorado**, Geological Society of America Special Papers.** v. 405, p. 233–253, 2006.

BISSCHOFF, A. A. The pseudotachylite of the Vredefort Dome. **Transactions of the Geological Society of South Africa,** v. 65, p. 207–225, 1962.

BISSCHOFF, A. A. The petrology of the igneous and metamorphic rocks in the Vredefort Dome and the adjoining parts of the Potchefstroom syncline. M.Sc. Thesis. **University of Pretoria, Pretoria, South Africa** p. 186,1969.

BISSCHOFF, A. A. The dioritic rocks of the Vredefort Dome. **Transactions of the Geological Society of South Africa,** v. 75, p. 31–45, 1972.

BISSCHOFF, A. A. Thermal metamorphism in the Vredefort Dome. **Transactions of the Geological Society of South Africa**, v. 85, p. 43–57, 1982.

BISSCHOFF, A. A. The history and origin of the Vredefort Dome. **South African Journal of Science,** v. 84, p. 413-417, 1988.

BISSCHOFF, A. A. The geology of the Vredefort Dome: Explanation of geological sheets 2627CA, CB, CC, CD, DA, DC, and 2727AA, AB, BA, map 1:50000 scale. **Council for Geoscience**, **Geological Survey of South Africa**. Pretoria., 1999.

BOON, J. D., ALBRITTON, C. C. Meteorite craters and their possible relationships to “cryptovolcanic structures”. **Field & Laboratory**, v. 5, p. 1–9, 1936.

BUCHANAN, P. C., REIMOLD, W. U. Planar deformation features and impact glass in inclusions from the Vredefort Granophyre, South Africa. **Meteoritics & Planetary Science**, v. 37, p. 807–822, 2002.

BUCHANAN, P. C., REIMOLD, W U., KOEBERL, C., KRUGER, F J. Rb–Sr and Sm–Nd isotopic compositions of the Rooiberg Group, South Africa: early Bushveld-related volcanism. **Lithos**, v. 75, n. 3, p. 373–388, 2004.

BÜHN, B., PIMENTEL, M. M., MATTEINI, M., DANTAS, E. L High spatial resolution analysis of Pb and U isotopes for geochronology by laser ablation multi-collector inductively coupled plasma mass spectrometry (LA-MC-ICP-MS). **Anais da Academia Brasileira de Ciências**, v. 81, n. 1, p. 99–114, mar. 2009.

CARTER, N. L. Basal quartz deformation lamellae; a criterion for recognition of impactites**. American Journal of Science**, v. 263, n. 9, p. 786-806, 1965.

CARTER, N.L. Dynamic deformation in quartz. In: French, B.M., Short, N.M. (Eds.), Shock Metamorphism of Natural Materials. **Mono Book Corporation, Baltimore**, p. 453–474, 1968.

CAWTHORN, R. G., EALES, H. V., WALRAVEN, F., CAWTHORN, A. R., UKEN, R., WATKEYS, M. K. The Bushveld complex. In: Johnson, M.R., Anhaeusser, C.R., Thomas, R.J. (Eds.), The Geology of South Africa. **Geological Society of South Africa, Johannesburg, and Council for Geoscience, Pretoria**, p. 261–281 (Chapter 11), 2006.

COETZEE, H., KRUGER, F.J. Geochronology and Srisotope geochemistry of the Losberg Complex and the limits of Bushveld Complex magmatism. **South African Journal of Geology**, v. 92, p. 37–41., 1994.

DALY, R. A. The Vredefort Ring-Structure of South Africa. **The Journal of Geology**, v. 55, n. 3, Part 1, p. 125–145, 1947.

DE WIT, M. J., DE RONDE., CORNEL E. J., TREDOUX, M., ROERING, C., HART, R. J., ARMSTRONG, R. A., GREEN, R. W. E., PEBERDY, E., HART, R. A. Formation of an Archaean continent. **Nature**, v. 357, n. 6379, p. 553–562, 1992.

DEPAOLO, D. J. Neodymium isotopes in the Colorado Front Range and crust–mantle evolution in the Proterozoic. **Nature**, v. 291, n. 5812, p. 193–196, 1981.

DIETZ,R. S. Meteorite impact suggested by orientation of shatter cones at the Kentland, Indiana, disturbance. **Science**, v. 105, p. 76, 1947.

DIETZ, R. S. Shatter cones in cryptoexplosion structures (meteorite impact?). **The Journal of Geology**, v. 67, p. 496–505, 1959.

DIETZ, R. S. Meteorite impact suggested by shatter cones in rock. **Science**, v. 131, p. 1781–1784, 1960.

DIETZ, R. S. Vredefort Ring Structure: Meteorite Impact Scar? **The Journal of Geology**, v. 69, n. 5, p. 499–516, 1961.

DRESSLER, B. O., REIMOLD, W. U. Terrestrial impact melt rocks and glasses. **Earth Science Reviews**, v. 56, n. 1, p. 205–284, 2001.

DRESSLER, B. O., REIMOLD, W. U. Order or chaos? Origin and mode of emplacement of breccias in floors of large impact structures. **Earth Science Reviews**, v. 67, n. 1–2, p. 1–54, 2004.

ERIKSSON, P. G., ALTERMANN, W., HARTZER, F. J. The Transvaal Supergroup and its precursors. In: Johnson, M.R., Anhaeusser, C.R., Thomas, R.J. (Eds.), The Geology of South Africa. **Geological Society of South Africa and Council for Geoscience**, Pretoria, p. 237–260 (Chapter 10), 2006.

FLETCHER P., REIMOLD W. U. Some notes and speculations on the pseudotachylites in the

Witwatersrand Basin and the Vredefort Dome. **South African Journal of Geology**, v. 92, p. 22–234, 1989.

FRENCH, B. M., KOEBERL, C. The convincing identification of terrestrial meteorite impact structures: What works, what doesn't, and why. **Earth Science Reviews**, v. 98, n. 1, p. 123–170, 2010.

FRENCH, B. M., NIELSEN, R. L. Vredefort bronzite granophyre: chemical evidence for origin as a meteorite impact melt. **Tectonophysics**, v. 171, n. 1–4, p. 119–138, 1990.

FRENCH, B.M., ORTH, C.J., QUINTANA, L. R. Iridium in the Vredefort Bronzite Granophyre: Impact melting and limits on a possible extraterrestrial component. **Proceedings of the Lunar and Planetary Science Conference** v. 19, p. 733–744, 1989.

GIBSON, R. L. Impact-induced melting of Archean granulites in the Vredefort Dome, South Africa. I: anatexis of metapelitic granulites. **Journal of Metamorphic Geology**, v. 20, n. 1, p. 57–70, 2002.

GIBSON, R. L. The Mesoarchaean Basement Complex of the Vredefort Dome—A Mid-Crustal Section Through the Central Kaapvaal Craton Exposed by Impact. In A. Kröner and A. Hofmann (eds.), The Archaean Geology of the Kaapvaal Craton, Southern Africa, **Regional Geology Reviews**, p. 109–132. 2019

GIBSON, R. L., REIMOLD, W. U. Shock pressure distribution in the Vredefort impact structure, South Africa. In: Kenkmann, T., Hörz, F., Deutsch, A. (Eds.), Large Meteorite Impacts and Planetary Evolution III, **Geological Society of America Special Paper**, v. 384, pp. 329–349, 2005.

GIBSON, R. L., REIMOLD, W. U. Geology of the Vredefort Impact Structure: A Guide to Sites of Interest. **Council for Geoscience memoir, Petroria**, v. 97, p. 181, 2008.

GIBSON, R. L., STEVENS, G. Regional metamorphism due to anorogenic intracratonic magmatism. **Geological Society, London, Special Publications**, v. 138, p. 121–135, 1998.

GIBSON, R. L., WALLMACH, T. Low pressure-high temperature metamorphism in the Vredefort Dome, South Africa: Anticlockwise pressure-temperature path followed by rapid decompression. **Geological Journal**, v. 30, n. 3-4, p. 319–331, 1995

GIBSON, R. L., ARMSTRONG, R. A., REIMOLD, W. U. The age and thermal evolution of the Vredefort impact structure: A single-grain U-Pb zircon study. **Geochimica et Cosmochimica Acta**, v. 61, n. 7, p. 1531–1540, 1997.

GIBSON, R. L., REIMOLD, W. U; STEVENS, G. Thermal-metamorphic signature of an impact event in the Vredefort dome, South Africa. **Geology**, v. 26, p. 787–790, 1998.

GIBSON, R. L., REIMOLD, W. U.; PHILLIPS, D.; LAYER, P. W. 40Ar/39Ar constraints on the age of metamorphism in the Witwatersrand Supergroup, Vredefort dome (South Africa). **South African Journal of Geology**, v. 103, n. 3–4, p. 175–190, 2000.

GIOIA, S., PIMENTEL, M. The Sm-Nd isotopic method in the Geochronology Laboratory of the University of Brasília**. Anais da Academia Brasileira de Ciencias**, v. 72, p. 219–245, 2000.

GOTTWALD M., KENKMANN T.; REIMOLD W. U. Terrestrial impact structures. **The TanDEM-X atlas**. Munich: Verlag Dr. Friedrich Pfeil. 608 p., 2020.

GRIEVE, R. A. Large-scale impact cratering on the terrestrial planets. **Advances in Space Research**, v. 12, p. 271–280, 1983.

GRIEVE, R. A. F. Terrestrial impact structures. **Annual Review of Earth and Planetary Sciences**v. 15, p. 245–270, 1987.

GRIEVE, R. A. F. The Terrestrial Cratering Record. **In: Peucker-Ehrenbrink B., Schmitz B. (eds)** Accretion of Extraterrestrial Matter Throughout Earth's History**.** Springer, Boston, MA., 2001.

GRIEVE, R. A. F., REIMOLD, W. U., MORGAN, J., RILLER, U., PILKINGTON, M. Observations and interpretations at Vredefort, Sudbury, and Chicxulub: Towards an empirical model of terrestrial impact basin formation. **Meteoritics and Planetary Science**, v. 43, n. 5, p. 855–882, 2008.

GRIEVE, R., THERRIAULT, A. Vredefort, Sudbury, Chicxulub: Three of a Kind? **Annual Review of Earth and Planetary Sciences**, v. 28, n. 1, p. 305–338, 2000.

GUMSLEY, A., STAMSNIJDER, J., LARSSON, E., SÖDERLUND, U., NÆRAA, T., DE KOCK, M., SAŁACIŃSKA, A., GAWĘDA, A., HUMBERT, F., ERNST, R. Neoarchean large igneous provinces on the Kaapvaal Craton in southern Africa re-define the formation of the Ventersdorp Supergroup and its temporal equivalentes. Geological **Society of America Bulletin** p. 132, 2020.

HALL, A. L., MOLENGRAAFF, G. A. F. The Vredefort Mountain Land in the southern Transvaal and the northern Orange Free State. **Verhandelingen, Koninklijke Akademie van Wetenschappen, Amsterdam**, v. 24, p. 183, 1925.

HARGRAVES, R. B. Shatter cones in the rocks of the Vredefort Ring. **Transactions of the Geological Society of South Africa** v. 64, p. 147–154, 1961.

HART, R. J., NICOLAYSEN, L. O., GALE, N. H. Radioelement concentrations in the deep profile through Precambrian basement of the Vredefort structure. **Journal of Geophysical Research: Solid Earth**, v. 86, n. B11, p. 10653-10661., 1981.

HENKEL, H., REIMOLD, W. U. Integrated geophysical modelling of a giant, complex impact structure: Anatomy of the Vredefort Structure, South Africa. **Tectonophysics**, v. 287, n. 1–4, p. 1–20, 1998.

HENKEL, H., REIMOLD, W. U. Magnetic Model of the Central Uplift of the Vredefort Impact Structure, LPSC XXX, **Lunar and Planetary Institute**, Houston, TX, Abstr, p. 1336 1999.

HECHT, L., WITTEK, A., RILLER, U., MOHR, T., SCHMITT, R., GRIEVE, R. Differentiation and emplacement of the Worthington Offset Dike of the Sudbury impact structure, Ontario. **Meteoritics & Planetary Science**. v.43, p. 1659-1679, 2008.

HUBER, M.S., KOVALEVA, E. RILLER, U. Modeling the geochemical evolution of impact melts in terrestrial impact basins: Vredefort granophyre dikes and Sudbury offset dikes. **Meteoritics Planetary Science,** v. 55, p. 2320-2337, 2020.

IVANOV, B. A. Numerical modeling of the largest terrestrial meteorite craters. **Solar System Research** v.39, p. 381-409, 2005.

JACKSON, M. C. A review of the late Archean volcano-sedimentary Dominion Group and implications for the tectonic setting of the Witwatersrand Supergroup, South Africa.

**Journal of African Earth Sciences (and the Middle East)**, v. 15, n. 2, p. 169–186, 1992.

JACKSON, M. C. Geochemistry and metamorphic petrology of Dominion Group metavolcanics in the Vredefort area, South Africa. **South African Journal of Geology**, v. 97, n. 1, p. 62–77, 1994.

JOURDAN, F., REIMOLD, W, U. IMPACT! – bolides, craters, and catastrophes. **Elements**, v. 8, p. 19–24, 2012.

KAMO, S. L., REIMOLD, W. U., KROGH, T. E., COLLISTON, W. P. A 2.023 Ga age for the Vredefort impact event and a first report of shock metamorphosed zircons in pseudotachylitic breccias and Granophyre. **Earth and Planetary Science Letters**, v. 144, n. 3–4, p. 369–387, 1996.

KILLICK A. M., REIMOLD W. U. Review of pseudotachylites in and around the Vredefort Dome, South Africa. **South African Journal of Geology,** v.93, p. 360– 365. 1990.

KOEBERL, C. The geochemistry and cosmochemistry of impacts. In: HOLLAND, H.D., TUREKIAN, K.K. (Ed.). **Treatise on Geochemistry**. 2nd. ed. Amsterdam: Elsevier, p. 73–118, 2014.

KOEBERL, C., REIMOLD W. U., SHIREY. S. B. Re-Os isotope study of the Vredefort granophyre: Clues to the origin of the Vredefort structure, South Africa. **Geology**, v. 24, p. 913–916, 1996.

KOVALEVA, E., HUBER, M.S., ROELOFSE, F., TREDOUX, M., PRAEKELT, H. Pseudotachylite vein hosted by a clast in the Vredefort Granophyre: characterization, origin and relevance. **South African Journal of Geology** v.121, n1, p. 51–68, 2018.

LANA, C. Structural and Petrogenetic Studies Related to the Geological Evolution of the Archaean Basement Complex of the Vredefort Dome. M.Sc. Thesis **University of the Witwatersrand, Johannesburg**, South Africa, 238pp. 2004.

LANA, C., GIBSON, R. L., KISTERS, A. F. M., REIMOLD, W. U. Archean crustal structure of the Kaapvaal craton, South Africa - evidence from the Vredefort dome. **Earth and Planetary Science Letters**, v. 206, n. 1–2, p. 133–144, 2003.

LANA C., GIBSON R. L., REIMOLD W. U. Geology of the Greenland greenstone complex, Vredefort dome, South Africa. **South African Journal of Geology**, 2003b.

LANA C., GIBSON R. L., REIMOLD W. U. Impact tectonics in the core of the Vredefort dome: Implication for formation of central uplifts in large impact structures. **Meteoritics and Planetary Science,** 2003c.

LANA, C., REIMOLD, W. U., GIBSON, R. L., KOEBERL, C., SIEGESMUND, S. Nature of the archean midcrust in the core of the Vredefort dome, Central Kaapvaal Craton, South Africa, Associate editor: B. R. Frost. **Geochimica et Cosmochimica Acta**, v. 68, n. 3, p. 623–642, 2004.

LEROUX, H., REIMOLD, W. U., DOUKHAN, J. C. A TEM investigation of shock metamorphism in quartz from the Vredefort dome, South Africa. **Tectonophysics**, v. 230, n. 3–4, p. 223–239, 1994.

LIEGER, D. Structural and geochemical analyses of fragment-rich pseudotachylite bodies and the Vredefort Granophyre of the Vredefort Impact Structure, South Africa. Ph.D.

Thesis. **Department of Earth Sciences, Free University of Berlin, Germany**, 212 pp. 2011.

LIEGER, D.; RILLER, U. Emplacement history of Granophyre dikes in the Vredefort Impact Structure, South Africa, inferred from geochemical evidence. **Icarus**, v. 219, n. 1, p. 168–180, 2012.

LUDWIG, K. Users manual for Isoplot/Ex: a geochronological toolkit for Microsoft Excel. **Berkeley Geochronology Center Special Publication**, v. 4, 76pp, 2008.

LUGMAIR, G. W.; MARTI, K. Lunar initial $^{143}Nd/^{144}Nd$: Differential evolution of the lunar crust and mantle. **Earth and Planetary Science Letters**, v. 39, n. 3, p. 349–357, 1978.

MARTINI, J. E. J. Coesite and stishovite in the Vredefort Dome, South Africa. **Nature**, v. 272, n. 5655, p. 715–717, 1978.

MARTINI, J. E. J. The nature, distribution and genesis of the coesite and stishovite associated with the pseudotachylite of the Vredefort Dome, South Africa. **Earth and Planetary Science Letters**, v. 103, n. 1, p. 285–300, 1991.

MARSH, J. S. The Dominion Group. In: Johnson, M.R., Anhaeusser, C.R., Thomas, R.J. (Eds.), The Geology of South Africa. **Geological Society of South Africa and Council for Geoscience**, Pretoria, p. 149–154 (Chapter 6), 2006.

MCCARTHY, T. The Witwatersrand Supergroup. In: The Geologyof South Africa. Johannesburg: **Geological Society of South Africa and Council for Geoscience**, p. 155-186, 2006.

MELOSH, H. J. Impact cratering : a geologic process. Oxford Monographs on Geology and Geophysics Series; **Oxford: Clarendon Press,** New York, 245 pp., 1989.

MELOSH, H. J. Planetary Surface Processes (Cambridge Planetary Science). **Cambridge University Press**, p. i-v, 2011.

MINNITT, R.C.A., REIMOLD, W.U., COLLISTON, W.P. The geology of the Greenlands Greenstone Complex andselected granitoid terranes in the southeastern quadrant of the Vredefort Dome. **Information Circular Economic Geology Research Unit**, University of Witwatersrand, Johannesburg, v. 281, p. 46, 1994.

MOSER, D. E. Dating the shock wave and thermal imprint of the giant Vredefort impact, South Africa. **Geology**, v. 25, n. 1, p. 7–10, 1997.

MOSER, D.E.; HART, R. Age of impact melting and metamorphism in the Vredefort structure, South Africa (abstract), **Joint Annual Meeting Geological Association of Canada/ Mineral Association Canada,** Program Abstract. v. 21, n. A-67, 1996.

NEL, L. T. The Geology of the Country Around Vredefort, an Explanation of the Geological Map. **Union of South Africa, Department of Mines and Industries, Geological Survey: Pretoria, South Africa**, 1927.

NICOLAYSEN, L. O. Tektites: ejecta from massive cratering events, caused by periodic escape and detonation of deep mantle fluids. In: **Int. Workshop Cryptoexplosions and Catastrophes in the Geological Record**. Parys, South Africa. p. Sec N3. 1987.

Nicolaysen, L. O., Ferguson, J. Cryptoexplosion structures, shock deformation and siderophile concentration related to explosive venting of fluids associated with alkaline ultramafic magmas. **Tectonophysics** v.171, p. 303-335, 1990.

OSINSKI, G., PIERAZZO, E. Impact Cratering: Processes and Products. **Published by Wiley-Blackwell,** p. 330, 2013.

OGILVIE, P. Metamorphic studies in the Vredefort Dome. PHD thesis, **University of the Witwatersrand**, **South Africa,** 737 pp. 2010.

PHILLIPS, G.N., POWELL, R. Origin of Witwatersrand gold: ametamorphic devolatisation-hydrothermal replacement model. **Applied Earth Sciences**, v. 120, n.3, p. 112-129, 2011.

POPPE, S., GALLAND, O., DE WINTER, N. J., GODERIS, S., CLAEYS, P., DEBAILLE, V., KERVYN, M. Structural and geochemical interactions between magma and sedimentary host rock: the Hovedøya case, Oslo Rift, Norway. **Geochemistry, Geophysics, Geosystems**, p. 1 -22, 2020.

POUJOL, M., ROBB, L., ANHAEUSSER, C., GERICKE, B. A review of the geochronological constraints on the evolution of the Kaapvaal Craton, South Africa. **Precambrian Research**, v. 127, p. 181–213, 2003.

PYBUS G.Q. Geological and mineralogical analysis of some mafic intrusives in the Vredefort Dome, Central Witwatersrand Basin. M.Sc. Thesis. **University of the Witwatersrand, Johannesburg, South Africa.**, 1995.

RACZEK, I., JOCHUM K. P., HOFMANN A. W. 2003. Neodymium and strontium isotope data for USGS reference materials BCR-1, BCR-2, BHVO-1, BHVO-2, AGV-1, AGV-2, GSP-1, GSP-2 and eight MPI-DING reference glasses, **Geostandard Newsletter**, v. 27, p. 173 – 179, 2003.

REIMOLD, W. U. Pseudotachylite - Generation by friction melting and shock brecciation? – A review and discussion. **Earth-Science Reviews**, v. 39, n. 3/4, p. 247–264, 1995.

REIMOLD, W. U. Exogenic and endogenic breccias: a discussion of major problematics. **Earth-Science Reviews**, v. 43, n. 1–2, p. 25–47, 1998.

REIMOLD, W. U., GIBSON, R. L. The melt rocks of the Vredefort impact structure - Vredefort Granophyre and pseudotachylitic breccias: Implications for impact cratering and the evolution of the Witwatersrand Basin. **Chemie der Erde - Geochemistry**, v. 66, n. 1, p. 1–35, 2006.

REIMOLD, W. U., KOEBERL, C. Impact structures in Africa: A review. **Journal of African Earth Sciences**, v. 93, p. 57–175, 2014.

REIMOLD, W. U., WALLMACH, T. The Vredefort structure under review. **South African Journal of Science**, v. 87, p. 412–417, 1991.

REIMOLD, W.U., COOPER, G.R.J., ROMANO, R., COWAN, D.R., KOEBERL, C. Investigation of Shuttle Radar Topography Mission data of the possible impact structure at Serra da Cangalha, Brazil. **Meteoritics and Planetary Science**, v. 41, p. 237-246, 2006.

REIMOLD, W.U., HORSCH, H., DURRHEIM, R. J. The “Bronzite” - granophyre from the Vredefort structure - a detailed analytical study and reflections on the genesis of one of Vredefort’s enigmas. **Journal of Chemical Information and Modeling**, v. 53, n. 9, p. 1689–1699, 1990.

REIMOLD, W.U., STEPHAN, T. AND JESSBERGER, E. K. Testing $^{40}Ar$-$^{39}Ar$ post-2 Ga ages

for pseudotachylite from the Vredefort Structure**.** 7 Int. Conf. on Geochronology, Cosmochronology and Isotope Geology. **Anais Canberra: Geol. Soc. Austral**, 1990b.

REIMOLD, W. U., PYBUS, G. Q., KRUGER, F., LAYER, P., KOEBERL, C.The Anna's Rust Sheet and related gabbroic intrusions in the Vredefort Dome-Kibaran magmatic event on the Kaapvaal Craton and beyond? **Journal of African Earth Sciences**, v. 31, p. 499–521, 2000.

REIMOLD, W. U., HOFFMANN, M., HAUSER, N., SCHMITT, R-T., ZAAG, P., MOHR-WESTHEIDE, T. A geochemical contribution to the discussion about the genesis of impact-related pseudotachylitic breccias: Studies of PTB in the Otavi and Kudu Quarries of the Vredefort Dome support the "In Situ Formation" hypothesis. **South African Journal of Geology**, v. 119, p. 453–472, 2016.

REIMOLD, W. U., HAUSER, N., HANSEN, B. T., THIRLWALL, M., HOFFMANN, M. The impact pseudotachylitic breccia controversy: Insights from first isotope analysis of Vredefort impact-generated melt rocks. **Geochimica et Cosmochimica Acta**, v. 214, p. 266–281, 2017.

REIMOLD, W. U., SCHULZ, T., KÖNIG, S., KOEBERL, C., HAUSER, N., WANNEK, D., SCHIMIDT, R-T. Genesis of the mafic granophyre of the Vredefort Impact Structure (South Africa): Implications of new geochemical and Se and Re-Os isotope data. In Reimold, W.U., and KOEBERL, C., eds., Large Meteorite Impacts and Planetary Evolution IV: **Geological Society of America Special paper**, v. 550, p. 235-254, 2021.

ROBB, L. J.; ROBB, V. M. Gold in the Witwatersrand basin. In: Wilson, M. G. C., Anhaeusser, C. R. (Eds.), **The Mineral Resources of South Africa. Council of Geoscience,** Pretoria, p. 294-349, 1998.

ROTHERY D.A., GILMOR I., S. M. A. An Introduction to Astrobiology**.** 3rd. ed. **Cambridge University Press**, 2018.

SCHMITZ, M., BOWRING, S., WIT, M. J., GARTZ, V. Subduction and terrane collision stabilize the western Kaapvaal craton tectosphere 2.9 billion years ago. **Earth and Planetary Science Letters**, v. 222, p. 363–376, 2004.

SCHRÖDER, S., BEUKES, N. J., ARMSTRONG, R. A. Detrital zircon constraints on the tectonostratigraphy of the Paleoproterozoic Pretoria Group, South Africa. **Precambrian Research***,* v. 278, p. 362-393, 2016.

SCHWARZMAN, E.C., MEYER, C.E., WILSHIRE, H. G. Pseudotachylite from the Vredefort Ring, South Africa, and the origin of some lunar breccias. **Geological Society of America Bulletin**, v. 94, p. 926–935, 1983.

SHAND., S. The pseudotachylyte of Parijs (O.F.S.) and its relation to 'trap-shotten gneiss' and 'flinty crush-rock'. **The Quarterly journal of the Geological Society of London**, v. 72, p. 198–221, 1916.

SIMPSON, C. The structure of the rim synclinorium of the Vredefort Dome **Transactions of the Geological Society of South Africa**, v.81, p.115-121, 1978.

SPRAY, J. G. Pseudotachylyte controversy: fact or friction? **Geology**, v. 23, n. 12, p. 1119 – 1122, 1995.

SPRAY, J., BIREN, M. Distinguishing friction- from shock-generated melt products in

hypervelocity impact structures. **Large Meteorite Impacts and Planetary Evolution VI.**, 2021

SPUDIS, P. D. The Geology of Multi-Ring Impact Basins: The Moon and Other Planets. **Cambridge University Press.**, 1993.

STEPTO, D. The geology and gravity field in the central core of the Vredefort structure. **Tectonophysics**, v. 171, n. 1, p. 75–103, 1990.

STÖFFLER, D., GRIEVE, R. Classification and Nomenclature of Impact Metamorphic Rocks: A Proposal to the IUGS Subcommission on the Systematics of Metamorphic Rocks. **Lunar and Planetary Science**., v. 25, p. 1347, 1994.

STÖFFLER, D., GRIEVE, R. A. F. Impactites, Chapter 2.11 in Fettes, D. and Desmons, J. (eds.) Metamorphic Rocks: A Classification and Glossary of Terms, Recommendations of the International Union of Geological Sciences, **Cambridge University Press**, v. 82-92, p. 111-125, and p. 126-242, 2007.

SUN, S.S. AND MCDONOUGH, W.F. Chemical and isotopic systematics of oceanic basalts; implications for mantle composition and processes. In: Magmatism in the ocean basins. Saunders, A.D. and Norry, M.J. (Editors), **Geological Society of London**, London. V. 42, p. 313-345, 1989.

TAYLOR, S. R. **Solar System Evolution: A New Perspective**. 2. ed. New York, NY, USA: Cambridge University Press, 488 pp., 2001.

THERRIAULT, A., REIMOLD, W., REID, A. M. Field relations and petrography of the Vredefort Granophyre. **South African Journal of Geology**, v. 99, p. 1–21, 1996.

THERRIAULT, A. M., GRIEVE, R. A. F.; REIMOLD, W. U. Original size of the Vredefort structure: Implications for the geological evolution of the Witwatersrand Basin. **Meteoritics and Planetary Science**, v. 32, n. 1, p. 71–77, 1997.

THERRIAULT, A. M., REIMOLD, W. U., REID, A. M. Geochemistry and impact origin of the Vredefort granophyre. **South African Journal of Geology**, v. 100, n. 2, p. 115–122, 1997b.

TUCKER, R., VILJOEN, R., VILJOEN, M. A Review of the Witwatersrand Basin - The World's Greatest Goldfield. **Episodes**. v, 39, n. 2, 105pp., 2016.

VAN DER WESTHUIZEN, W., DE BRUIYN, H., MEINTJES, P. G. The Ventersdorp Supergroup. In: Johnson, M.R., Anhaeusser, C.R., Thomas, R.J. (Eds.), The Geology of South Africa. **Geological Society of South Africa and Council for Geoscience,** Pretoria, p. 187–208 (Chapter 8)., 2006.

WALRAVEN F., ARMSTRONG R. A., KRUGER F. J. A chronostratigraphic framework for the north-central Kaapvaal Craton, the Bushveld Complex and the Vredefort Structure. **Tectonophysics** v.171 p. 23–48. 1990.

WALRAVEN, F., ELSENBROEK, J. H. Geochronology of the Schurwedraai Alkali Granite and associated nepheline syenite and implications for the origin of the Vredefort structure. **South African Journal of Geology**, v. 94, n. 2–3, p. 228–235, 1991.

WANNEK D. S. Geologische Untersuchungen zur Genese des Vredefort Granophyrs im Nordwesten des Vredefort Doms. M.Sc. Thesis (unpubl.). **Freie Universität Berlin, Berlin, German**, 186pp., 2015.

WEIS, P., BECK, H.P., GÜNTHER, D. Characterizing ablation and aerosol generation during elemental fractionation on absorption modified lithium tetraborate glasses using LA-ICP-MS. **Analytical and Bioanalytical Chemistry**, v. 381, p. 212–224, 2005.

WIELAND, F., REIMOLD, W.U., GIBSON, R.L. “New Observations on Shatter Cones in the Vredefort Impact Structure, South Africa, and Evaluation of Current Hypotheses for Shatter Cone Formation.” **Meteoritics & Planetary Science**, v.41 n.11, p: 1737–59. 2006.

WILLEMSE, J. On the old granite of the Vredefort region and some of its associated rocks. **Transactions of the Geological Society of South Africa ,**v. 40, p. 195–206, 1937.

WILSHIRE, H. G. Pseudotachylite from the Vredefort Ring, South Africa. **The Journal of Geology**, v. 79, n. 2, p. 195–206, 1971.

YANG, L. Accurate and precise determination of isotopic ratios by MC-ICP-MS: A review. **Mass Spectromy. Reviews**, v.28, p.990-1011, 2009.

# 7. APPENDIX

Appendix 1 - Map with all points visited during the field work on Rensburgdrif Farm (study area) and Rietikul Farm (yellow rectangle).

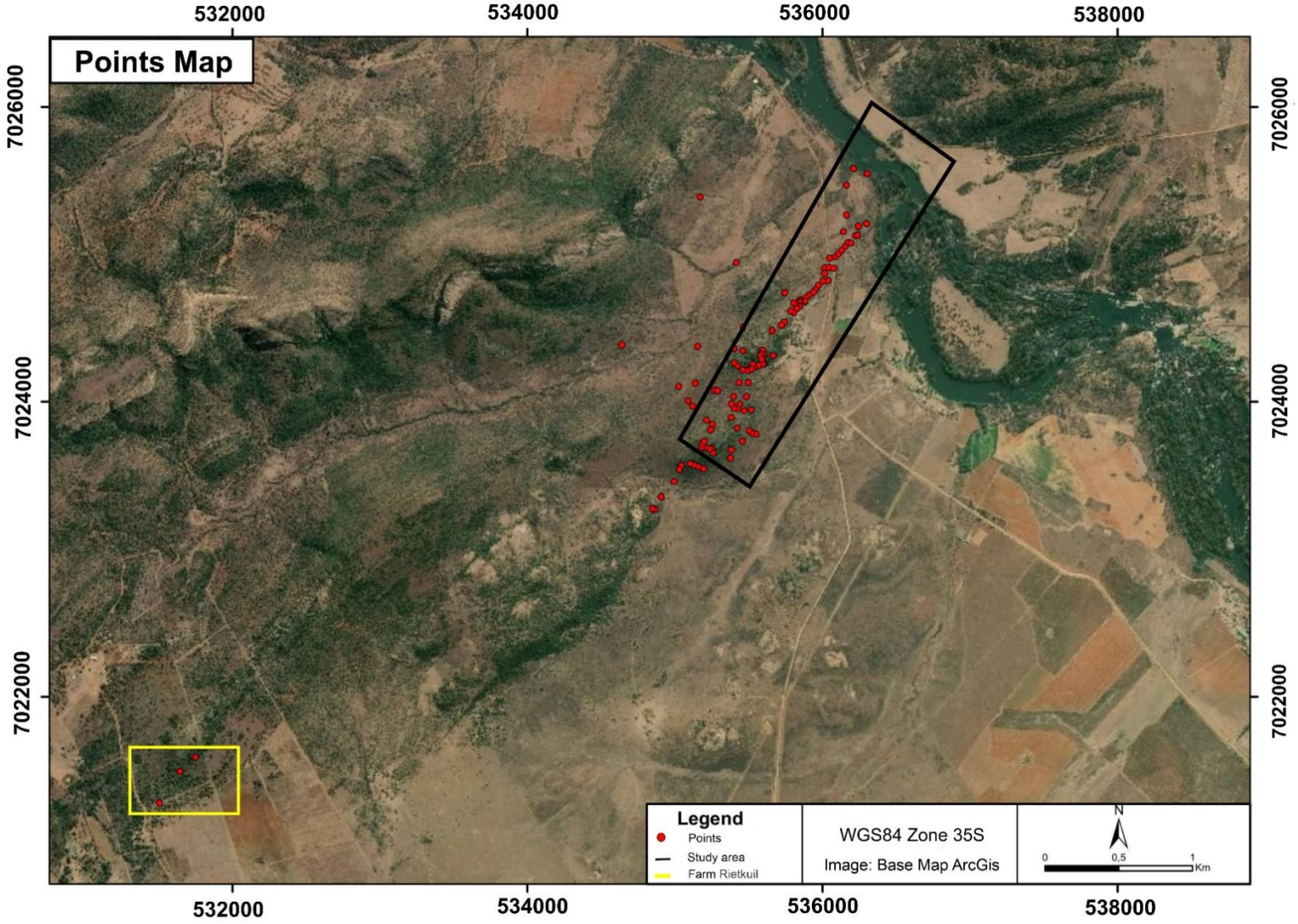

Appendix 2 - Map of the study area with points where the samples were collected during the field trip. The yellow dot is the profile across the dike (AR-38). All of these samples were geochemically and isotopically analyzed.

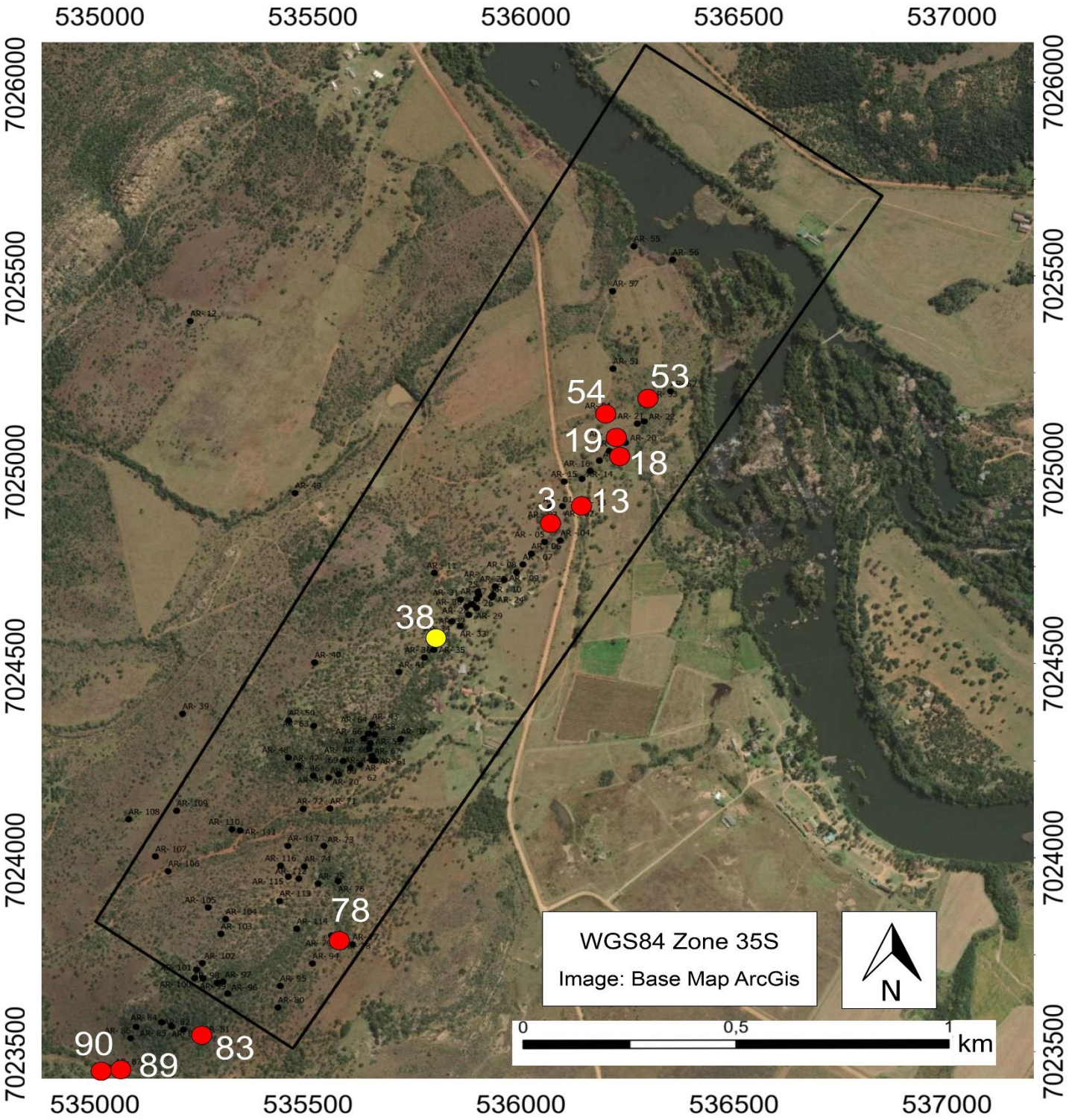

Appendix 3 – Latitude-longitude coordinates of our locations, samples No are related to location numbers (projected coordinate system: WGS 1984 UTM zone 35S).

| Points | UTM E | UMT N | Altitude |
|---|---|---|---|
| AR - 01 | 536017 | 7024908 | 1356 |
| AR - 02 | 536045 | 7024910 | 1353 |
| AR - 03 | 536016 | 7024869 | 1355 |
| AR - 04 | 536040 | 7024822 | 1352 |
| AR - 05 | 536003 | 7024818 | 1358 |
| AR - 06 | 535972 | 7024788 | 1359 |
| AR - 07 | 535952 | 7024760 | 1357 |
| AR - 08 | 535937 | 7024740 | 1357 |
| AR - 09 | 535908 | 7024720 | 1359 |
| AR - 10 | 535879 | 7024676 | 1364 |
| AR - 11 | 535744 | 7024738 | 1363 |
| AR- 12 | 535171 | 7025388 | 1354 |
| AR- 13 | 536078 | 7024904 | 1345 |
| AR- 14 | 536091 | 7024981 | 1353 |
| AR- 15 | 536049 | 7024974 | 1351 |
| AR- 16 | 536110 | 7025001 | 1351 |
| AR- 17 | 536132 | 7025028 | 1349 |
| AR- 18 | 536155 | 7025053 | 1349 |
| AR- 19 | 536174 | 7025078 | 1349 |
| AR- 20 | 536193 | 7025074 | 1346 |
| AR- 21 | 536221 | 7025123 | 1348 |
| AR- 22 | 536237 | 7025129 | 1345 |
| AR- 23 | 535887 | 7024703 | 1349 |
| AR- 24 | 535882 | 7024681 | 1366 |
| AR- 25 | 535846 | 7024689 | 1364 |
| AR- 26 | 535849 | 7024680 | 1370 |
| AR- 27 | 535844 | 7024671 | 1366 |
| AR- 28 | 535833 | 7024657 | 1364 |
| AR- 29 | 535843 | 7024647 | 1364 |
| AR- 30 | 535820 | 7024651 | 1367 |
| AR- 31 | 535806 | 7024669 | 1369 |
| AR- 32 | 535825 | 7024630 | 1360 |
| AR- 33 | 535805 | 7024601 | 1367 |
| AR- 34 | 535786 | 7024613 | 1378 |
| AR- 35 | 535743 | 7024540 | 1379 |
| AR- 36 | 535721 | 7024520 | 1379 |
| AR- 37 | 535665 | 7024310 | 1401 |
| AR- 38 | 535730 | 7024540 | 1372 |
| AR- 39 | 535153 | 7024375 | 1384 |
| AR- 40 | 535463 | 7024507 | 1391 |
| AR- 41 | 535661 | 7024482 | 1390 |
| AR- 42 | 534641 | 7024384 | 1401 |
| AR- 43 | 535598 | 7024349 | 1440 |
| AR- 44 | 535547 | 7024236 | 1386 |
| AR- 45 | 535496 | 7024210 | 1388 |
| AR- 46 | 535460 | 7024215 | 1385 |
| AR- 47 | 535425 | 7024241 | 1388 |
| AR- 48 | 535401 | 7024262 | 1386 |
| AR- 49 | 535417 | 7024944 | 1399 |
| AR- 50 | 535402 | 7024358 | 1394 |
| AR- 51 | 536164 | 7025265 | 1345 |
| AR- 52 | 536299 | 7025207 | 1345 |
| AR- 53 | 536243 | 7025188 | 1343 |
| AR- 54 | 536144 | 7025150 | 1345 |
| AR- 55 | 536213 | 7025581 | 1338 |
| AR- 56 | 536304 | 7025546 | 1338 |
| AR- 57 | 536163 | 7025465 | 1338 |
| AR- 59 | 535594 | 7024299 | 1400 |
| AR- 60 | 535598 | 7024266 | 1399 |
| AR- 61 | 535605 | 7024254 | 1398 |
| AR- 62 | 535598 | 7024255 | 1410 |
| AR- 63 | 535461 | 7024344 | 1396 |
| AR- 64 | 535597 | 7024348 | 1440 |
| AR- 65 | 535589 | 7024324 | 1410 |
| AR- 66 | 535579 | 7024311 | 1409 |
| AR- 67 | 535591 | 7024285 | 1391 |
| AR- 68 | 535570 | 7024244 | 1388 |
| AR- 69 | 535530 | 7024253 | 1385 |
| AR- 70 | 535520 | 7024219 | 1377 |
| AR- 71 | 535499 | 7024131 | 1377 |
| AR- 72 | 535436 | 7024130 | 1382 |
| AR- 73 | 535485 | 7024034 | 1382 |
| AR- 74 | 535439 | 7023981 | 1392 |
| AR- 75 | 535471 | 7023937 | 1388 |
| AR- 76 | 535518 | 7023943 | 1382 |
| AR- 77 | 535552 | 7023780 | 1376 |
| AR- 78 | 535522 | 7023788 | 1381 |
| AR- 79 | 535503 | 7023803 | 1380 |
| AR- 80 | 535377 | 7023617 | 1368 |
| AR- 81 | 535194 | 7023545 | 1408 |
| AR- 82 | 535155 | 7023560 | 1412 |
| AR- 83 | 535127 | 7023569 | 1420 |
| AR- 84 | 535104 | 7023579 | 1420 |
| AR- 85 | 535044 | 7023567 | 1412 |
| AR- 86 | 535031 | 7023538 | 1402 |
| AR- 87 | 534995 | 7023458 | 1385 |
| AR- 88 | 534906 | 7023353 | 1379 |
| AR- 89 | 534867 | 7023270 | 1413 |
| AR- 90 | 534848 | 7023275 | 1423 |
| AR- 91 | 531646 | 7021491 | 1486 |
| AR- 92 | 531750 | 7021588 | 1534 |
| AR- 93 | 531507 | 7021279 | 1463 |
| AR- 94 | 535458 | 7023731 | 1390 |
| AR- 95 | 535382 | 7023673 | 1404 |
| AR- 96 | 535259 | 7023653 | 1436 |
| AR- 97 | 535248 | 7023684 | 1441 |
| AR- 98 | 535234 | 7023681 | 1448 |
| AR- 99 | 535201 | 7023692 | 1446 |
| AR- 100 | 535181 | 7023693 | 1449 |
| AR- 101 | 535186 | 7023715 | 1410 |
| AR- 102 | 535199 | 7023732 | 1442 |
| AR- 103 | 535243 | 7023807 | 1430 |
| AR- 104 | 535254 | 7023845 | 1431 |
| AR- 105 | 535213 | 7023875 | 1415 |
| AR- 106 | 535119 | 7023969 | 1406 |
| AR- 107 | 535089 | 7024007 | 1413 |
| AR- 108 | 535026 | 7024103 | 1402 |
| AR- 109 | 535139 | 7024125 | 1414 |
| AR- 110 | 535269 | 7024077 | 1392 |
| AR- 111 | 535288 | 7024074 | 1395 |
| AR- 112 | 535426 | 7023950 | 1399 |
| AR- 113 | 535381 | 7023892 | 1410 |
| AR- 114 | 535421 | 7023820 | 1413 |
| AR- 115 | 535401 | 7023955 | 1395 |
| AR- 116 | 535383 | 7023983 | 1395 |
| AR- 117 | 535400 | 7024034 | 1388 |
| AR- 118 | 535566 | 7024577 | 1392 |

Appendix 4 - Table of EPMA data for Feldspar in Felsic and Mafic Granophyre, and epidiorite.

| Felsic Granophyre - AR 38M | | | | | | | | | | Mafic Granophyre - AR 38G | | | | | | | | | | | | |
|---|---|---|---|---|---|---|---|---|---|---|---|---|---|---|---|---|---|---|---|---|---|---|
| wt% | plagioclase | | | | | | | | | K-feld | | plagioclase | | | | | | | | K-feld | | |
| SiO2 | 53.26 | 52.79 | 52.27 | 54.15 | 54.56 | 53.51 | 52.47 | 61.51 | 53.22 | 64.46 | 64.11 | 56.83 | 54.352 | 53.189 | 55.08 | 55.21 | 63.37 | 63.03 | 64.73 | 64.99 | 64.68 | 64.99 |
| Al2O3 | 29.05 | 28.92 | 29.20 | 27.04 | 27.10 | 27.96 | 28.89 | 23.86 | 29.06 | 18.62 | 18.68 | 26.816 | 27 | 28.156 | 26.36 | 26.45 | 22.21 | 22.15 | 18.33 | 18.35 | 18.00 | 18.525 |
| Cr2O3 | 0.05 | bdl | bdl | bdl | 0.03 | bdl | bdl | bdl | 0.04 | 0.04 | bdl | 0.03 | bdl | bdl | bdl | 0.05 | 0.03 | bdl | bdl | 0.06 | bdl | 0.06 |
| MgO | 0.03 | 0.07 | 0.05 | 0.04 | 0.11 | 0.02 | 0.04 | bdl | 0.04 | bdl | bdl | bdl | 0.07 | 0.08 | 0.05 | 0.05 | bdl | bdl | bdl | bdl | bdl | bdl |
| CaO | 12.05 | 11.97 | 12.34 | 11.38 | 10.85 | 11.84 | 12.59 | 5.45 | 12.12 | 0.05 | 0.16 | 9.52 | 11.01 | 12.14 | 10.26 | 10.32 | 4.13 | 4.09 | 0.08 | 0.14 | bdl | 0.54 |
| MnO | bdl | bdl | bdl | 0.03 | 0.02 | bdl | bdl | bdl | 0.03 | bdl | bdl | 0.04 | 0.03 | 0.01 | bdl | 0.02 | bdl | bdl | bdl | bdl | bdl | bdl |
| FeO | 0.47 | 0.56 | 0.47 | 0.55 | 0.31 | 0.24 | 0.55 | 0.22 | 0.54 | 0.16 | 0.15 | 0.57 | 1.17 | 1.12 | 0.77 | 0.83 | 0.09 | 0.15 | 0.15 | 0.09 | 0.08 | 0.68 |
| Na2O | 5.27 | 5.17 | 5.08 | 5.44 | 5.32 | 5.23 | 4.65 | 8.62 | 4.91 | 1.48 | 1.58 | 6.72 | 5.82 | 5.08 | 6.16 | 6.22 | 9.36 | 9.77 | 1.70 | 2.19 | 1.51 | 4.28 |
| K2O | 0.17 | 0.18 | 0.09 | 0.10 | 0.13 | 0.05 | 0.11 | 0.23 | 0.19 | 14.13 | 14.27 | 0.07 | 0.07 | 0.06 | 0.27 | 0.31 | 0.20 | 0.19 | 14.22 | 13.54 | 14.68 | 10.48 |
| Total | 100.35 | 99.65 | 99.49 | 98.73 | 98.42 | 98.86 | 99.29 | 99.89 | 100.14 | 98.94 | 98.95 | 100.59 | 99.52 | 99.83 | 98.94 | 99.48 | 99.38 | 99.37 | 99.20 | 99.36 | 98.94 | 99.56 |
| Ab % | 43.8 | 43.5 | 42.5 | 46.1 | 46.7 | 44.3 | 39.8 | 73.2 | 73.2 | 13.7 | 14.3 | 56 | 49 | 43 | 51 | 51 | 80 | 80 | 37 | 15 | 20 | 13 |
| An % | 55.3 | 55.6 | 57.1 | 53.3 | 52.6 | 55.4 | 59.6 | 25.5 | 25.5 | 0.3 | 0.8 | 44 | 51 | 57 | 47 | 47 | 19 | 19 | 3 | 0 | 1 | 0 |
| Or % | 0.9 | 1.0 | 0.5 | 0.6 | 0.7 | 0.3 | 0.6 | 1.3 | 1.3 | 86.1 | 84.9 | 0 | 0 | 0 | 1 | 2 | 1 | 1 | 60 | 84 | 80 | 86 |

| Epidiorite - AR 54 | | | | | | | | | | | | | | |
|---|---|---|---|---|---|---|---|---|---|---|---|---|---|---|
| wt% | plagioclase | | | | | | | | | | | | | |
| SiO2 | 53.18 | 54.03 | 53.94 | 51.84 | 54.27 | 58.40 | 57.95 | 47.44 | 47.39 | 46.75 | 53.21 | 50.52 | 49.41 | 47.49 |
| Al2O3 | 29.00 | 28.53 | 28.34 | 30.07 | 27.94 | 25.29 | 25.89 | 32.40 | 32.53 | 32.77 | 28.97 | 30.24 | 31.77 | 31.97 |
| Cr2O3 | bdl | 0.02 | bdl | 0.05 | bdl | 0.07 | bdl | bdl | bdl | bdl | bdl | bdl | bdl | bdl |
| MgO | bdl | bdl | bdl | bdl | bdl | bdl | 0.03 | bdl | bdl | bdl | bdl | 0.15 | bdl | bdl |
| CaO | 12.52 | 11.55 | 11.54 | 14.02 | 10.68 | 7.85 | 8.20 | 16.69 | 16.83 | 17.32 | 12.10 | 14.63 | 15.60 | 16.91 |
| MnO | 0.02 | 0.01 | 0.00 | 0.03 | 0.01 | 0.00 | 0.00 | 0.02 | 0.00 | 0.02 | 0.02 | 0.00 | 0.02 | 0.00 |
| FeO | 0.04 | 0.07 | 0.01 | 0.04 | 0.10 | 0.20 | 0.20 | 0.05 | 0.04 | 0.08 | 0.04 | 0.11 | 0.06 | 0.07 |
| Na2O | 4.95 | 5.61 | 5.61 | 4.31 | 5.74 | 7.63 | 7.62 | 2.36 | 2.19 | 2.02 | 5.34 | 3.75 | 3.21 | 2.23 |
| K2O | 0.07 | 0.09 | 0.11 | 0.06 | 0.05 | 0.12 | 0.10 | 0.04 | 0.02 | 0.02 | 0.07 | 0.11 | 0.04 | 0.02 |
| Total | 99.77 | 99.90 | 99.56 | 100.41 | 98.79 | 99.56 | 99.99 | 99.00 | 98.98 | 98.97 | 99.74 | 99.52 | 100.11 | 98.68 |
| Ab % | 41.5 | 46.6 | 46.5 | 35.6 | 49.2 | 63.3 | 62.4 | 20.3 | 19.0 | 17.4 | 44.2 | 31.5 | 27.1 | 19.2 |
| An % | 58.1 | 53.0 | 52.9 | 64.1 | 50.5 | 36.0 | 37.1 | 79.5 | 80.9 | 82.5 | 55.4 | 67.9 | 72.7 | 80.6 |
| Or % | 0.4 | 0.5 | 0.6 | 0.3 | 0.3 | 0.6 | 0.5 | 0.2 | 0.1 | 0.1 | 0.4 | 0.6 | 0.2 | 0.1 |

Appendix 5 - Table of EPMA data for Pyroxene in Felsic and Mafic Granophyre.

| | Felsic Granophyre - 38M | | | | | | | | | | | | | | | Mafic Granophyre - 38G | | | | | | | |
|---|---|---|---|---|---|---|---|---|---|---|---|---|---|---|---|---|---|---|---|---|---|---|---|
| wt% | Px | | | | | | | | | | | | | | | Px | | | | | | | |
| SiO2 | 51.05 | 51.12 | 50.99 | 51.09 | 51.64 | 52.42 | 52.61 | 53.82 | 53.31 | 50.13 | 50.12 | 50.90 | 50.25 | 49.78 | 49.53 | 51.57 | 51.24 | 50.81 | 51.52 | 50.07 | 50.15 | 50.26 | 51.87 |
| Al2O3 | 1.42 | 1.37 | 1.00 | 1.69 | 1.33 | 1.82 | 2.46 | 1.14 | 1.97 | 1.01 | 1.17 | 1.63 | 1.18 | 1.15 | 0.50 | 1.59 | 1.41 | 1.36 | 0.44 | 1.88 | 0.90 | 2.35 | 0.65 |
| Cr2O3 | 0.43 | 0.26 | 0.12 | 0.40 | 0.31 | 0.43 | 0.53 | 0.31 | 0.56 | 0.17 | 0.28 | 0.37 | 0.10 | 0.08 | 0.07 | 0.35 | 0.25 | 0.36 | 0.15 | 0.33 | 0.19 | 0.34 | 0.23 |
| MgO | 19.67 | 21.60 | 18.46 | 21.78 | 22.70 | 24.82 | 26.17 | 27.07 | 26.33 | 17.79 | 17.76 | 19.76 | 17.79 | 17.98 | 15.51 | 20.74 | 19.41 | 18.94 | 10.89 | 12.87 | 17.49 | 13.59 | 12.20 |
| CaO | 1.17 | 0.95 | 1.79 | 1.25 | 1.26 | 1.26 | 1.23 | 1.10 | 1.14 | 1.79 | 1.41 | 1.07 | 1.61 | 1.71 | 1.77 | 1.79 | 2.04 | 2.02 | 20.52 | 16.59 | 1.80 | 17.81 | 20.59 |
| MnO | 0.52 | 0.45 | 0.59 | 0.48 | 0.43 | 0.42 | 0.34 | 0.42 | 0.39 | 0.64 | 0.59 | 0.46 | 0.56 | 0.64 | 0.73 | 0.46 | 0.49 | 0.52 | 0.53 | 0.41 | 0.62 | 0.32 | 0.34 |
| FeO | 24.89 | 23.21 | 25.57 | 21.98 | 21.82 | 18.36 | 16.13 | 16.08 | 15.96 | 26.80 | 26.72 | 24.68 | 26.49 | 26.90 | 30.11 | 22.82 | 24.69 | 25.01 | 16.01 | 15.85 | 27.54 | 15.14 | 14.27 |
| Na2O | 0.04 | 0.00 | 0.04 | 0.04 | 0.02 | 0.06 | 0.02 | 0.03 | 0.02 | 0.03 | 0.02 | 0.03 | 0.03 | 0.02 | 0.02 | bdl | 0.03 | 0.03 | 0.23 | 0.22 | 0.02 | 0.26 | 0.33 |
| K2O | bdl | bdl | bdl | bdl | bdl | bdl | bdl | bdl | bdl | bdl | 0.02 | 0.02 | bdl | bdl | bdl | bdl | bdl | bdl | bdl | bdl | bdl | bdl | bdl |
| Total | 99.18 | 98.96 | 98.56 | 98.71 | 99.51 | 99.61 | 99.49 | 99.97 | 99.67 | 98.36 | 98.07 | 98.93 | 98.01 | 98.24 | 98.24 | 99.33 | 99.56 | 99.06 | 100.29 | 98.21 | 98.70 | 100.07 | 100.48 |
| Wo | 2 | 2 | 4 | 3 | 3 | 3 | 2 | 2 | 2 | 3 | 4 | 4 | 4 | 3 | 2 | 4 | 4 | 4 | 4 | 42 | 35 | 37 | 42 |
| En | 57 | 61 | 54 | 62 | 63 | 68 | 72 | 73 | 72 | 52 | 52 | 46 | 52 | 52 | 57 | 59 | 55 | 55 | 51 | 31 | 38 | 39 | 35 |
| Fs | 41 | 37 | 43 | 36 | 35 | 29 | 25 | 25 | 25 | 44 | 45 | 51 | 45 | 45 | 41 | 37 | 40 | 41 | 46 | 27 | 27 | 25 | 23 |

Appendix 6 - Table of EPMA data for Amphibole in Felsic and Mafic Granophyre, and epidiorite

| | Felsic - AR 38M | | Mafic - AR 38G | | Epidiorite - AR 54 | | | | | | | | | | | | | | |
|---|---|---|---|---|---|---|---|---|---|---|---|---|---|---|---|---|---|---|---|
| wt% | amph | | amph | | amphibole | | | | | | | | | | | | | | |
| SiO2 | 53.47 | 50.05 | 48.34 | 48.34 | 52.50 | 51.74 | 51.41 | 54.20 | 50.74 | 50.53 | 51.03 | 50.39 | 51.97 | 50.25 | 51.82 | 51.46 | 51.84 | 49.35 | 45.29 | 44.40 |
| Al2O3 | 1.50 | 4.61 | 5.27 | 4.69 | 3.89 | 4.19 | 4.03 | 2.33 | 4.16 | 4.76 | 3.54 | 5.36 | 4.11 | 5.38 | 4.53 | 3.98 | 4.26 | 6.08 | 11.95 | 12.92 |
| Cr2O3 | 0.24 | 0.08 | 0.11 | 0.24 | 0.12 | 0.12 | 0.06 | 0.07 | 0.13 | bdl | bdl | 0.50 | 0.14 | 0.44 | 0.10 | 0.06 | bdl | bdl | 0.04 | 0.05 |
| MgO | 15.66 | 13.25 | 13.30 | 12.60 | 16.26 | 15.68 | 15.61 | 16.73 | 15.85 | 15.15 | 16.09 | 14.74 | 15.80 | 14.80 | 15.21 | 16.53 | 15.97 | 13.83 | 11.02 | 10.44 |
| CaO | 7.25 | 10.85 | 11.25 | 10.57 | 12.86 | 12.70 | 12.66 | 12.99 | 12.69 | 12.73 | 12.63 | 12.68 | 12.75 | 12.78 | 12.89 | 12.76 | 12.71 | 12.74 | 12.45 | 12.51 |
| MnO | 0.53 | 0.34 | 0.18 | 0.37 | 0.25 | 0.19 | 0.18 | 0.20 | 0.21 | 0.20 | 0.23 | 0.18 | 0.26 | 0.21 | 0.22 | 0.24 | 0.22 | 0.22 | 0.25 | 0.24 |
| FeO | 18.36 | 16.72 | 16.36 | 18.49 | 11.30 | 11.18 | 11.29 | 11.25 | 10.96 | 11.42 | 11.25 | 12.26 | 11.36 | 11.99 | 11.82 | 10.92 | 11.62 | 13.45 | 14.26 | 14.25 |
| Na2O | 0.25 | 0.66 | 1.21 | 1.04 | 0.37 | 0.32 | 0.35 | 0.13 | 0.39 | 0.44 | 0.34 | 0.56 | 0.38 | 0.52 | 0.40 | 0.36 | 0.38 | 0.64 | 1.04 | 1.11 |
| K2O | 0.11 | 0.34 | 0.70 | 0.45 | 0.09 | 0.13 | 0.12 | 0.05 | 0.12 | 0.14 | 0.12 | 0.20 | 0.13 | 0.19 | 0.11 | 0.11 | 0.12 | 0.23 | 0.41 | 0.47 |
| Total | 97.37 | 96.90 | 96.73 | 96.78 | 97.63 | 96.23 | 95.70 | 97.97 | 95.24 | 95.37 | 95.23 | 96.88 | 96.91 | 96.57 | 97.10 | 96.40 | 97.12 | 96.53 | 96.72 | 96.39 |
| | ferri-actinolitic hornbl | | ferri-magn-hbl | | actinolite | | | | actinolitic hornblende | | | | | | | | | magnesio-hornblende | | |

Appendix 7 - Table of geochemical analyses of major elements for samples of Epidiorite, Granite, and Granophyre (felsic and mafic) from the literature.

| | Reimold 1990 | | | | | Therriault 1997 | | | | | | Lieger 2011 | | | | Wannek 2015 | | |
|---|---|---|---|---|---|---|---|---|---|---|---|---|---|---|---|---|---|---|
| Sample | (BG-CM) | (USA209-1) | (USA209-2) | (BG-3) | (BG-4) | VAT8a | (VAT69) | (AU14A) | (VAT 113) | (VAT 141) | (AU13) | (453A2) | Epidiorite | (188B2) | (188A1) | 38 | 41 | 11 |
| Lithology | Granite | Epidiorite | Epidiorite | Granophyre dike 1 | Granophyre | Granophyre dike 2 | Granophyre dike 4 | Granophyre dike 5 | Granophyre dike 7 | Granophyre dike 8 | Granophyre dike 9 | Granitoide | Epidiorite | Granophyre | Granophyre dike 7 | Epidiorite (38) | Granophyre (41) | Mafic Granophyre |
| SiO2 | 82.00 | 50.30 | 49.80 | 67.00 | 67.50 | 66.00 | 68.89 | 66.29 | 63.90 | 68.20 | 66.14 | 73.12 | 51.18 | 61.93 | 68.64 | 53.30 | 66.70 | 62.00 |
| TiO2 | 0.24 | 0.30 | 0.70 | 0.50 | 0.50 | 0.59 | 0.56 | 0.53 | 0.59 | 0.47 | 0.49 | 0.24 | 0.30 | 0.66 | 0.51 | 0.60 | 0.51 | 0.61 |
| Al2O3 | 8.90 | 11.60 | 12.20 | 13.00 | 12.70 | 12.82 | 12.60 | 12.67 | 12.86 | 12.60 | 12.57 | 14.47 | 14.65 | 13.51 | 12.45 | 13.00 | 12.80 | 13.20 |
| Fe2O3 | 2.80 | 12.10 | 12.00 | 7.00 | 7.20 | 7.50 | 8.01 | 7.35 | 8.83 | 7.33 | 7.56 | 1.40 | 7.55 | 9.55 | 7.36 | 10.70 | 7.28 | 9.16 |
| MnO | 0.05 | 0.10 | 0.20 | 0.14 | 0.14 | 0.13 | 0.13 | 0.17 | 0.14 | 0.15 | 0.15 | 0.03 | 0.12 | 0.15 | 0.14 | 0.16 | 0.14 | 0.16 |
| MgO | 1.15 | 12.80 | 12.70 | 3.50 | 3.50 | 3.26 | 3.53 | 3.68 | 3.87 | 3.81 | 3.99 | 0.24 | 9.28 | 3.72 | 3.35 | 8.67 | 3.58 | 4.06 |
| CaO | 0.80 | 10.20 | 10.00 | 3.70 | 3.80 | 3.89 | 3.73 | 4.19 | 5.21 | 4.06 | 4.21 | 1.07 | 13.41 | 5.89 | 3.91 | 9.65 | 3.96 | 5.60 |
| Na2O | 1.80 | 1.70 | 1.90 | 2.70 | 2.50 | 2.28 | 2.22 | 2.82 | 2.76 | 2.75 | 2.58 | 5.25 | 1.37 | 3.44 | 2.76 | 2.10 | 2.62 | 2.89 |
| K2O | 2.20 | bd | 0.10 | 2.40 | 2.10 | 2.32 | 2.11 | 2.15 | 1.90 | 2.23 | 2.18 | 3.28 | 0.08 | 1.68 | 1.99 | 0.53 | 2.21 | 1.87 |
| P2O5 | 0.04 | 0.15 | 0.10 | 0.10 | 0.10 | 0.11 | 0.11 | 0.11 | 0.13 | 0.11 | 0.09 | 0.08 | 0.02 | 0.12 | 0.11 | 0.08 | 0.11 | 0.12 |
| LOI | 0.00 | 0.50 | 0.30 | 0.05 | 0.00 | 0.02 | 0.21 | 0.04 | 0.32 | 0.00 | 0.05 | 0.96 | 1.08 | 0.01 | 0.01 | 1.25 | 0.04 | 0.05 |
| Sum | 99.98 | 99.98 | 100.00 | 100.09 | 100.04 | 98.92 | 99.90 | 100.00 | 100.51 | 101.71 | 100.01 | 100.14 | 99.04 | 100.66 | 101.21 | 99.80 | 99.90 | 99.90 |

| Pybus 1995 | | | | | Jackson 1994 | | | | | | | | | | Willemse 1937 | | | | | Hall and Molengraaf 1925 | | |
|---|---|---|---|---|---|---|---|---|---|---|---|---|---|---|---|---|---|---|---|---|---|---|
| UP54a | UP54b | UP56 | UP57 | UP58 | 90PAR1 | 90PAR3 | 90PAR5 | 90PAR8 | 90PAR10 | 90VRE1 | 90VRE3 | 91VRE1 | 91VRE2 | 91VRE4 | 1 | 2 | 3 | 4 | 5 | I | II | III |
| Epidiorite | Epidiorite | Epidiorite | Epidiorite | Epidiorite | Metabasalts DGL | Metabasalts DGL | Metabasalts DGL | Metabasalts DGL | Metabasalts DGL | Metabasalts DGL | Metabasalts DGL | Metabasalts DGL | Metabasalts DGL | Metabasalts DGL | Basic Granophyre | Basic Granophyre | Basic Granophyre | Basic Granophyre | Basic Granophyre | Enstatite Granophyre | Enstatite Granophyre | Enstatite Granophyre |
| 55.06 | 55.13 | 53.46 | 53.46 | 53.76 | 55.2 | 53.7 | 53.58 | 55.11 | 54.51 | 57.23 | 56.55 | 54.47 | 50.6 | 55.23 | 67.4 | 63.7 | 67.45 | 69.2 | 67.4 | 67.4 | 63.7 | 67.45 |
| 0.43 | 0.45 | 0.58 | 0.54 | 0.47 | 0.67 | 0.74 | 0.6 | 1.07 | 0.78 | 1,077 | 1.08 | 0.74 | 0.75 | 0.74 | 0.4 | 0.5 | 0.4 | 0.78 | 0.53 | 0.4 | 0.5 | 0.4 |
| 14.64 | 14.39 | 12.08 | 13.93 | 14.5 | 13.69 | 15.23 | 17.71 | 14.49 | 13.23 | 14.83 | 14.4 | 13.61 | 15.91 | 13.9 | 12.5 | 12.75 | 12.2 | 12.5 | 12.71 | 12.5 | 12.75 | 12.2 |
| 9.57 | 9.68 | 11.81 | 10.07 | 9.91 | 11.46 | 10.42 | 10.53 | 12.81 | 11.05 | 11.62 | 12.98 | 12.01 | 12.6 | 10.99 | 7.85 | 9.4 | 7.73 | 6.1 | 7.1 | 6.5 | 7.6 | 6.15 |
| 0.13 | 0.13 | 0.17 | 0.15 | 0.16 | 0.14 | 0.14 | 0.21 | 0.27 | 0.15 | 0.13 | 0.15 | 0.23 | 0.26 | 0.19 | 0.15 | 0.1 | 0.15 | 0.14 | 0.1 | 0.15 | 0.1 | 0.15 |
| 7.98 | 8.06 | 9.51 | 9.07 | 6.9 | 6.81 | 6.6 | 4.51 | 3.18 | 8.36 | 4.01 | 3.87 | 7.42 | 5.8 | 7.4 | 3.9 | 4.2 | 4.1 | 3.08 | 3.35 | 3.9 | 4.2 | 4.1 |
| 9.94 | 9.91 | 10.38 | 11.34 | 10.9 | 10.65 | 11.88 | 12.22 | 10.54 | 9.59 | 9.43 | 9.21 | 8.96 | 13.28 | 8.88 | 4.5 | 5.8 | 4.4 | 3.48 | 3.94 | 4.5 | 5.8 | 4.4 |
| 2.13 | 2.17 | 1.92 | 1.65 | 1.63 | 1.08 | 0.88 | 0.34 | 2.06 | 1.89 | 1.33 | 1.49 | 2.3 | 0.58 | 2.41 | 1.6 | 2.4 | 1.7 | 2.38 | 2.83 | 1.6 | 2.4 | 1.7 |
| 0.52 | 0.54 | 0.57 | 0.36 | 0.38 | 0.15 | 0.24 | 0.1 | 0.25 | 0.25 | 0.09 | 0.02 | 0.11 | 0.1 | 0.13 | 1.85 | 1.8 | 2 | 2.38 | 2.34 | 1.85 | 1.8 | 2 |
| 0.06 | 0.07 | 0.06 | 0.06 | 0.06 | 0.13 | 0.15 | 0.2 | 0.19 | 0.18 | 0.24 | 0.25 | 0.16 | 0.13 | 0.13 | 0.3 | 0.2 | 0.1 | 0.25 | 0.18 | 0.3 | 0.2 | 0.1 |
| 0.22 | 0.15 | 0 | 0.29 | 0.52 | 1.17 | 0.86 | 0.36 | 0.41 | 0.52 | 0.34 | 0.25 | 0.53 | 0.5 | 0.56 | | | | | | 0.05 | 0.05 | 0.05 |
| 99.7 | 99.7 | 99.4 | 99.9 | 98.2 | | | | | | | | | | | 99.9 | 100.4 | 99.9 | 100.08 | 100.22 | 99.9 | 100.4 | 99.9 |

Appendix 8 -Table of geochemical analyses of trace elements for samples of Epidiorite, DGL, Granite, and Granophyre (felsic and mafic) from the literature.

| | Reimold 1990 | | | | | Therrialut 1997 | | | | | | Lieger 2011 | | | |
|---|---|---|---|---|---|---|---|---|---|---|---|---|---|---|---|
| Lithology | Granite | | Epidiorite | Granophyre | | Granophyre | | | | | | Granitoid | Epidiorite | Granophyre | |
| Samples | (BG) | (BG) | (USA209) | (BG-3) DIKE 1 | (BG-4) | dike 2 (VAT8a) | dike 4 (VAT69) | dike 5 (AU14A) | dike 7 (VAT 113) | dike 8 (VAT 141) | dike 9 (AU13) | (453A2) | | dike 7 (188B2) | dike 7 (188A1) |
| Sc | 12 | 14 | 24 | 13 | 14 | | | | | | | | | | |
| Cr | 85 | 89 | 261 | 87 | 89 | 291 | 291 | 438 | 360.9 | 316.7 | 452 | 104 | 985 | 250 | 396 |
| Co | 25 | 27 | 66 | 25 | 27 | 21 | 23 | 23 | 22 | 21 | 22 | <6 | 40 | 31 | 25 |
| Ni | 93 | 134 | 439 | 93 | 100 | 87 | 92.8 | 96 | 114.4 | 103.9 | 101 | 9 | 217 | 81 | 106 |
| Cu | | | | | | 43 | 40 | 46 | 45 | 34 | 43 | <6 | 63 | 55 | 48 |
| Zn | | | | | | 53 | 62 | 59 | 62 | 54 | 58 | 35 | 58 | 80 | 61 |
| Rb | 65 | 84 | 4 | 78 | 65 | 79 | 79 | 74 | 67 | 76 | 81 | 113 | 7 | 60 | 66 |
| Sr | | | | | | 243 | 243 | 240 | 228 | 228 | 220 | 240 | 99 | 222 | 232 |
| Y | | | | | | 16 | 16 | 16 | 19 | 15 | 19 | 15 | 13 | 22 | 18 |
| Zr | 117 | 165 | nd | 137 | 132 | 157 | 157 | 155 | 143 | 145 | 148 | 184 | 38 | 142 | 145 |
| Nb | | | | | | 8 | 7 | 7 | 7 | 8 | 8 | 6 | 3 | 7 | 6 |
| Ba | 438 | 512 | 44 | 497 | 512 | 475 | 519 | 477 | 432 | 426 | 436 | 616 | 61 | 406 | 516 |

| | Wannek 2015 | | | Pybus 1995 | | | | | Jackson 1994 | | | | | | | | | | | | | | |
|---|---|---|---|---|---|---|---|---|---|---|---|---|---|---|---|---|---|---|---|---|---|---|---|
| Epidiorite | Granophyre | M. Granophyre | Granite | Epidiorite | | | | | Meta-lava (DGL) | | | | | | | | | | | | | | |
| Ave. (38) | Ave.(41) | Ave.(38) | | UP54a | UP54b | UP56 | UP57 | UP58 | 90PAR1 | 90PAR3 | 90PAR5 | 90PAR8 | 90PAR10 | 90VRE1 | 90VRE3 | 91VRE1 | 91VRE2 | 91VRE4 | DB251 | DB278 | DB68 | DB248 | DB255 |
| 37 | 14 | 18 | <5 | | | | | | | | | | | | | | | | | | | | |
| 665 | 301 | 244 | <5 | 435 | 435 | 768 | 584 | 155 | 855 | 821 | 696 | 19 | 784 | 11 | 11 | 917 | 890 | 892 | 315 | 45 | 40 | 986 | 716 |
| 47 | 21 | 26 | <5 | 42 | 42 | 58 | 42 | 36 | 57 | 52 | 55 | 56 | 50 | 44 | 46 | 50 | 64 | 51 | 35 | 40 | 30 | 48 | 49 |
| 195 | 99 | 94 | <5 | 178 | 178 | 263 | 215 | 128 | 315 | 293 | 257 | 39 | 279 | 41 | 45 | 270 | 363 | 294 | 202 | 101 | 83 | 292 | 259 |
| 66 | 47 | 56 | <15 | 46 | 46 | 73 | 49 | 87 | 58 | 62 | 27 | 20 | 83 | 53 | 72 | 51 | 6 | 75 | 50 | 39 | 58 | 64 | 72 |
| 77 | 57 | 69 | 32 | 61 | 61 | 74 | 65 | 63 | 86 | 85 | 64 | 107 | 88 | 100 | 107 | 94 | 93 | 81 | 84 | 126 | 115 | 95 | 83 |
| 25 | 73 | 63 | 172 | 27 | 29 | 33 | 22 | 23 | 13 | 20 | 12 | 6 | 14 | 11 | 12 | 3 | 6 | 6 | 17 | 11 | 41 | 26 | 25 |
| 204 | 225 | 222 | 180 | 219 | 220 | 176 | 162 | 183 | 611 | 623 | 431 | 503 | 434 | 827 | 802 | 558 | 255 | 575 | 426 | 193 | 491 | 310 | 370 |
| 14 | 16 | 18 | <10 | 11 | 12 | 13 | 12 | 13 | 15 | 17 | 16 | 24 | 18 | 25 | 23 | 16 | 18 | 14 | 15 | 28 | 26 | 17 | 15 |
| 66 | 144 | 138 | 171 | 57 | 56 | 59 | 46 | 56 | 93 | 100 | 77 | 149 | 111 | 163 | 166 | 95 | 98 | 95 | 106 | 191 | 181 | 95 | 87 |
| | | | | 4 | 4 | 4 | 4 | 4 | 4.8 | 5.2 | 4.7 | 6.4 | 5.5 | 6.8 | 7.3 | 4.4 | 4.5 | 3.6 | 4.1 | 7.9 | 6.5 | 5 | 4.2 |
| 183 | 445 | 397 | 562 | 194 | 183 | 177 | 118 | 96 | 132 | 96 | 63 | 89 | 125 | 172 | 95 | 32 | 50 | 100 | 653 | 407 | 405 | 570 | 295 |

Appendix 9 - Table of geochemical analyses of rare earth elements (REE) for samples of Epidiorite and Granophyre (felsic and mafic) from the literature. Reimold et al. 1990 and Wannek 2015.

| | Reimold 1990 | | | Wannek 2015 | | | | | | | | | | | | |
|---|---|---|---|---|---|---|---|---|---|---|---|---|---|---|---|---|
| Lithology | Epidiorite | | | Granophyre | | Gran. Type 1 | | | | Gran. Type 2 | | Mafic | | | | |
| Samples | (USA209) | (E32) | (E35) | (BG-3) DIKE 1 | (BG-4) | D1 | 17 | 20 | 31 | 25 | 43 | (DW-SA24) | DW-SA33 | DW-SA11 | DW-SA30 | DW-SA41 |
| La | 6.9 | 5.2 | 5.38 | 36 | 34 | 26.7 | 28 | 29.1 | 27 | 26.7 | 27.3 | 24.6 | 25 | 25.5 | 26 | 25.4 |
| Ce | nd | 12 | 7.3 | 46 | 44 | 52.4 | 53.9 | 56.5 | 53 | 52.1 | 53.5 | 48.3 | 49.3 | 49.2 | 51.7 | 49.5 |
| Pr | | 1.58 | 1.01 | | | 5.66 | 5.79 | 6.01 | 5.67 | 5.7 | 5.87 | 5.21 | 5.39 | 5.28 | 5.62 | 5.13 |
| Nd | bd | 7.7 | 4.03 | 21 | 29 | 20.6 | 20.8 | 22.4 | 20.6 | 19.9 | 20.2 | 19.2 | 19.9 | 21 | 20.8 | 13.9 |
| Sm | 2.2 | 2.09 | 1.29 | 4.5 | 4.5 | 3.7 | 3.95 | 3.75 | 3.81 | 3.58 | 3.64 | 3.56 | 4 | 3.93 | 3.65 | 3.68 |
| Eu | 0.4 | 0.7 | 0.51 | 0.9 | 1 | 0.92 | 0.9 | 0.92 | 0.79 | 0.82 | 0.87 | 0.91 | 0.86 | 0.87 | 1.03 | 0.88 |
| Gd | | 2.5 | 1.67 | | | 2.78 | 3.09 | 3.21 | 2.88 | 2.81 | 2.9 | 3.11 | 3.37 | 3.32 | 3.23 | 3.17 |
| Tb | 0.49 | 0.38 | 0.32 | 0.5 | 0.5 | 0.38 | 0.43 | 0.42 | 0.43 | 0.44 | 0.41 | 0.56 | 0.51 | 0.48 | 0.48 | 0.5 |
| Dy | | 2.33 | 1.98 | | | 2.55 | 2.62 | 2.65 | 2.4 | 2.42 | 2.7 | 3.18 | 3.32 | 2.7 | 2.94 | 2.72 |
| Ho | | 0.5 | 0.42 | | | 0.51 | 0.53 | 0.49 | 0.49 | 0.52 | 0.51 | 0.66 | 0.69 | 0.59 | 0.6 | 0.56 |
| Er | | 1.35 | 1.3 | | | 1.45 | 1.37 | 1.33 | 1.38 | 1.4 | 1.3 | 1.74 | 1.97 | 1.58 | 1.59 | 1.45 |
| Tm | | 0.2 | 0.19 | | | 0.2 | 0.19 | 0.2 | 0.19 | 0.23 | 0.22 | 0.25 | 0.27 | 0.24 | 0.26 | 0.25 |
| Yb | bd | 1.26 | 1.23 | 0.8 | 0.8 | 1.38 | 1.29 | 1.42 | 1.26 | 1.36 | 1.39 | 1.82 | 1.94 | 1.49 | 1.63 | 1.52 |
| Lu | bd | 0.17 | 0.19 | 0.13 | 0.13 | 0.21 | 0.18 | 0.22 | 0.18 | 0.18 | 0.22 | 0.29 | 0.28 | 0.25 | 0.27 | 0.27 |

Appendix 10 - Results of isotopic analysis of Epidiorite, Granite and Granophyre from the literature (Reimold et al., 2017). Samples analyzed at Royal Holloway University, London. fc = as measured and corrected for fractionation; 87Sr/86Sr(T) = measured values recalculated to impact time (2020 Ma). Uncertainties on isotope ratios are given as the least significant digits of the values.

| Sample | Lithology Type | Age (Ma)* | Rb [µg/g] | 2se | Sr [µg/g] | 2se | $^{87}Rb/^{86}Sr$ | $^{87}Sr/^{86}Sr_{[fc]}$ | 2se | $^{87}Sr/^{86}Sr_{(T)}$ |
|---|---|---|---|---|---|---|---|---|---|---|
| **Reimold et al., 2017** | | | | | | | | | | |
| Hybrid 24 | M. Granophyre | 2020 | 56.8 | 0.01 | 214.4 | 0.01 | 0.7653 | 0.7342 | 0.000015 | 0.7119 |
| Hybrid 33 | M. Granophyre | 2020 | 56.9 | 0.01 | 218.7 | 0.015 | 0.7522 | 0.7338 | 0.000011 | 0.7119 |
| DGL 26 | Metabasalts | 2020 | 6.6 | 0.01 | 470.7 | 0.03 | 0.0403 | 0.7036 | 0.000012 | 0.7024 |
| DGL 14 | Metabasalts | 2020 | 2.1 | 0.01 | 415.3 | 0.03 | 0.0147 | 0.7045 | 0.000039 | 0.7041 |
| RG-2+4 | PTB Quarry | 2020 | 144.9 | 0.29 | 185.8 | 0.02 | 2.2688 | 0.8036 | 0.000012 | 0.7376 |
| RG1 | Rand Granite Quarry | 2020 | 197.0 | 0.39 | 167.3 | 0.01 | 3.4420 | 0.8466 | 0.000011 | 0.7464 |
| TMW38B | Leeukop-PTB | 2020 | 109.5 | 0.22 | 282.6 | 0.07 | 1.1221 | 0.7509 | 0.000013 | 0.7183 |
| TMW39 | Leuukop-Granite | 2020 | 141.6 | 0.28 | 241.2 | 0.03 | 1.7031 | 0.7724 | 0.000011 | 0.7228 |
| TMU5 | PTB Leeukop | 2020 | 123.5 | 0.25 | 254.5 | 0.05 | 1.4062 | 0.7611 | 0.000012 | 0.7202 |
| TMW144 | Granite Leeukop | 2020 | 113.7 | 0.23 | 289.2 | 0.05 | 1.1374 | 0.7482 | 0.000010 | 0.7151 |
| P2TM3 | Kudu-PTB | 2020 | 45.7 | 0.09 | 455.0 | 0.30 | 0.2898 | 0.7132 | 0.000011 | 0.7048 |
| TMW19 | Kudu-Amphi | 2020 | 26.7 | 0.05 | 337.0 | 0.20 | 0.2286 | 0.7096 | 0.000011 | 0.7029 |
| WUR-VG | F. Granophyre | 2020 | 89.7 | 0.18 | 208.5 | 0.03 | 1.2466 | 0.7561 | 0.000010 | 0.7198 |
| VPU5 | F. Granophyre | 2020 | 62.9 | 0.13 | 227.3 | 0.04 | 0.8002 | 0.7359 | 0.000009 | 0.7126 |
| VPU5 | Duplicate dissoln | 2020 | 63.0 | 0.13 | 227.3 | 0.05 | 0.8012 | 0.7359 | 0.000012 | 0.7126 |
| VG2 | F. Granophyre | 2020 | 75.2 | 0.15 | 214.2 | 0.01 | 1.0156 | 0.7441 | 0.000013 | 0.7145 |
| VPU11 | Contam. Granophyre | 2020 | 66.1 | 0.13 | 233.4 | 0.02 | 0.8185 | 0.7360 | 0.000012 | 0.7122 |
| VPU20 | Kudu granite | 2020 | 73.2 | 0.15 | 561.4 | 0.10 | 0.3764 | 0.7187 | 0.000011 | 0.7078 |
| VPU21 | Epidiorite | 2020 | 63.4 | 0.13 | 234.1 | 0.03 | 0.7824 | 0.7346 | 0.000013 | 0.7118 |
| VPU23 | F. Granophyre | 2020 | 66.2 | 0.13 | 227.1 | 0.03 | 0.8421 | 0.7367 | 0.000013 | 0.7122 |

| Sample | Lithology Type | Age (Ma)* | Sm [µg/g] | 2se | Nd [µg/g] | 2se | $^{147}Sm/^{144}Nd$ | $^{143}Nd/^{144}Nd_{[fc]}$ | 2se | $\varepsilon Nd_{(0)}$ | $^{143}Nd/^{144}Nd_{(T)}$ |
|---|---|---|---|---|---|---|---|---|---|---|---|
| **Reimold et al., 2017** | | | | | | | | | | | |
| Hybrid 24 | M. Granophyre | 2020 | 3.34 | 0.01 | 18.28 | 0.001 | 0.1112 | 0.510929 | 0.000014 | -33.51 | 0.509450 |
| Hybrid 33 | M. Granophyre | 2020 | 3.76 | 0.01 | 20.44 | 0.002 | 0.1120 | 0.510930 | 0.000010 | -33.49 | 0.509442 |
| DGL 26 | Metabasalts | 2020 | 4.13 | 0.01 | 18.97 | 0.002 | 0.1328 | 0.511329 | 0.000021 | -25.71 | 0.509563 |
| DGL 14 | Metabasalts | 2020 | 3.21 | 0.01 | 13.46 | 0.002 | 0.1453 | 0.511544 | 0.000013 | -21.51 | 0.509612 |
| RG-2+4 | PTB Quarry | 2020 | 11.04 | 0.002 | 75.30 | 0.004 | 0.0893 | 0.510358 | 0.000004 | -44.65 | 0.509171 |
| RG1 | Rand Granite Quarry | 2020 | 6.62 | 0.002 | 48.02 | 0.002 | 0.0840 | 0.510233 | 0.000004 | -47.09 | 0.509116 |
| TMW38B | Leeukop-PTB | 2020 | 4.14 | 0.001 | 23.98 | 0.001 | 0.1052 | 0.510695 | 0.000004 | -38.08 | 0.509295 |
| TMW39 | Leuukop-Granite | 2020 | 2.03 | 0.001 | 11.00 | 0.000 | 0.1124 | 0.510827 | 0.000004 | -35.50 | 0.509332 |
| TMU5 | PTB Leeukop | 2020 | 4.72 | 0.002 | 28.69 | 0.001 | 0.1002 | 0.510630 | 0.000004 | -39.34 | 0.509298 |
| TMW144 | Granite Leeukop | 2020 | 1.73 | 0.000 | 10.37 | 0.000 | 0.1015 | 0.510606 | 0.000004 | -39.81 | 0.509256 |
| P2TM3 | Kudu-PTB | 2020 | 2.99 | 0.001 | 16.52 | 0.001 | 0.1102 | 0.510839 | 0.000004 | -35.27 | 0.509374 |
| TMW19 | Kudu-Amphi | 2020 | 2.57 | 0.001 | 11.99 | 0.001 | 0.1307 | 0.511325 | 0.000004 | -25.79 | 0.509587 |
| WUR-VG | F. Granophyre | 2020 | 3.87 | 0.001 | 21.67 | 0.001 | 0.1089 | 0.510818 | 0.000004 | -35.68 | 0.509370 |
| VPU5 | F. Granophyre | 2020 | 3.68 | 0.001 | 21.12 | 0.001 | 0.1060 | 0.510796 | 0.000004 | -36.11 | 0.509386 |
| VPU5 | Duplicate dissoln | 2020 | 3.68 | 0.001 | 21.15 | 0.001 | 0.1060 | 0.510798 | 0.000004 | -36.07 | 0.509388 |
| VG2 | F. Granophyre | 2020 | 3.57 | 0.001 | 20.39 | 0.001 | 0.1066 | 0.510795 | 0.000004 | -36.13 | 0.509377 |
| VPU11 | Contam. Granophyre | 2020 | 3.97 | 0.001 | 21.99 | 0.001 | 0.1099 | 0.510856 | 0.000004 | -34.94 | 0.509395 |
| VPU20 | Kudu granite | 2020 | 2.45 | 0.001 | 20.49 | 0.001 | 0.0728 | 0.510058 | 0.000004 | -50.50 | 0.509090 |
| VPU21 | Epidiorite | 2020 | 4.01 | 0.001 | 21.98 | 0.001 | 0.1111 | 0.510898 | 0.000004 | -34.12 | 0.509420 |
| VPU23 | F. Granophyre | 2020 | 3.82 | 0.001 | 21.90 | 0.001 | 0.1062 | 0.510814 | 0.000004 | -35.76 | 0.509402 |